Transport of terrestrially derived nutrients along the Western Antarctic Peninsula, Anvers Island

by

Jared Crenshaw

April, 2015

Director of Thesis: D. Reide Corbett

Major Department: Geological Sciences

The mechanisms that supply Fe to the surface waters off the coast of the Western Antarctic Peninsula (WAP) play a key role in the global climate cycle by fueling primary production in this vast and globally important environment. This study investigates the shore-normal mixing rate of nearshore waters using naturally-occurring radioactive isotopes. This mixing could transport nutrients derived from an unevaluated source (i.e., submarine groundwater discharge; SGD) offshore along the WAP. Stable isotopes of water (i.e., ^{2}H, ^{18}O) and radioactive groundwater tracers (i.e., $^{223,224,226,228}Ra$, ^{222}Rn) were used to evaluate the potential source of these nutrients and nearshore water masses. During the austral summers of 2012-2013 and 2013-2014, seawater samples were collected along the WAP offshore of Anvers Island aboard the *R/V Laurence M. Gould* (LMG) to observe water-column and tracer dynamics in nearshore and offshore environments in order to evaluate the source and horizontal mixing of water across the continental shelf.

Short- and long lived radium (Ra) isotopes and radon-222 (^{222}Rn) are used to evaluate the rates that water masses mix in shelf waters. Porewaters collected near Palmer Station were found to be elevated in short-lived Ra isotopes and ^{222}Rn, demonstrating that these tracers are valuable

to delineating terrestrially derived water masses as has been reported in temperate and tropical shelf systems. Offshore surface waters were depleted in short-lived Ra isotopes and ^{222}Rn relative to porewaters, and within the range of those measured in other regions of the WAP and temperate nearshore environments. Using the full suite of parameters measured, comparisons of freshwater delivery to coastal waters are compared across seasons, with increased freshwater observed during the late austral summer, 2014. Horizontal mixing rates of water masses within glacial fjords along the WAP ranged from 570 to 6820 m^2s^{-1}. Short-lived Ra isotopes were used to estimate the timing of the most recent sediment-water interaction in surface waters. Estimates ranged between 15-25 days offshore of Anvers Island. Fluorescence was elevated in several nearshore locations and found to be coincident with the high tracer activities used in this study to evaluate the distribution of terrestrial meltwater, suggesting the importance of glacial melt as a source of bio-limiting nutrients.

A Thesis

Presented To the Faculty of the Department of Geological Sciences

East Carolina University

In Partial Fulfillment of the Requirements for the Degree

Masters of Science in Geology

by

Jared Crenshaw

April, 2015

Transport of terrestrially derived nutrients along the Western Antarctic Peninsula, Anvers Island

by

Jared Crenshaw

APPROVED BY:

DIRECTOR OF
THESIS: _____
D. Reide Corbett, PhD

COMMITTEE MEMBER: _____
J. P. Walsh, PhD

COMMITTEE MEMBER: _____
Terri Woods, PhD

COMMITTEE MEMBER: _____
Kimberly Null, PhD

CHAIR OF THE DEPARTMENT
OF GEOLOGICAL SCIENCES: _____
Steve Culver, PhD

DEAN OF THE
GRADUATE SCHOOL: _____
Paul J. Gemperline, PhD

Acknowledgements

I would like to thank Drs. Reide Corbett, J. P. Walsh, Terri Woods, and Kimberly Null for their support and guidance on this project and throughout my time at East Carolina University. This research would not have been possible without the collaboration of Dr. Richard Peterson, Dr. Rich Viso, Leigha Peterson, and David Sybert. I would like to thank the captain and crew of the *R/V Laurence M. Gould*, the scientists and support staff of Palmer Station the U.S. Antarctic Program, and the many graduate students who not only assisted in sample analyses at ECU, but devoted significant amounts of time to assist with field efforts in the Antarctic. Finally, I thank my wife for her dedication, support, and encouragement throughout my studies at ECU. This research was funded by the National Science Foundation, grant number 1142090.

Table of Contents

List of Tables

List of Figures

List of Symbols

A_x= Tracer activity at distance x from the shoreline

A_0= Tracer activity of source water

K_h= Eddy diffusion coefficient

λ= Decay Constant

m= slope of the Ln of ^{222}Rn activity with distance from the shoreline

AR_{obs}= observed activity ratio of ^{224}Ra/^{223}Ra

AR_i= ^{224}Ra/^{223}Ra activity ratio of source water

t= time in days

1. Introduction

Over the past hundred years, average global temperatures have been increasing. The most drastic warming has taken place in climate-sensitive regions at high latitudes, including the Western Antarctic Peninsula (WAP; Schofield et al., 2010; Figure 1). Annual mean atmospheric temperatures along the WAP have increased by about 3°C over the past 60 years (Meredith and King, 2005). Due to recent warming, glaciers between 64°S and 66°S are currently receding at a rate of ~ 57 meters per year (Cook et al, 2005). Warming air temperatures have resulted in sea-ice reduction and increased glacial melt inputs that have the potential to impact salinity and temperature dynamics in surface waters along the shoreline (Hakkinen, 2003; Turner et al., 2006; Ducklow et al., 2007). The surface waters of the Southern Ocean play a key role in global climate and carbon cycles by hosting some of the world's largest phytoplankton blooms, which sequester up to one billion metric tons of CO_2 per year (Takahashi et al., 2012).

Recent studies (Hawkings et al., 2014; Bhatia et al., 2013) have emphasized the potential importance of glacial inputs to Fe budgets in polar regions, and how these inputs can fuel primary productivity in Fe-limited environments like the Southern Ocean (Klink et al., 2004; Martinson et al., 2008; Martinson, 2012; Takahashi et al., 2012). The fertile surface waters along the shelf of the WAP are influenced by large inputs of glacial melt from the peninsula (Dierrsen et al., 2002). The objective of this study is to evaluate the transport of Fe-rich waters from the Antarctic continent into the biologically productive waters along the western coast of the WAP utilizing a suite of naturally occurring stable- and radioisotopes as tracers of terrestrially derived water masses.

1.1 Sources of Nutrients to the Southern Ocean

Aeolian sediment from arid regions of the African continent was thought to be a primary source of Fe to the surface waters of the Southern Ocean (Cassar et al., 2007); however, recent studies in the Antarctic seasonal sea ice zone (SSIZ) show that aeolian dust plays a minor role in the overall Fe budget (Winton et al., 2014). An additional source of Fe to offshore surface waters along the WAP is vertical mixing (Klink et al. 2004, Martinson et al. 2008, Martinson 2012). Vertical mixing occurs when currents encounter bathymetric features such as seamounts. Changes in bathymetry force bottom waters, resuspended sediments, and associated nutrients to the surface. For example, in areas where the Antarctic Circumpolar Current encounters seamounts, increased Fe concentrations down-current have been shown to stimulate primary production in surface waters (Holm-Hansen et al., 2005).

Continentally-derived freshwater inputs often enter coastal waters during meltwater pulses along the WAP. These pulses create large freshwater lenses that can extend 50 m in the water column and as far as 100 km offshore (Dierssen et al., 2002). Meltwater pulses have the potential to develop density gradients that can drive surface currents, laterally transporting continentally-derived nutrients (e.g. Fe) offshore (Dierssen et al., 2002; Moffat et al., 2008). Dierssen et al. (2002) found that over 70% of the phytoplankton blooms observed offshore of Anvers Island occurred shortly after pulses of meltwater discharged from local glaciers into surface waters.

Glacial meltwater can enter the nearshore coastal zone through calving, basal melt, and subglacial melt, which passes over or through sediments or other geologic material before reaching the ocean. The process of water moving through the subsurface and discharging into the sea is referred to as submarine groundwater discharge (SGD; Figure 2). Meltwater that interacts

with rocks and sediments before reaching the sea is of particular importance because it incorporates biologically important macro- and micro-nutrients before discharge to the ocean (Johannes, 1980; Corbett et al., 1999; McCoy et el., 2011; Null et al., 2012). Terrestrial inputs and associated constituent fluxes have not previously been measured along the WAP. It is important to investigate meltwater as a source of nutrients along the WAP since rapid warming in this region may lead to an increase in the amount of water that passes over or through geologic material and is ultimately delivered to the coastal ocean.

1.2 Radiotracers and Coastal Processes

Submarine groundwater discharge may include meltwater and recirculated seawater that has interacted with the substrate (Burnett et al., 2003). For the purposes of this study, SGD is defined as the total discharge into a water body across the sediment-water interface, regardless of the water source and the mechanisms that result in such discharge (Burnett et al., 2003). Therefore, as defined, SGD may include both fresh and saline sources of groundwater (Figure 2). SGD can contribute considerable amounts of Fe and other nutrients to nearshore environments, often delivering more than local river systems (Bugna et al., 1996; Moore, 1996; Windom et al., 2006; Viso et al., 2010).

Groundwater in coastal environments can be traced from the land-ocean boundary across continental shelves using radium isotopes (Charette et al., 2001; Hwang et al., 2005; Peterson et al., 2009) and radon (Corbett et al., 2000; Burnett et al., 2006; McCoy et al., 2007a; McCoy et al., 2007b). Radium and radon (^{224}Ra $t_{1/2}$ = 3.63 d, ^{223}Ra $t_{1/2}$ = 11.43 d, ^{228}Ra $t_{1/2}$ =5.75 y, ^{226}Ra $t_{1/2}$ =1600 y, ^{222}Rn $t_{1/2}$=3.83 d) are naturally occurring radioisotopes that are enriched in groundwater relative to seawater (Moore, 1996; Cable et al., 1996; Burnett, 2003). Radium is

generated naturally by the decay of thorium, which is present in soils, rocks, and sediments. Thorium is highly particle reactive in the marine environment. Radium is particle reactive in freshwater environments. When Ra-enriched water enters the marine environment, Ra desorbs from particles and moves with the associated water-mass. The pathways of terrestrially-derived water masses, such as meltwater and SGD, can be identified by evaluating the spatial distribution of radon- and radium-enriched waters (Moore, 1996).

The transport rate of radium-enriched water can be calculated by using the decay rates of short- and long-lived radium isotopes (Moore 2000). Radon-222 is generated by the decay of its parent ^{226}Ra which is found in sediments and along continental margins. Conveniently, ^{222}Rn decays on about the same timescale as ^{224}Ra, which is commonly used in mixing calculations. Here Ra isotopes and ^{222}Rn are used to evaluate surface water mixing rates along the coast of the WAP. Studies using radium and radon isotopes to evaluate mixing rates have been conducted in several coastal environments (Hancock et al. 2006; Peterson et al. 2008; Knee et al. 2011), and in other regions along the WAP (Dulaiova, 2009; Annett et al., 2013).

Mixing and lateral transport rates of shelf-derived Fe and Ra from continental shelves to offshore waters have recently been established along the northern WAP (Charette et al., 2007; Dulaiova et al, 2009; Ardelan et al., 2010; Annett et al., 2012). However, great variability in the magnitude of lateral transport has been reported, and therefore site-specific mixing rates across the continental shelf near Anvers Island and in other areas along the WAP need to be established to evaluate the transport of continentally-derived inputs to high-nutrient-low-chlorophyll (HNLC) waters along the continental shelf.

2. Study Area

The WAP extends northward from the western Antarctic continent. This region is the warmest of the Antarctic and the most rapidly warming region in the world. The rugged topography and warmer maritime climate of the peninsula differentiates the WAP from other regions of the continent that are colder and covered by ice sheets that obscure underlying topographic features. Air temperatures along the western coast of the WAP are dominated by the influence of the Bellingshausen Sea, causing air temperatures to be about 7°C warmer than the eastern coast of the Peninsula, which is influenced by the cooler Weddell Sea (Reynolds, 1981; Morris and Vaughan, 1994; Vaughan et al., 2003). During the summer months ambient air temperatures commonly exceed 0°C at sea level along the western coast of the peninsula. Winter temperatures average -8.6°C (Vaughan et al., 2003).

Several glacial fjords line the coast of the WAP and were sampled as part of this research. Flandres Bay is a glacial fjord protected from the open ocean by Anvers Island and several smaller islands. The 16-km-wide bay is flanked by mountains on both sides, and maximum depth is ~400 m. The mouth of Flandres Bay opens to the Gerlache Strait that runs between Anvers Island and the Antarctic Continent. Barilari Bay and Beascochea Bay are both similarly flanked by rugged mountains, and open to the Grandidier Channel (Figure 1). These glacial fjords are characterized by high relief, with mountains along either sides sloping to depths of up to 1500m.

The continental shelf of the WAP is about 200km wide near Anvers Island and has an average depth of around 450m (Martinson et al., 2008). The aforementioned depth excludes many of the deep canyons that incise the continental shelf such as the Palmer Deep which reaches a maximum depth of about 1500m (Domack et al., 2006, Martinson et al., 2008).

Surface water characteristics along the WAP change seasonally. Most of the water between the surface and the permanent pycnocline (~150m) during the summer months is termed Antarctic Surface Water (AASW). AASW ranges in temperature from -1.5 – 1.0° C and ranges in salinity from 33.0 - 33.7 (Klinck et al., 2004). During the winter, a relatively cooler and saltier water mass develops near the surface (Winter Water). Winter Water temperatures are generally cooler than -1.8°C, with a salinity of about 34.1 (Klinck et al., 2004). During the summer months, remnants of Winter Water linger between AASW and the pycnocline (Klinck et al., 2004). Subpycnocline waters are classified as Circumpolar Deep Water (CDW), which is subdivided into Upper CDW and Lower CDW. CDW ranges in temperature from 1.0 - 2.0° C and has salinities of 34.6 - 34.74. Several authors (Klinck et al., 2004; Martinson et al., 2008; Meredith et al., 2013) cite frequent incursions of Upper CDW into coastal regions of the continental shelf and apparent mixing with surface waters.

Cyclonic circulation patterns along the WAP were identified in early oceanographic studies along the WAP, and further described by Savidge and Amft (2009). Long-term averages of Acoustic Doppler Current Profiler (ADCP) data collected by research vessels along the peninsula suggest that a cyclonic cell rotates around Anvers Island (Figure 3). Surface waters offshore of Anvers Island flow south and form part of the Antarctic Peninsula Coastal Current (APCC), an along-shore surface current which occurs along the west coast of the peninsula during the summer months (Moffat et al., 2008). The development of the APCC is thought to be initiated by meltwater inputs along the Peninsula, although the origin of these waters is poorly understood. The APCC has been observed as far north as Barbarant and Anvers Islands (Savidge and Amft, 2009), and flows southward, eventually making its way into Marguerite Bay and farther south

(Moffat et al., 2008). In the Gerlache Strait surface currents move to the north toward the Bransfield Straight (Savidge and Amft, 2009).

3. Methods

3.1 Sample collection and analysis

During the austral summers of 2012-2013 and 2013-2014, seawater samples were collected along the WAP offshore of Anvers Island aboard the *R/V Laurence M. Gould* (LMG) to observe water-column and tracer dynamics in nearshore and offshore environments (Figure 4). During each field season, seawater was collected at 1-3 depths (surface, mid-depth, and bottom) along three transects and within glacial fjords for analysis of a suite of parameters including radium isotopes (^{223,224,226,228}Ra), ^{222}Rn, oxygen and deuterium ratios in seawater (δ^{18}O and δD), and nutrient and trace metal concentrations (NO_3^-+NO_2^-, NH_4^+, HPO_4^{2-}, SiO_2, total dissolved Fe).

At each site, the CTD with rosette was lowered multiple times from the ship to within a few meters of the sea-floor. Temperature, salinity, density, beam transmission, conductivity, oxygen, and fluorescence were continuously recorded. Along the cruise track during the 2014 field season, the hull mounted ADCP was used to measure current velocities between 37 and 97m.

3.2 Ra Isotopes

Large volumes (280L-360L) of seawater were collected at 1-3 depths (surface, mid-depth, and bottom) at each station for Ra analysis using 30L Niskin bottles. Samples were transferred to modified aquarium tanks for processing. Radium was quantitatively removed from the seawater by gravity filtering (rate of ~1 L min^{-1}) through MnO_2-coated acrylic fiber (i.e., Mn fibers; Moore and Reid, 1973).

Upon the completion of gravity filtering, the fibers were rinsed with radium-free fresh water and partially dried with compressed air (Sun and Torgerson, 1998; Kim et al., 2001). ^{223}Ra and ^{224}Ra were immediately analyzed using a Radium Delayed Coincidence Counter (RaDeCC; Figure 5; Moore and Arnold, 1996). Samples were recounted after 4-6 weeks for ^{228}Th. Analytical uncertanties were 0.08 dpm m^{-3} for ^{223}Ra and 0.15 dpm m^{-3} for ^{224}Ra.

After correcting for ^{228}Th supported ^{224}Ra, samples were analyzed for the longer-lived radium isotopes (^{226}Ra and ^{228}Ra). Although specifically designed to measure activities of ^{223}Ra and ^{224}Ra, the RaDeCC system was used to measure ^{226}Ra using methods introduced by Waska et al. (2008). The Mn fibers were placed into a column fitted with ball-valves to allow the system to be opened and closed as necessary. Prior to measurement, fibers were placed into the columns with the valves closed for 3-10 days. This allowed for the ingrowth of ^{222}Rn from ^{226}Ra. During the initial measurement process, the modified columns containing the fibers are placed into a closed air-loop with the RaDeCC system for 25 minutes. A small diaphragm pump circulates helium throughout the system at approximately 6L min^{-1}. After 25 minutes the pump is turned off and the ball valves are closed to isolate the system from the sample, preventing additional ^{222}Rn ingrowth. For the next three hours, the daughter isotopes of ^{223}Ra and ^{224}Ra (^{219}Rn and ^{220}Rn) decay, and the count rate represents only that of ^{222}Rn and its short-lived daughters (i.e., ^{218,214}Po) generated by the decay of ^{226}Ra (Figure 6). After the three hour equilibration period, decays within the Lucas cell are counted with the RaDeCC software (Waska et al., 2008; Peterson et al., 2009).

3.3 Radon

Radon analyses were completed by collecting 6L of seawater directly from a Niskin bottle with a 3/8" diameter tube at each location and depth. Seawater was siphoned into a 6L Nalgene bottle with a filling-venting cap to minimize radon evasion. Each seawater sample was analyzed with a RAD-7 radon-in-air monitor (Durridge Co., Inc.). The RAD-7 uses a silicon semiconductor at ground potential to measure the short-lived Po isotopes emitted by ^{222}Rn decay (Burnett and Dulaiova, 2003).

3.4 Nutrients, $\delta^{18}O$ and δD

A 60 mL seawater sample was collected at each sampling location and depth for nutrient analyses ($NO_3^-+NO_2^-$, NH_4^+, HPO_4^{2-}, SiO_2). Each sample was filtered through a 0.45 µm filter into an acid-cleaned 60 mL polypropylene bottle. Samples collected during the 2012-2013 field season were stored at -20 °C and shipped to the UNC Coastal Studies Institute for analysis on a Lachat Quickchem Autoanalyser. Samples collected during the 2013-2014 season were analyzed at Palmer Station on a Lachat Quickchem Autoanalyser.

Seawater samples were collected for $\delta^{18}O$ and δD analyses at each location and depth at the same time as nutrient samples. To minimize degassing, water was allowed to overflow a 20mL scintillation vial for 10 seconds. After the scintillation vial was completely filled with seawater with no head space, the cap was placed on the vial. Samples were sealed with parafilm and stored inverted at +4°C. Samples were shipped to Ohio State University for analysis on a Picarro water isotope ($\delta^{18}O$ and δD) analyzer. Calculated values are relative to Vienna Standard Mean Ocean Water (VSMOW).

3.5 Sediment Analyses

Bottom sediments were collected at each station with a Smith McIntyre Grab Sampler. The grab sampler collects sediments from the upper few centimeters of the substrate. Once the sampler was brought aboard the ship, sediments were collected into Whirl-Pak plastic bags, stored at 4 °C, and sent to East Carolina University for analyses.

Diffusion of ^{222}Rn from bottom sediments into the overlying water may be an important source of radon and should be evaluated. These diffusive ^{222}Rn fluxes were obtained using a "sediment equilibration" technique described by Martens et al. (1980). Although this approach does not include influences from bioturbation or resuspension, an accurate and representative diffusive flux may be obtained without using in situ methods. Fluxes from several sites across the shelf were estimated by equilibrating approximately 200 g of wet sediment with 6 L of Ra-free tap water in sealed containers. After ~4 weeks, the ^{222}Rn in the water phase was measured via the RAD-7 system utilizing methods described above. A radon flux was estimated using

$$J = \left(\lambda D_S\right)^{1/2}\left(C_{eq} - C_o\right) \qquad (1)$$

where λ is the decay constant for radon (min^{-1}); D_S is the effective wet bulk sediment diffusion coefficient in the sediments ($m^2 \cdot min^{-1}$); C_{eq} is the radon concentration in pore fluids in equilibrium with radium in the sediments determined by the sediment equilibration experiments ($dpm \cdot m^{-3}$; wet sediment); and C_O is the radon concentration in the overlying water at the sediment-water interface multiplied by the calculated sediment porosity to obtain a wet sediment equivalent ($dpm \cdot m^{-3}$). The effective wet sediment diffusion coefficient (D_S) used for these calculations is based on literature values corrected for the average temperature variations and

tortuosity conditions for the study area [(6.99 X 10^{-5} $m^2 \cdot d^{-1}$; (Ullman and Aller, 1982; Peng et al., 1974)].

Sediment desorption experiments were done to evaluate the impact of salinity on Ra-enriched sediments. About 100g of wet sediment was added to 4L of Ra-free salt water. After sitting for 48 hours, the solution was passed through Mn fibers. The fibers were subsequently analyzed as described above for short- and long-lived Ra isotopes using the RaDeCC system.

Four sediment samples from the sea floor and one from beneath a glacier terminus on Anvers Island were chosen for analysis via X-ray fluorescence spectrometry with a PANalytical Axios, low-power, wavelength-dispersive, XRF spectrometer. Sediments were ground to <240 mesh and mixed with 20% cellulose binder. Once homogenized, the mixture was pressed into a 37mm round pellet and analyzed for FeO. The spectrometer was calibrated by measuring 16 standards with known elemental compositions. Calibration yielded a 5.39 ppm lower detection limit and measurements accuracy within 0.001%.

4. Results

4.1 Physical Parameters

During the cruises, surface water temperatures varied from -1.49 – 2.79° C, with an average of 0.54° C. The warmest waters were observed in Flandres Bay and regions closer to shore. The coldest surface temperatures were measured along T-3 in 2012 and in Barilari Bay during the February 2014 cruise (Figure 7). Temperature minima (-2°C) existed during both field seasons throughout the study area at 50-100m depth. These temperature minima were not present closer to the shoreline, where density gradients across the permanent pycnocline ~150m were less prevalent. Salinities ranged from 31.2 – 34.1 at the surface with an average of 33.2. Fresher waters were found closest to shore in Flandres Bay, Beschochea Bay, and Barilari Bay (Figure 7).

The mixed layer extended to about 150m depth in offshore waters where several authors have reported a permanent pycnocline. Closer to land, these temperature and salinity (and thus density) gradients were generally not as prominent (Figures 8 and 9). Near Vernadsky Station a large fresher water mass in the upper 20m of the water column extended from the shoreline to about 60km offshore in December 2012, and about 18km from the shoreline in February of 2014. Along T-3 in 2012, temperature and salinity profiles suggested vertical mixing throughout the water column was occurring at about 80km offshore. During the 2014 field season CTD casts were performed at the same location (80km offshore along T-3), and suggested that the 150m pycnocline was present along the entire length of T-3. Deeper waters within the study area ranged in temperature from -0.51 – 1.58° C, with an average of 1.07° C. Salinities in deeper waters ranged from 34.2 – 34.7, with an average of 34.6.

A plot of instantaneous current vectors generated by the ship's Acoustic Doppler Current Profiler (ADCP) during the 2014 cruise shows highly variable current velocities along the shelf near Anvers Island (Figure 10). The currents measured during the 2014 cruise differ from current vectors presented by Savidge and Amft (2009), which are averages of ADCP data collected by the *Laurence M. Gould* and *Nathaniel B. Palmer* over 6 years along the WAP. Note that our dataset has not been post processed to remove tidal fluctuations, but represents directional flow paths during the time the ship passed over those locations.

4.2 Radium

Short-lived radium isotopes were measured in surface waters offshore of Anvers Island and in Flandres Bay during the 2012 and 2014 cruises (Figure 11-12). The activities of ^{223,224}Ra in surface waters of the Grandidier Channel, Gerlache Strait, and Beascochea and Barilari Bays were measured during the 2014 cruise. Surface waters had 0.1 – 1.0 dpm m^{-3} ^{223}Ra, 0.1 – 12.8 dpm m^{-3} ^{224}Ra, and 26.3 – 980 dpm m^{-3} ^{226}Ra, while deep waters had 0.2 – 1.7 dpm m^{-3} ^{223}Ra, 0.2 – 16.1 dpm m^{-3} ^{224}Ra, and 21.8 – 470 dpm m^{-3} ^{226}Ra.

4.3 Radon

Surface ^{222}Rn activities ranged from 0.3-0.8 dpm L^{-1} while deeper waters ranged from 0.1 – 1.1 dpm L^{-1} (Figures 11-12). Like radium, surface waters were found to be enriched in ^{222}Rn in the vicinity of Anvers Island and Flandres Bay in December of 2012 (0.2-0.6 dpm L^{-1}), and at several locations in bottom waters. In 2014, ^{222}Rn-enriched surface waters were observed offshore Barilari Bay and in Flandres Bay (0.3 - 0.75 dpm L^{-1}).

4.4 Nutrients and Fluorescence

Orthophosphate concentrations in surface waters ranged from 0.04-0.78 µmol L^{-1}. Nitrate concentrations in surface waters ranged from 0.9-7.3 µmol L^{-1}. Nitrate and phosphate concentrations showed similar patterns (Figures 13-14). Generally, bottom water concentrations were higher than surface water values, and surface water concentrations along the coast were lower than offshore waters. Deep water orthophosphate and nitrate concentrations ranged from 0.6-0.8 µmol $L^{-1}$and 3.8-8.4 µmol L^{-1}, respectively. In 2012, maximum fluorescence values were observed along T-1 in Ra-enriched waters about 57 km offshore of Anvers Island (Figure 15-b). During the 2014 cruise, surface waters in Flandres, Barilari, and Beascochea Bays had the lower phosphate concentrations, corresponding to sites with the highest fluorescence values. As expected, fluorescence was generally higher nearshore (Figures 14-16).

Ammonium concentrations in surface waters ranged from below detection to 5.4 µmol L^{-1} (Figure 13-14). In deeper waters, ammonium concentrations range from below detection to 1.3 µmol L^{-1}. Patterns in the distribution of ammonium differ from patterns observed in phosphate and nitrate, although ammonium was similarly depleted in some areas (Beascochea and Barilari Bays) (Figures 13-14). Increased ammonium concentrations in surface waters were observed in the vicinity of Vernadsky Station and in Flandres Bay. Silica concentrations in surface waters varied from 18.0-41.3 µmol L^{-1} (Figure 13-14). Surface waters in Flandres Bay and in the Gerlache Strait were enriched relative to offshore surface waters and fjords to the south. In deeper waters, silicate concentrations range from 40.6-50.4 µmol L^{-1}.

4.5 $\delta^{18}O$ and δD

Deuterium values in surface and deep waters ranged from -12.1 to -3.7 ‰ and -11.2 - -0.5 ‰, respectively. ^{18}O values in surface and deep waters ranged from -1.9 - 0.4 and -1.36 – 0.02 ‰, respectively. The distribution of $\delta^{18}O$ and δD are very similar (Figures 15-16). Surface waters near Vernadsky Station and in Flandres Bay were depleted in D relative to adjacent surface and bottom waters. Surface waters along the 2012 southern transect at about 25 km offshore were enriched in $\delta^{18}O$ and δ D relative to adjacent surface waters. In surface waters along the 2012 northern transect, $\delta^{18}O$ and δ D were enriched relative to adjacent surface waters. In the center of the study area, along T-2 in 2012, surface waters were depleted in $\delta^{18}O$ and δ D relative to adjacent surface waters. Measurements taken at T-2 were the lowest observed during both offshore cruises, but were within the range of previously measured values along the peninsula (Meredith et al., 2008).

4.6 Sediment Experiments

Marine sediments analyzed via XRF averaged 4.3% Fe. The sediment sample taken from the glacial terminus contained 4.1% Fe. Sediments that were equilibrated in a sealed container for at least 21 days generated 0.26-8.86 dpm g^{-1} ^{222}Rn with an average of 3.11 dpm g^{-1}. Sediments evaluated for Ra desorption upon interaction with salt water released between 0.20-1.65 dpm g^{-1} ^{223}Ra with an average of 0.98 dpm g^{-1}. The same sediments desorbed between 2.18-5.56 dpm g^{-1} ^{224}Ra with an average of 3.51 dpm g^{-1}.

5. Discussion

5.1 Tracer Signatures of Freshwater Sources

Along the shoreline of the WAP and nearby islands, fresher water masses were observed in the upper layers of the water column (Figure 9). These salinity differences in the upper parts of the water column co-varied with physical and geochemical parameters that have been used to identify glacial melt such as $\delta^{18}O$. The light isotopic signature of glacial ice has been used previously to trace melt inputs along the Antarctic continental shelf (Weiss et al., 1979; Schlosser et al., 1990; Weppernig et al., 1996; Meredith et al., 2008). Water isotope data presented in the study suggests that meltwater plumes exist ~14 km offshore of Barilari and Beascochea Bays.

Porewater and glacial meltwaters were enriched in Ra and Rn relative to seawater, and depleted in ^{18}O. Nearshore meltwaters had a similar geochemical signature, proving the use of these isotopes as valuable meltwater tracers. Porewater samples from Anvers Island had average activities of 2.33 and 54.08 dpm m^{-3} for ^{223}Ra and ^{224}Ra respectively, which are high relative to average surface water values observed offshore (Table 1). Glacial ice was also enriched in Ra isotopes relative to surface waters along the WAP. On average, glacial ice had activities of 6.2 and 115.8 dpm m^{-3} for $^{223, 224}Ra$, respectively (Null, in prep). Surface seawater activities averaged 0.4 and 2.8 dpm m^{-3} for $^{223, 224}Ra$, respectively. The relative enrichment of Ra and Rn in terrestrially derived waters is used to identify and evaluate the freshwater inputs observed along the shoreline of the WAP. Radium activities measured in this study are within the range of Ra activities measured in surface waters at other locations along the WAP (Annett et al., 2013;

Dulaiova et al., 2009) and in other coastal environments (Moore, 2000; Kim et al., 2008; Hwang et al., 2005; Moore, 2006).

5.2 Tracer Variability with Proximity to the Shoreline

Changes in surface salinity, temperature, and tracer activities vary with the amount of meltwater entering the nearshore environment. These parameters and others change with the progression of the austral summer as more melt water enters the nearshore environment. The averages of surface temperature and salinity values (Table 2) remain within the limits of AASW defined by Klinck et al. (2004) with the exception of nearshore salinity in 2014 (32.7±0.1). These waters were fresher on average than AASW, which suggests that local glacial inputs are mixing with nearshore surface waters. Data from the December 2012 cruise suggest little change in surface seawater characteristics with distance from the shoreline. This cruise took place during the early weeks of the austral summer when the melt season was just beginning. A notable difference is that offshore waters were much cooler than surface waters nearshore. Glacial melt signals weren't as prominent across the shelf. The 2014 cruise took place during the latter phases of the austral summer. At this point in the season, there were many differences in the physical and geochemical characteristics of surface seawater nearshore relative to offshore waters. Nearshore surface waters had lower salinity, temperature, $\delta^{18}O$ and δD values, and higher $^{223,224}Ra$ activities relative to offshore surface waters. These changes show an increased amount of meltwater influence with the progression of the austral summer and the utility of these geochemical tracers in identifying melt waters. The location and intensity of meltwater inputs can impact and influence the prolific phytoplankton blooms that take place along the WAP (Dierssen et al., 2002). In order to gain an understanding of how quickly these water masses can

be distributed along the WAP, mixing models were employed to evaluate coastal and cross-shelf mixing.

5.3 Estimating Nearshore Mixing

Mixing rates were estimated within two fjords where degassing was reduced based on the calculated flux of Rn from the sea surface to the atmosphere in these areas for the 24 hours prior to sample collection (Table 3). Values presented here are possibly an underestimate of mixing rates due to the potential impact of degassing.

A linear mixing model that evaluates mixing as a function of activity with distance from the shoreline and accounts for radioactive decay of the tracer is used to calculate mixing rates. This model is based on the assumptions that: (1) the system is at steady state, and (2) a constant flux at the landward boundary providing a constant initial concentration (A_0), and (3) there is no offshore source of the tracer. If the distribution of ^{222}Rn can be described as a function of diffusion rather than advection, then the eddy diffusion coefficient (K_h) can be calculated via:

$$A_x = A_0 \exp[-x(\mathrm{sqrt}(\lambda/K_h))] \qquad (2)$$

where A_x is the activity at distance x from the coast; A_0 is the activity at the coast (x = 0); and λ is the decay constant (Moore, 2000)

Mixing rates were calculated in two fjords, Flandres and Beascochea Bays. In Flandres Bay, mixing rates were 1210±180 and 570±130 $m^2 s^{-1}$ for the 2012 and 2014 cruises, respectively (Figure 16). As mentioned for the shelf, significant difference may represent variability in mixing rates during different times of the season. The December 2012 measurements were taken during the early weeks of the summer while 2014 measurements were made during the late

weeks of February, towards the end of the summer. During both sampling campaigns, surface waters in the fjord were extremely calm.

Mixing to the open ocean may be limited from Flandres Bay because it is protected by Anvers Island. Glaciers flank the bay on either side, likely providing multiple sources of terrestrially derived nutrients, fresh water, and the tracers (Figure 17). Elevated ^{222}Rn activities observed suggest that large terrestrial inputs exist within the fjord. Water and associated nutrients exported from Flandres Bay likely travel to the north within the Gerlache Strait and into the Bransfield Strait (Figure 3; Savidge and Amft 2012).

Mixing in Beascochea Bay was estimated at 6820±740 m^2 s^{-1} in (Figure 18) using measurements spanning a distance of ~31 km. Similar to Flandres Bay, Beascochea Bay is flanked by glaciers, but opens to the relatively unprotected Grandidier Channel at its mouth. Unfortunately, we have no information regarding flow paths leaving Beascochea Bay.

Mixing rates estimated here were within the range of other rates calculated along the WAP. To the north, Dulaiova et al. (2009) estimated mixing rates via Ra isotopes along the South Shetland Islands between 596-63000 m^2 s^{-1} in open ocean waters, where the Antarctic Circumpolar Current nears the northern edge of the peninsula. South of our study area Annett et al. (2013) calculated mixing rates using Ra isotopes within Marguerite Bay of 0.13 -1.0 m^2 s^{-1}. These are several orders of magnitude lower than those calculated in this study and may represent the more protected embayment of that study.

The mixing rates may be underestimates because of Rn degassing and the inherent assumptions of the model. The calculations are based on the assumption that there is only one point source of Rn within the fjord. Other sources of Rn throughout the fjord such as glacial

inputs along the shoreline could result in elevated activities away from what we are assuming is a point source. Finally, the mixing rates calculated are based on a linear diffusion model, but advection may impact the data. For example, onshore advection would yield data with a concave up trend, while offshore advection would result in a data with a concave down pattern (Moore, 2000). Data presented here generally fit a straight line, suggesting that the transport rates estimations within these fjords are a good estimation of an effective horizontal eddy coefficient (Charette et al., 2007; Annett et al., 2012).

The suite of short- and long-lived radium isotopes can be used to estimate rates of nearshore and cross-shelf mixing. Using differences in the half-lives and the likely source of these radium isotopes near shore (i.e., glacial meltwater), it is possible to calculate the elapsed time between the last interaction with the continental shelf and sample collection (Moore, 2003). More specifically, the age of a water mass on the continental shelf can be calculated using the decay rates of the short-lived radium isotopes as follows:

$$t = ln((AR)_i/(AR)_{obs}))1/\lambda_{224}-\lambda_{223} \quad (3)$$

where AR_{obs} is the observed $^{224}Ra/^{223}Ra$ activity ratio at each sample location, AR_i is the $^{224}Ra/^{223}Ra$ activity ratio of the source area, and λ_{224} and λ_{223} are the decay constants for each radionuclide (d^{-1}). The equation here was solved for *t* (days), and defines the "age" of water at the corresponding site. This calculation is based on the assumption that the activity ratio of the source $(AR)_i$ is constant in the area (Table 4). Porewaters measured near Palmer Station demonstrated the highest activity ratios while bottom waters along the shelf had the lowest. The age values presented here are derived using an initial activity ratio $(AR)_I$ of 20.9, which is an average of the terrestrial samples collected from porewaters, streams, and glacial ice. Radium

ages are estimated for surface waters in Flandres Bay during the 2012 cruise. Ages range from 2.3 - 20.2 days with the youngest surface waters closest to the glacial terminus and the oldest waters nearing the Gerlache Strait.

5.4 Evaluating Cross-Shelf Mixing

Radium ages are estimated for samples acquired along T-1 as described by equation 3 above. Ages range from 5-25 days with the youngest ages at the shoreline, increasing in age with distance from the shoreline (Figure 19). Values presented here are within the range of ages presented by Moore (2003) along the South Atlantic Bight. An outlier within this data set is the "younger" water mass observed at about 80km offshore in surface waters. This water mass had a younger age than adjacent samples, meaning that it has had a more recent interaction with terrestrial materials, and may not have been delivered to that region by the same mechanisms as the adjacent waters. Given the variability of this area, delivery of this "younger" water mass via an along shore current such as the Antarctic Peninsula Coastal Current, or vertical upwelling is plausible. While the results presented here provide insight regarding mixing rates within isolated fjords, more quantitative studies need to be done to gain a true understanding of how nutrients derived from the terrestrial environment are circulated about the continental shelf.

Estimating cross-shelf mixing via ^{222}Rn proved to be more problematic. Figure 20 shows plots of the natural logarithm of ^{222}Rn activities measured along T-5 and T-4. Mixing models using terrestrially derived tracers were based on the assumption that there was a single source of tracers emanating from the continental margin and that lateral transport in other directions and vertical transport were negligible. In reality, Surface currents and circulation dynamics in this region are much more complex than the models used here to evaluate them. ADCP data collected

as part of this study (Figure 9) and composite data presented by Savidge and Amft (2012; Figure 3) show that circulation patterns can be complicated, and vary over different timescales. The predominant trends shown in Figure 9 differ from instantaneous measurements along the 2014 cruise track. However, unlike the shelf, the fjords provide an area where the assumptions essential for this type of unidirectional circulation model are more plausible. Because the offshore areas are more exposed to longshore currents and vertical transport, mixing rates are likely much higher than what is estimated above for the glacial fjords.

5.5 Seasonal variability - Nutrient Transport and Shelf Productivity

The December 2012 survey was conducted at the beginning of the austral summer. Surface waters ranged in salinity from 32.6 – 34.8 with an average of 33.7. Ra values in surface waters averaged 1.5 dpm/m^3. During the months of November and December from 1995-2013, atmospheric temperatures ranged from -1.4 – 2.3°C and averaged 0.0.4°C (Palmer Station Antarctica LTER, 2014). The average atmospheric temperature for November and December 2012 was -0.1 °C (Figure 20). The 2014 cruise took place during the latter part of February, as the summer season was coming to an end. Surface waters ranged in salinity from 31.2 – 33.6 and averaged 32.9. Ra values for surface waters in 2014 averaged 3.03 dpm m^{-3}. Atmospheric temperatures for the months of January and February from 1995-2012 ranged from 1.0 – 3.5° C and averaged 2.2° C (Figure 21). January and February 2014 atmospheric temperatures at Palmer Station averaged 0.9° C (Figure 20). As the season progresses, above freezing air temperatures are more common, and there are fewer hours of darkness. The increased temperatures and exposure to sunlight enhance glacial melting, progressively releasing vast quantities of meltwater into the surface ocean.

Depending on the characteristics of the aquifer material and the residence time of water within the aquifer, water entering the nearshore environment via SGD has the potential to be enriched in nutrients that are critical for primary production (Moore, 1996; Charette and Buesseler, 2004; Charette and Sholkovitz, 2005; Viso et al., 2010). In many environments, Fe is enriched in groundwater relative to seawater. A recent study conducted in Greenland, interactions between meltwater from the ice-sheet and basal bedrock led to an estimated discharge of as much as 2.7 Tg yr^{-1} of bioavailable Fe along the margins and offshore of the Greenland Ice Sheet (Bhatia et al., 2013). Similar results were observed in the nearshore environment adjacent to the Patos Lagoon, Brazil where an estimate of $3.2x10^5$ mol day^{-1} of Fe was transported across the continental shelf (Windom et al., 2006). Iron fluxes of at least the same magnitude are expected along the WAP near Anvers Island. Using Fe concentrations reported by Dulaiova et al. (2009), between $8.1x10^3$ and $9.7x10^4$ mol day^{-1} Fe was transported away from the shore in the fjords, helping to fuel primary productivity.

An ongoing study along the WAP (Null et al., in prep) found that porewaters and streams flowing into Arthur Harbor (adjacent to Palmer Station) were enriched in Fe, Rn, and Ra relative to surface seawater. Given that meltwater interacts with sediments composed of ~4% Fe, it is likely that sediments entrained in meltwater inputs supply Fe to surface waters along the WAP. The highest fluorescence values reported in this study were measured in the Gandidier Channel seaward of Barilari Bay. These waters were enriched in ^{222}Rn, ^{223}Ra, and ^{224}Ra relative to surface waters offshore where primary productivity was lower. These surface waters were clearly fresher, colder, and depleted in ^{18}O and D relative to adjacent surface waters (Figure 15), suggesting that glacial melt comprises a higher percentage of surface waters in the Grandidier Channel near Barilari Bay. Given that phytoplankton blooms are commonly limited by Fe

availability along the WAP (Klink et al., 2004; Martinson et al., 2008; Martinson, 2012; Takahashi et al., 2012), it is hypothesized that glacial melt is fueling primary productivity by supplying Fe to the surface ocean.

Several authors (Bugna et al., 1996; Moore, 1996; Dierrsen et al., 2002; Windom et al., 2006; Viso et al., 2010) have studied the link between the terrestrial environment and primary productivity in the surface ocean with respect to bio-limiting nutrients. The WAP is unique in that it has a vast reservoir of frozen water covering the majority of the land surface that partially melts during summer months. This study suggests that primary productivity along the WAP could be linked to bio-limiting nutrients provided by these seasonal meltwater inputs. Mixing rates in the surface waters observed in nearby Beascochea Bay and within Flandres Bay are slow relative to those calculated along the northern tip of the WAP (Dulaiova et al., 2008), and within the range of those calculated in Marguerite Bay (Annett et al., 2012). In the calmer protected areas where these rates were calculated, the Fe supplied by the Antarctic continent could be consumed by phytoplankton before mixing with waters across the shelf.

In this study, higher surface fluorescence values were observed close to the shoreline where the tracers used in this study suggest that glacial melt inputs are present. Farther offshore, surface fluorescence values were lower. Given this spatial distribution, it is possible that the extent and location of phytoplankton blooms are controlled by the location, intensity, and mixing of meltwater inputs along the coast. Circulation dynamics, especially those that control the distribution of meltwater, are impacted by changes in surface water temperature and salinity. As atmospheric temperatures along the WAP rise, the volume of meltwater that enters the surface ocean will increase. This change in meltwater dynamics with respect to the duration of warmer

atmospheric temperatures is observed in this study over the changing seasons, although the same concepts could be applied over longer time scales.

6. Conclusions

Terrestrially derived water masses introduce and transport bio-limiting nutrients along and across the shelf of the WAP. As atmospheric temperatures along the WAP rise, the increasing frequency and intensity of meltwater pulses along the WAP has the potential to have a profound impact on global carbon and climate cycles. Terrestrial water can be identified via natural tracer concentrations ($^{223,\ 224}$Ra, ^{222}Rn, δ^{18}O, δD). Porewater and glacial meltwaters were enriched in Ra and Rn relative to seawater, and depleted in ^{18}O and D. Nearshore meltwaters had a similar geochemical signature, proving the use of these isotopes as valuable meltwater tracers.

These tracers should vary in concentration as a function of meltwater delivery to coastal waters. Given the difference in season between the two cruises (2012 – early austral summer; 2014 – late austral summer), the higher activities in Ra and Rn observed nearshore in 2014 are likely attributed to an increase in meltwater. This increased freshwater delivery was also seen in the salinity and water isotopes nearshore compared to the offshore values in 2014.

Calculated horizontal mixing rates of water masses within glacial fjords along the WAP ranged from 570 to 6820 m^2s^{-1}. Radium ages along an open ocean transect offshore of Anvers Island are estimated between 15 – 25 days. Mixing rates estimated here were within the range of other rates calculated along the WAP and suggest a rapid transport mechanism for moving freshwater further offshore. Using Fe concentrations reported by Dulaiova et al. (2009), between $8.1x10^3$ and $9.7x10^4$ mol day^{-1} Fe was transported away from the shore in the fjords, helping to fuel primary productivity.

Based on data collected offshore of Anvers Island during the 2012-2013 and 2013-2014 austral summers, the flux of bio-limiting nutrients from the Antarctic continent across the continental shelf was evaluated. More work is needed to further evaluate the Fe flux and Fe

budget in surface waters along the WAP to gain a true understanding of how continental inputs play a role in this globally important ecologic system. Findings presented here suggest the Antarctic continent provides a significant source of Fe to the continental shelf, possibly driving primary productivity along the shelf.

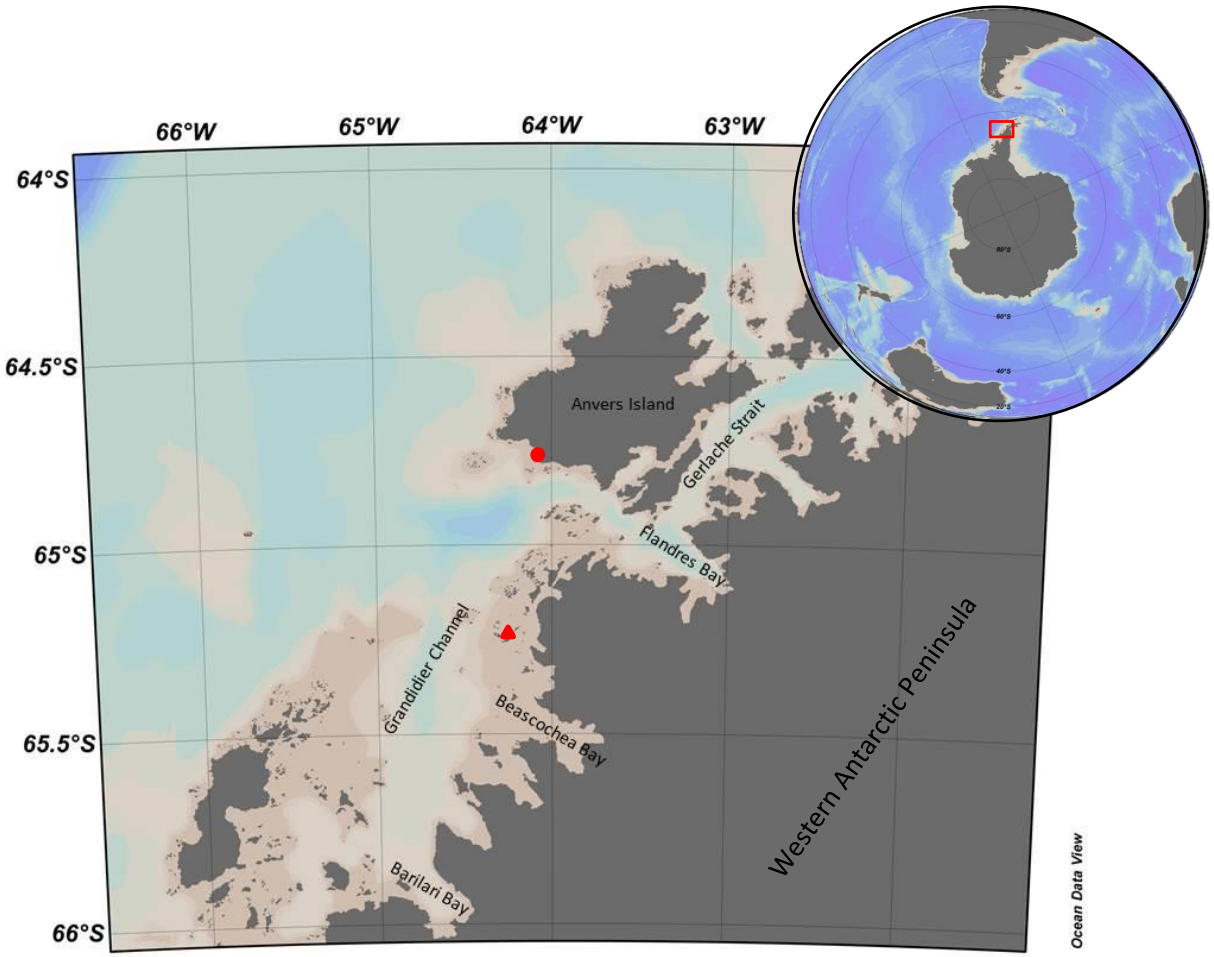

Figure 1: Map of study area. Red circle denotes the approximate location of Palmer Station. Red triangle denotes the approximate location of Vernadsky Station.

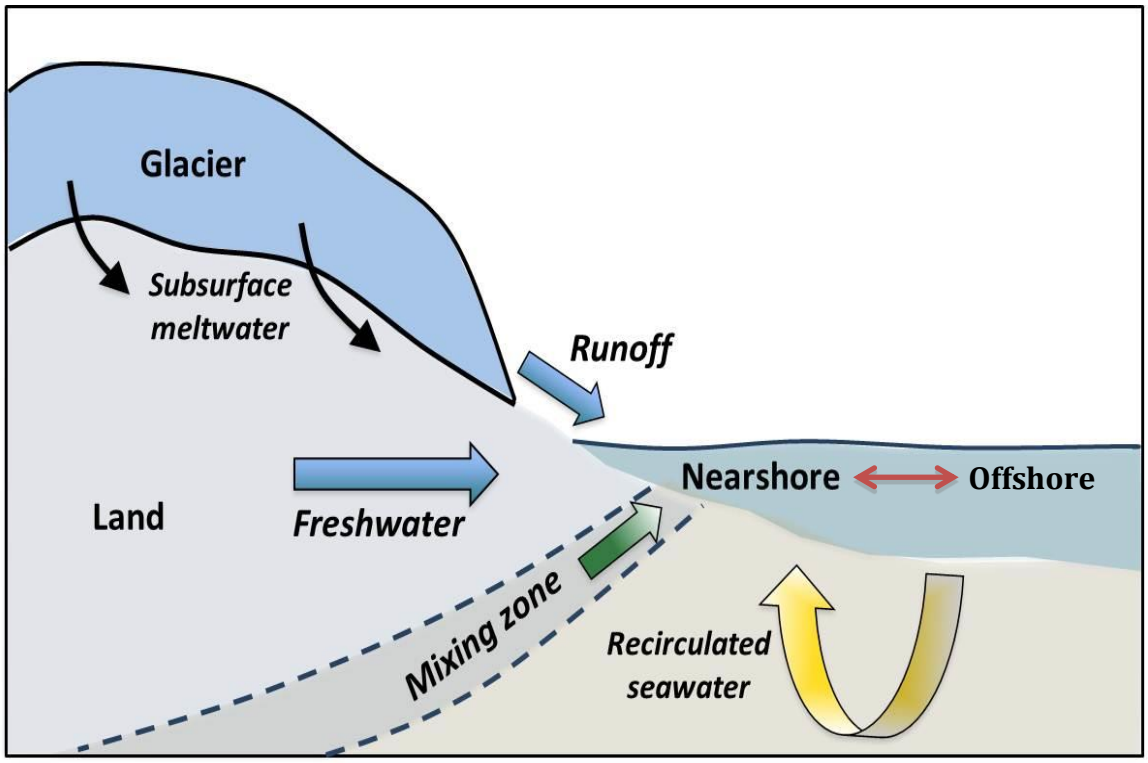

Figure 2: Schematic diagram of submarine groundwater discharge in glacial environments (Modified with permission from Kimberly Null)

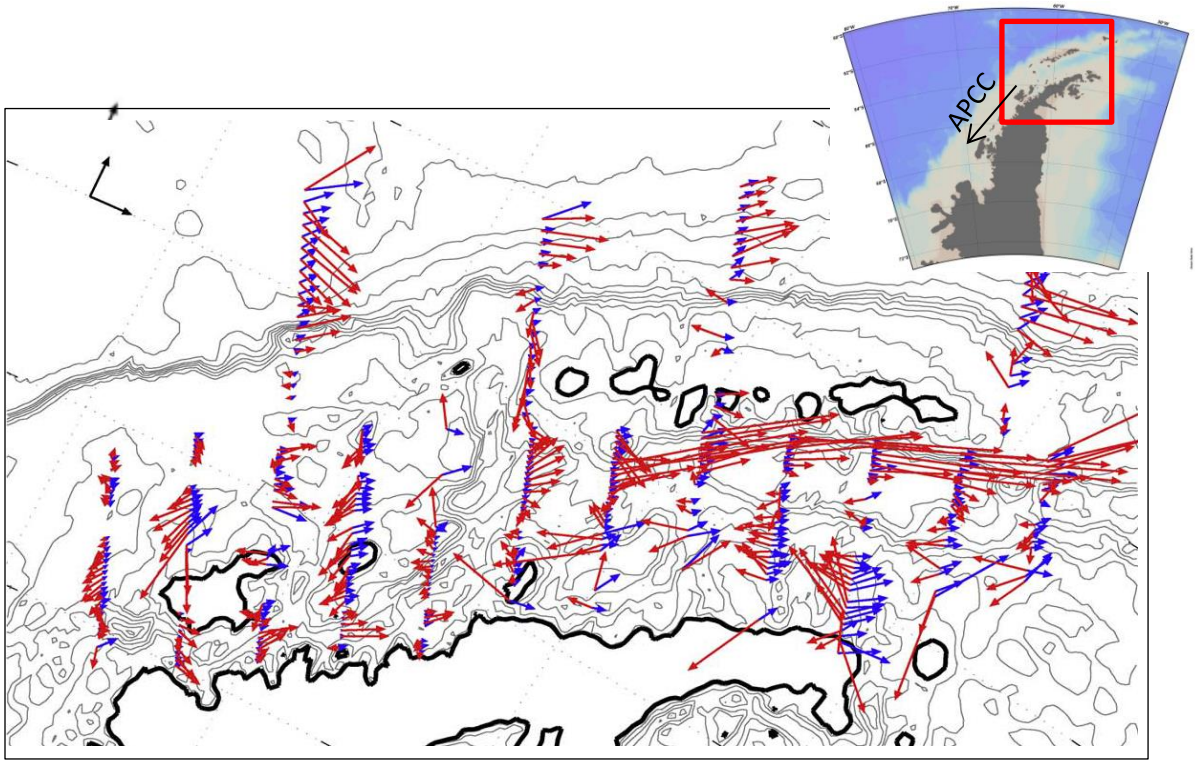

Figure 3: Surface currents(modified from Savidge and Amft 2009). Red arrows are average current velocities between 40m and 200m depth measured aboard the *R/V Nathaniel Palmer* and *R/V Laurence M. Gould* from 1999-2005. Blue arrows show error associated with measurements. Length of north arrow displays the vector length for a 0.1m/s current velocity. Green circle denotes the approximate position of Palmer Station on Anvers Island.

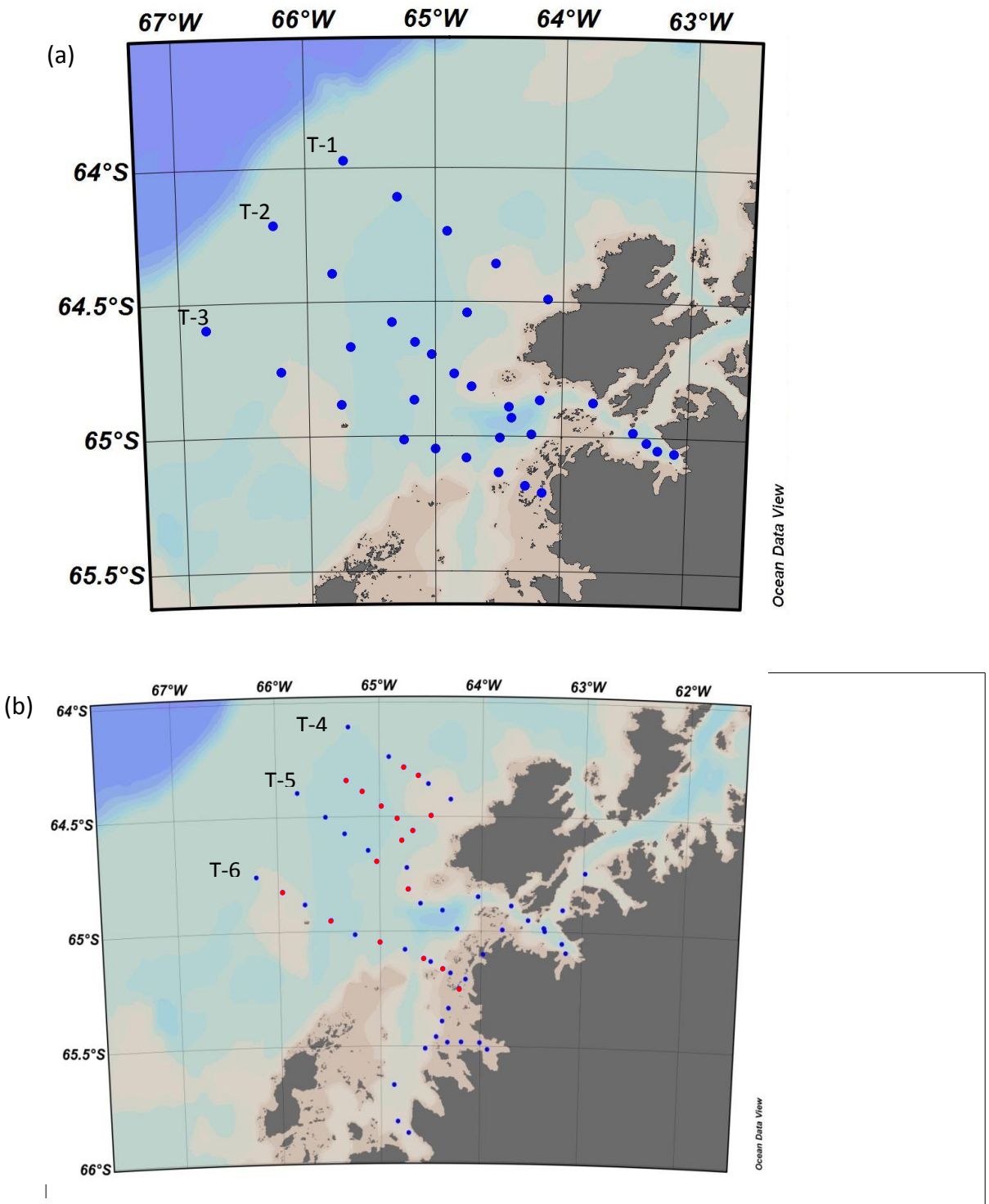

Figure 4: Sample collection sites along the 2012 (a.) and 2014 (b.) cruises offshore of the Western Antarctic Peninsula. Samples collected by the ships intake are marked by red dots. These samples were determined to be unreliable and were not included in any tracer analyses. Blue dots represent stations where samples were collected with the ship's rosette.

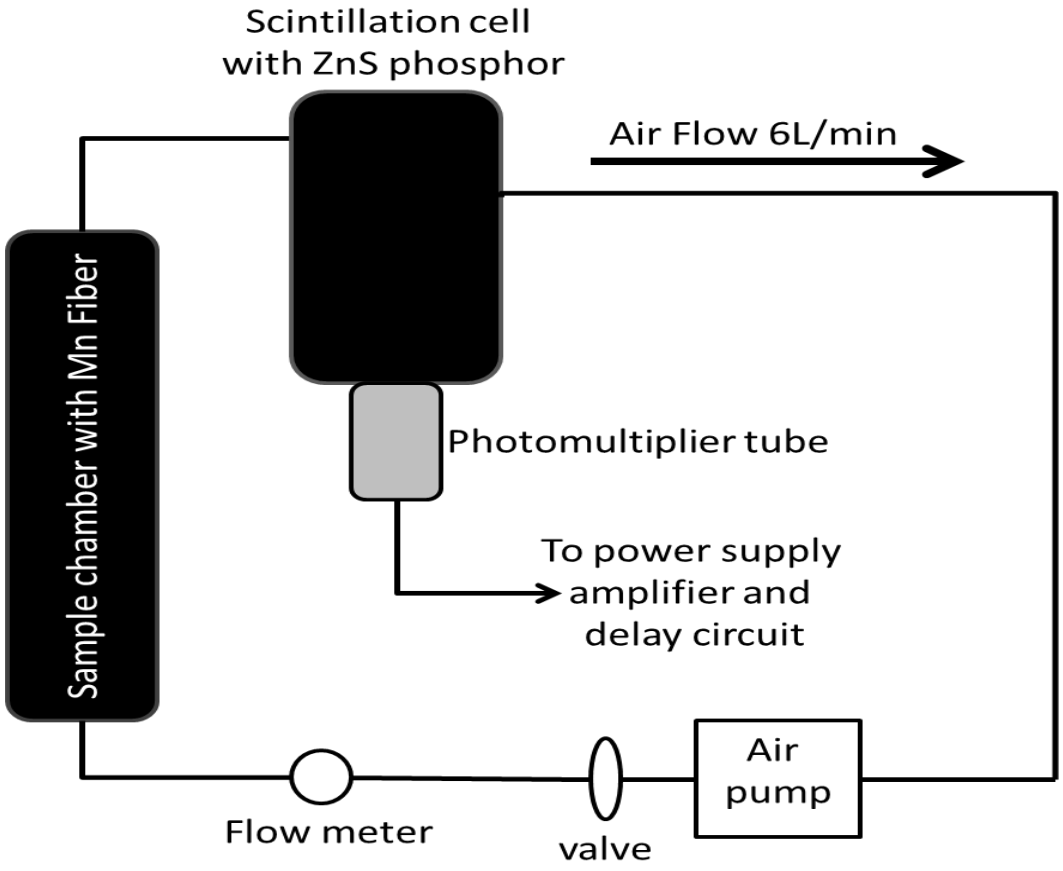

Figure 5: Schematic diagram of the Radium Delayed Coincidence Counting (RaDeCC) system (Reproduced from Moore and Arnold, 1996).

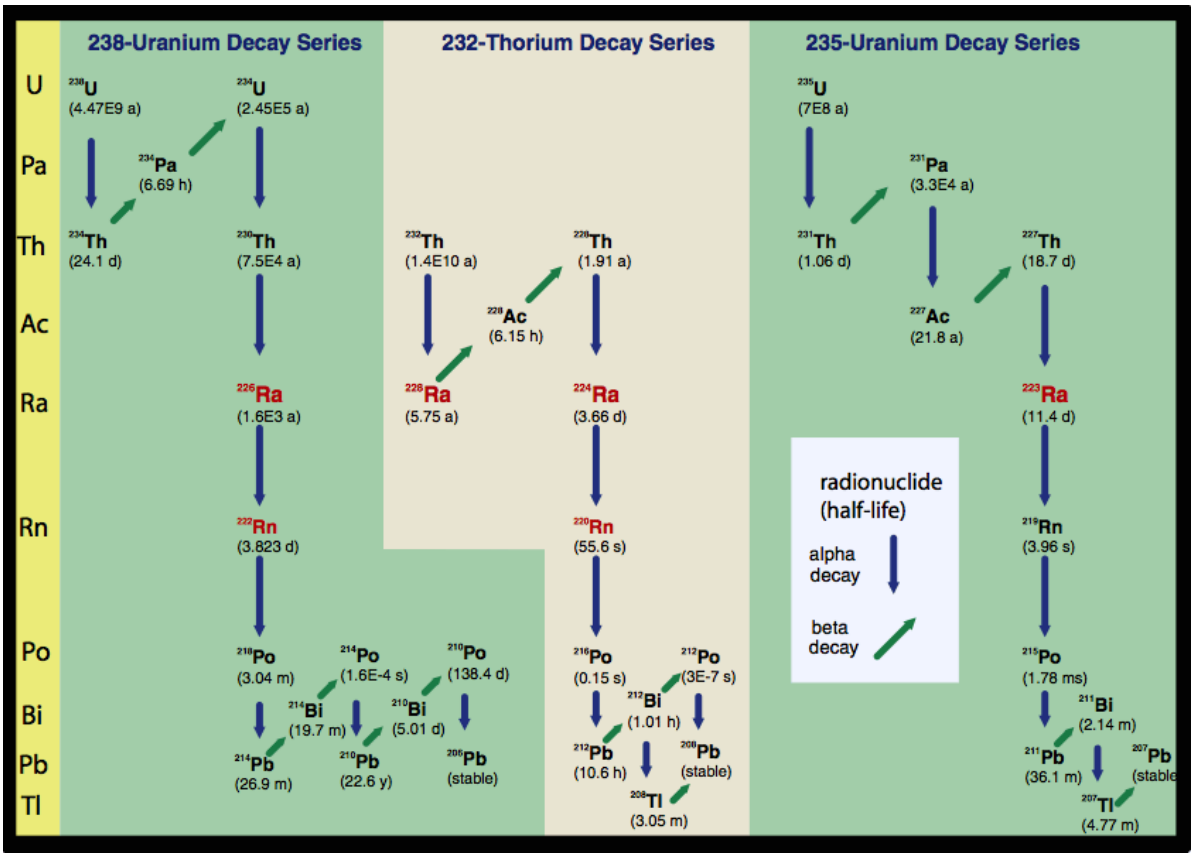

Figure 6. ^{238}U, ^{232}Th, and ^{235}U decay chains (usgs.gov).

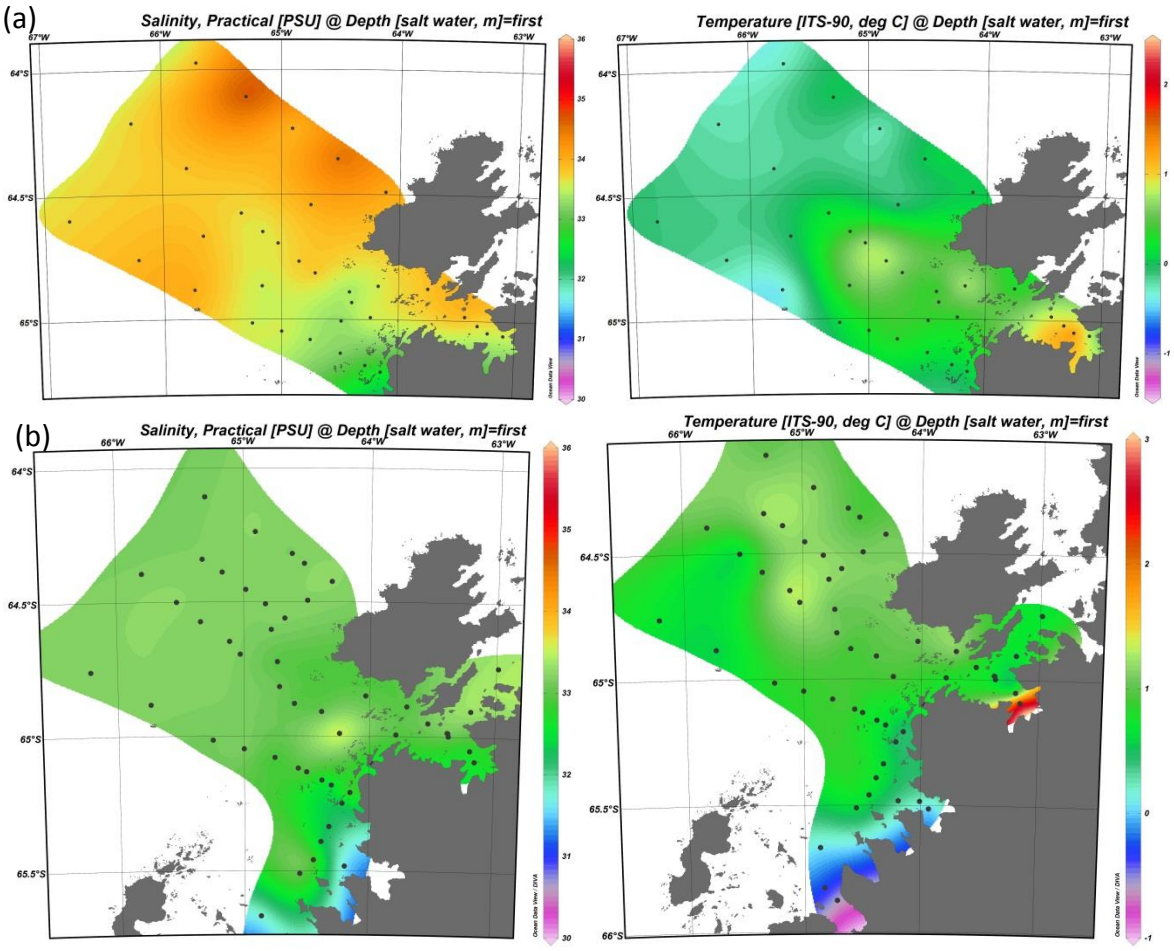

Figure 7. Surface salinity and temperature along the 2012 (a) and 2014 (b) cruises.

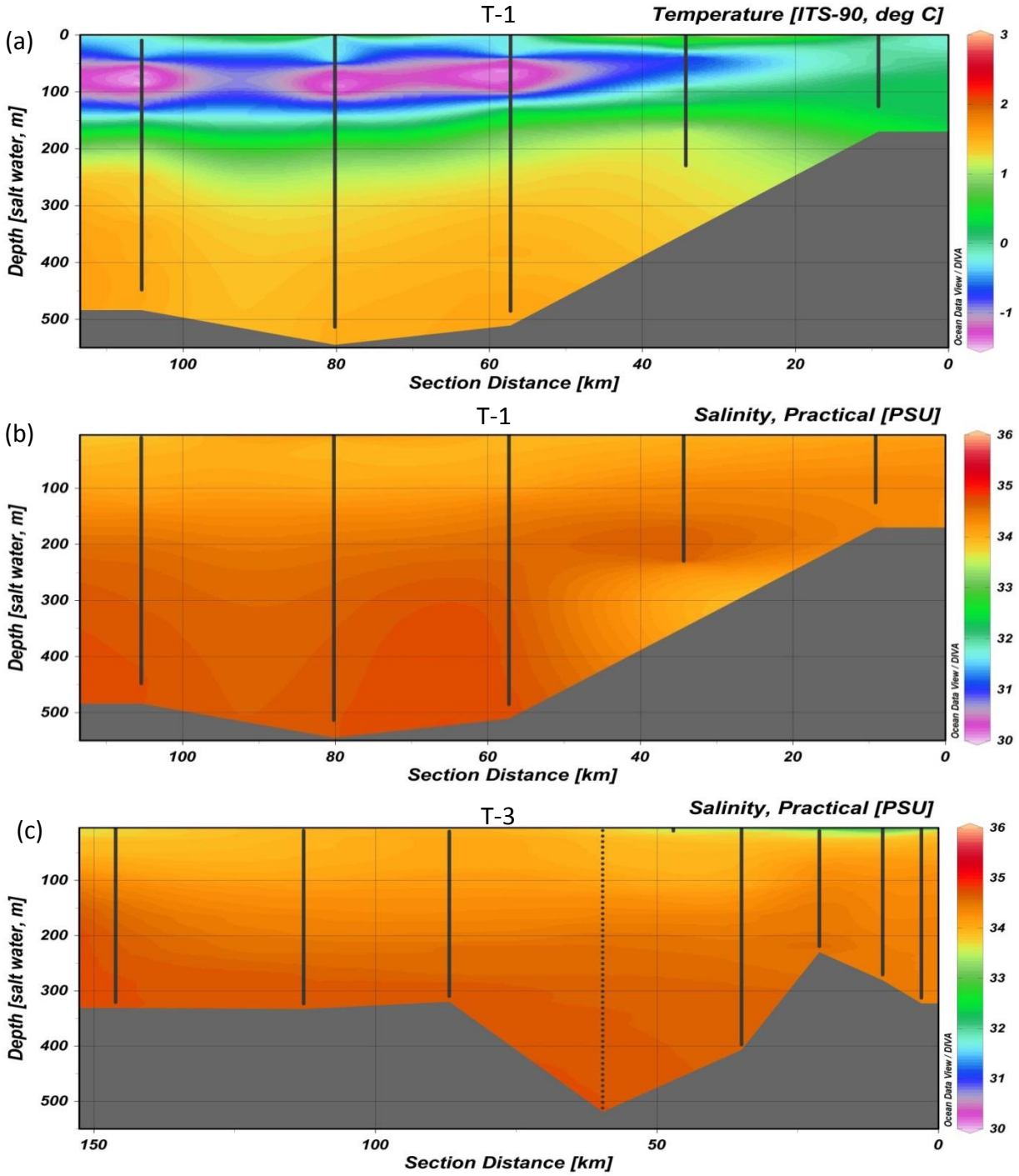

Figure 8: Cross sections of physical parameters from the 2012 cruise T-1 (a,b) and T-3(c).

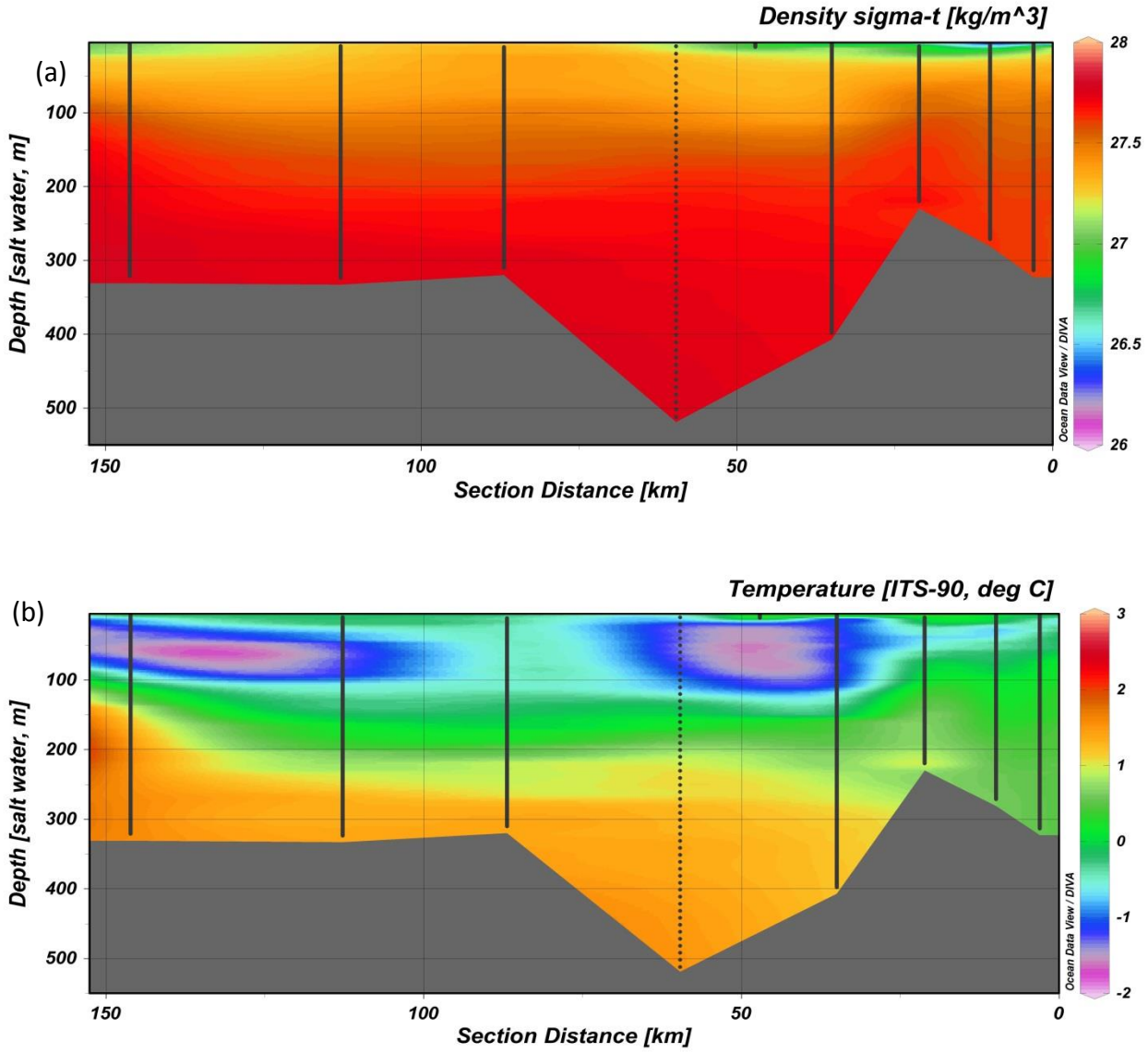

Figure 9: Cross sections of density (a) and temperature (b) along T-3.

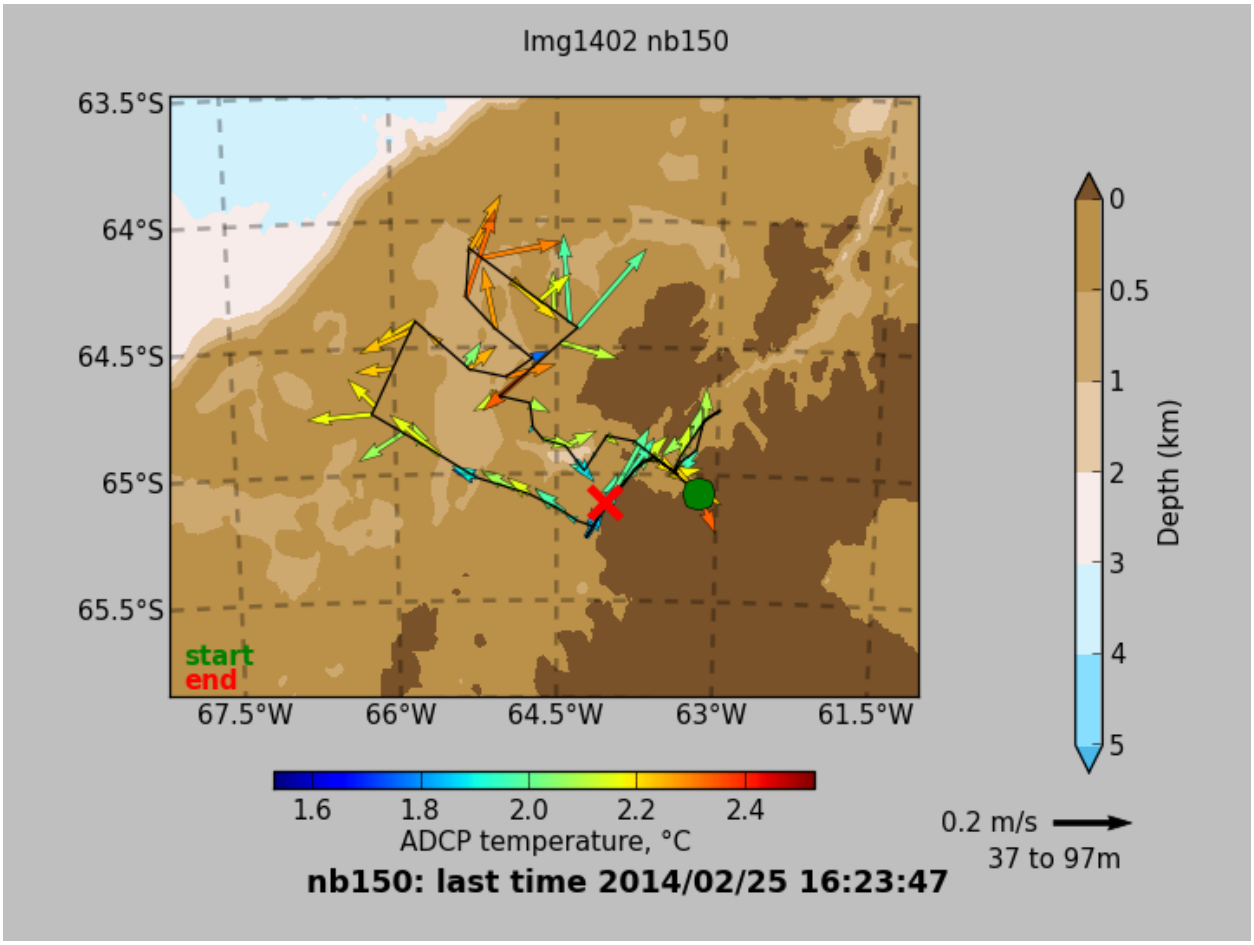

Figure 10: Shipboard ADCP measurements from 2014 cruise.

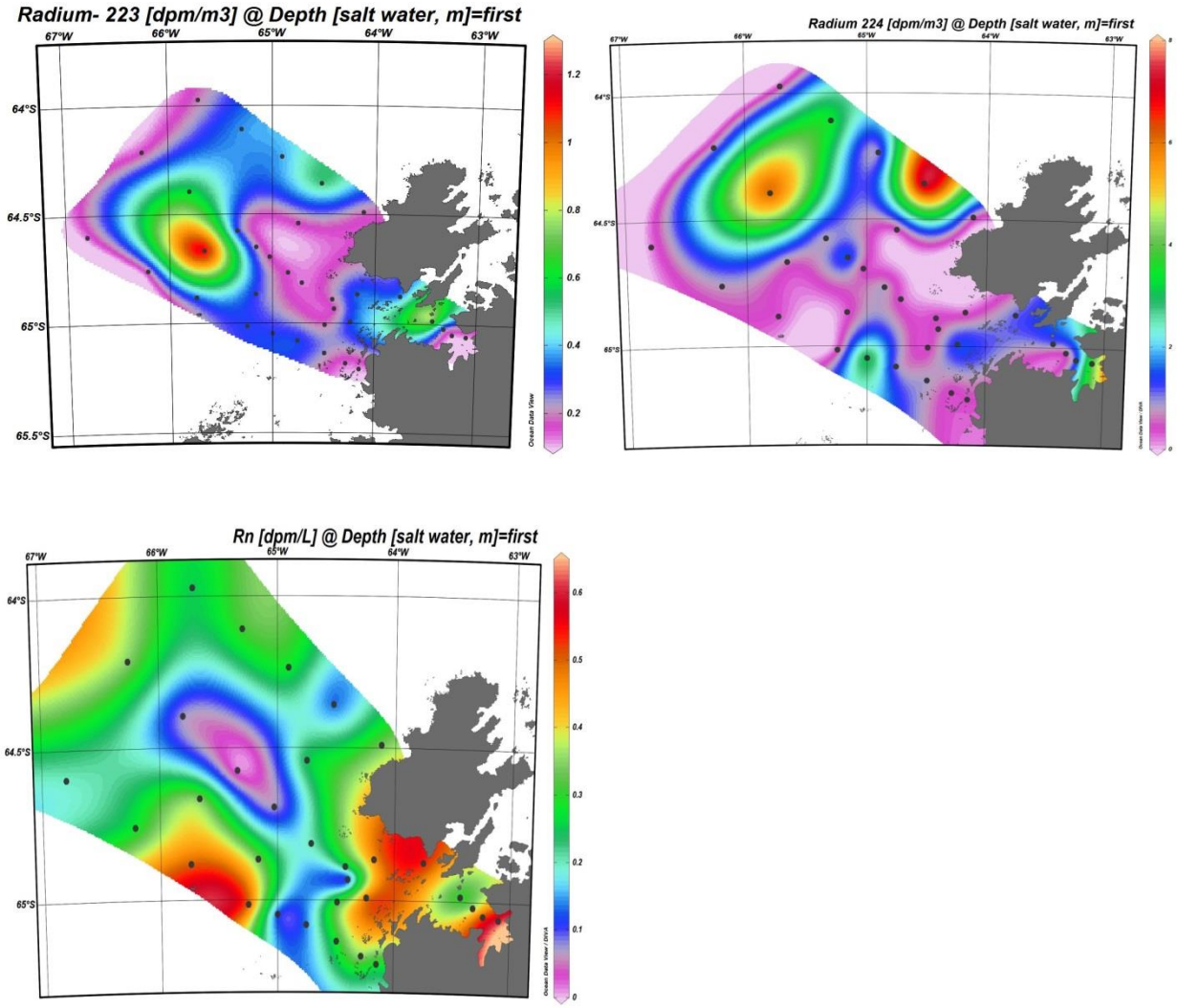

Figure 11. Surface water ^{223,224}Ra and ^{222}Rn activities along the 2012 cruise track.

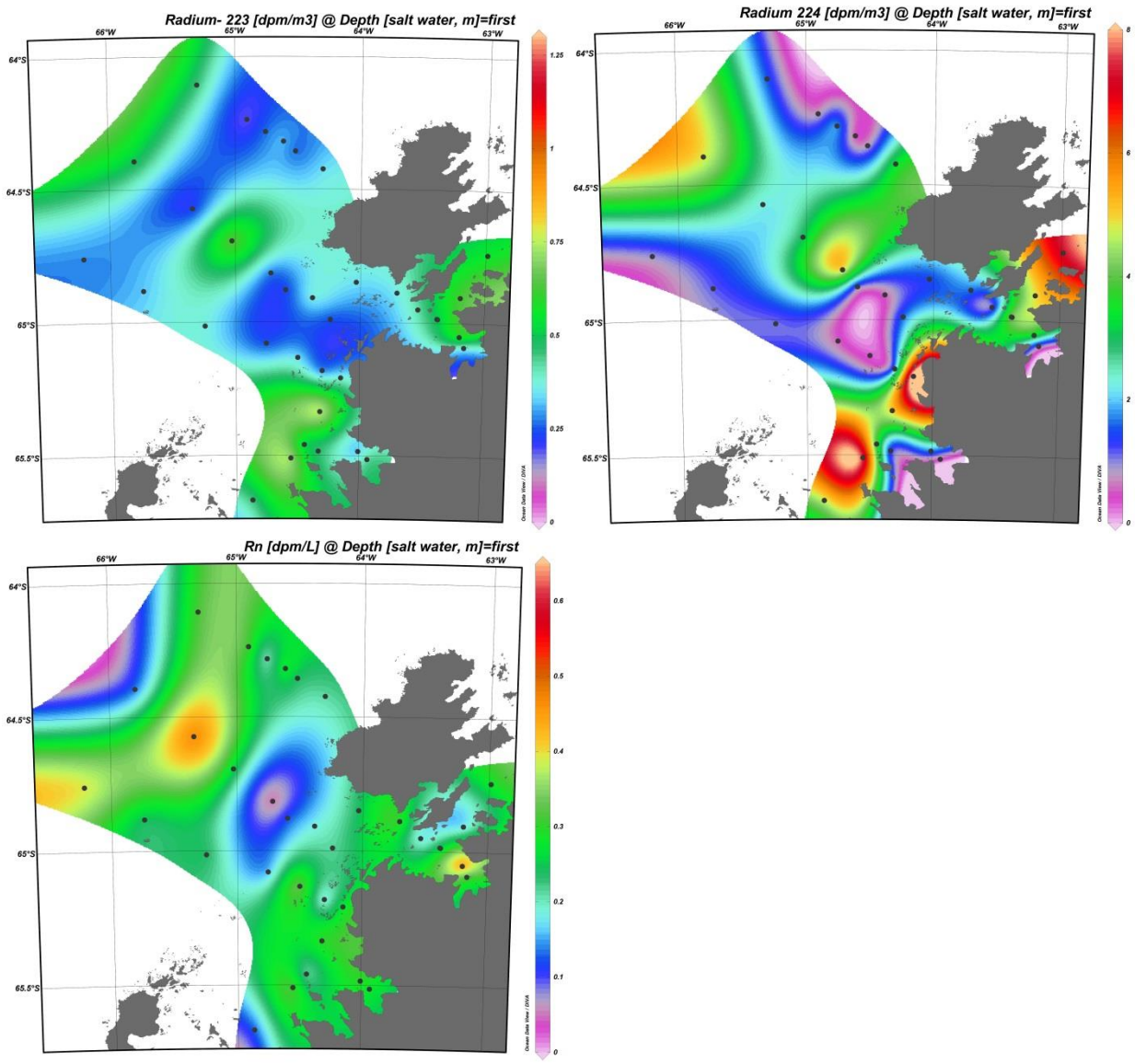

Figure 12. Surface water ^{223,224}Ra and ^{222}Rn activities along the 2014 cruise track.

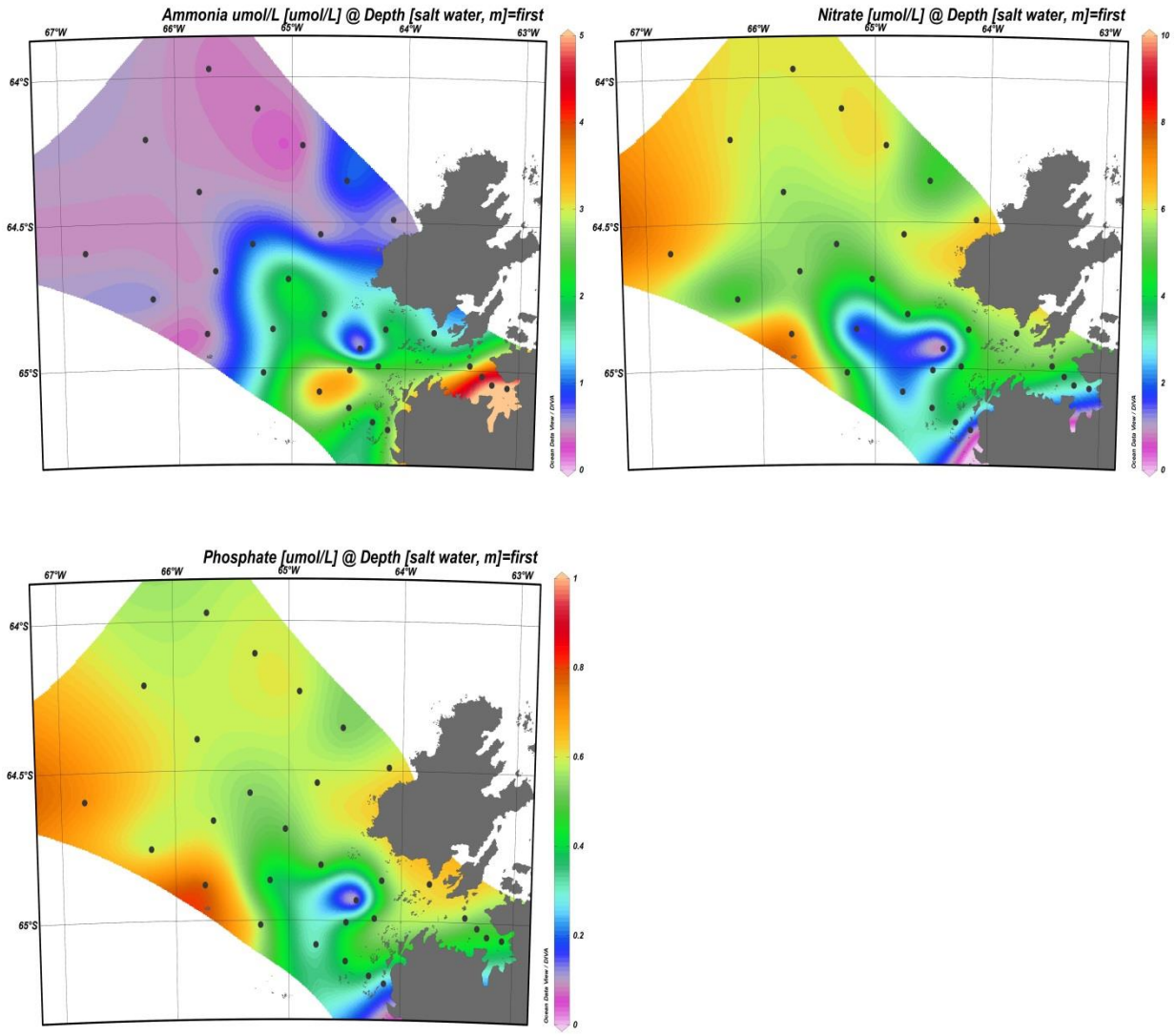

Figure 13: Nutrient concentrations in surface waters along the 2012 cruise track.

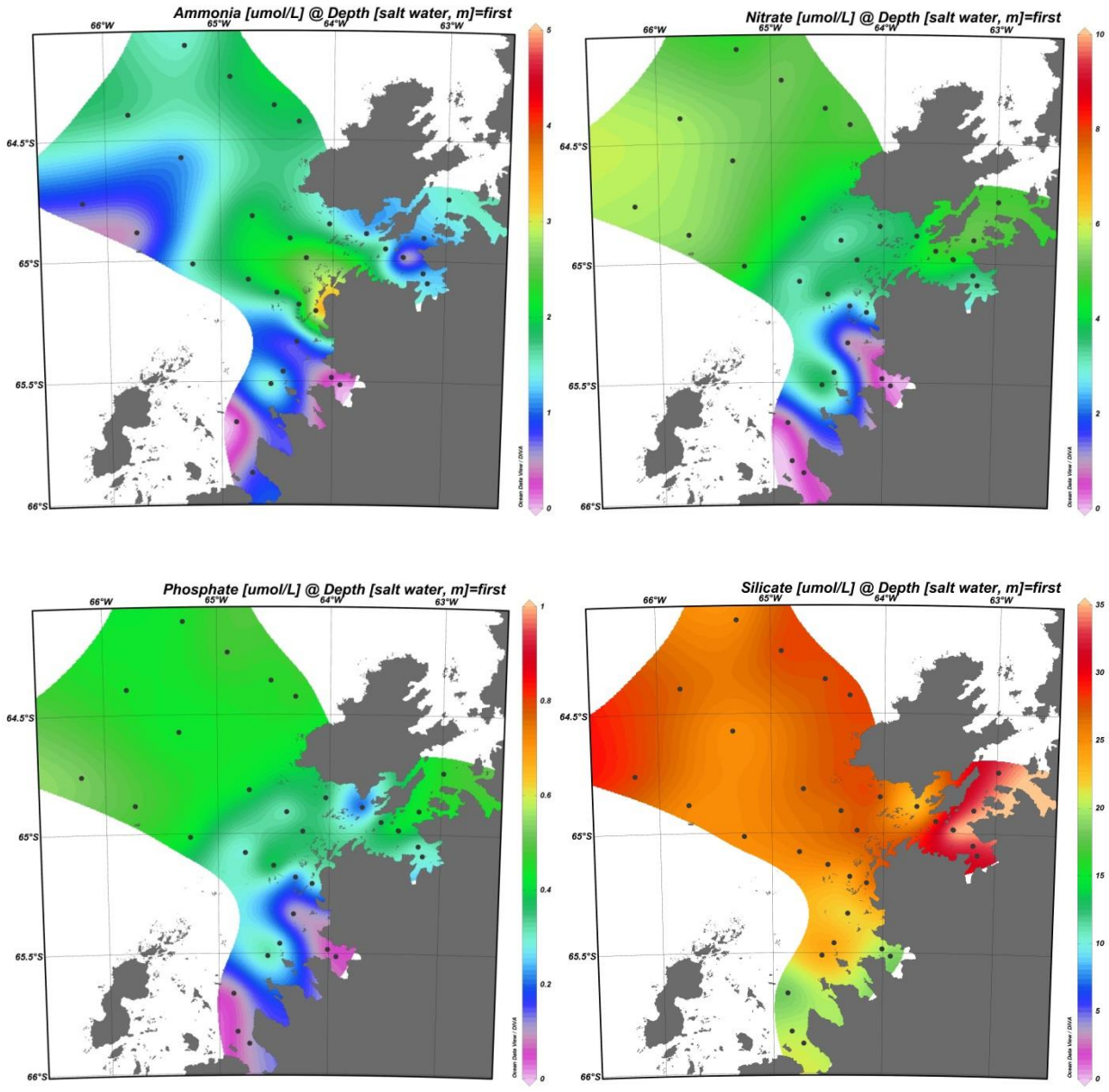

Figure 14. Surface water nutrient concentrations along the 2014 cruise track.

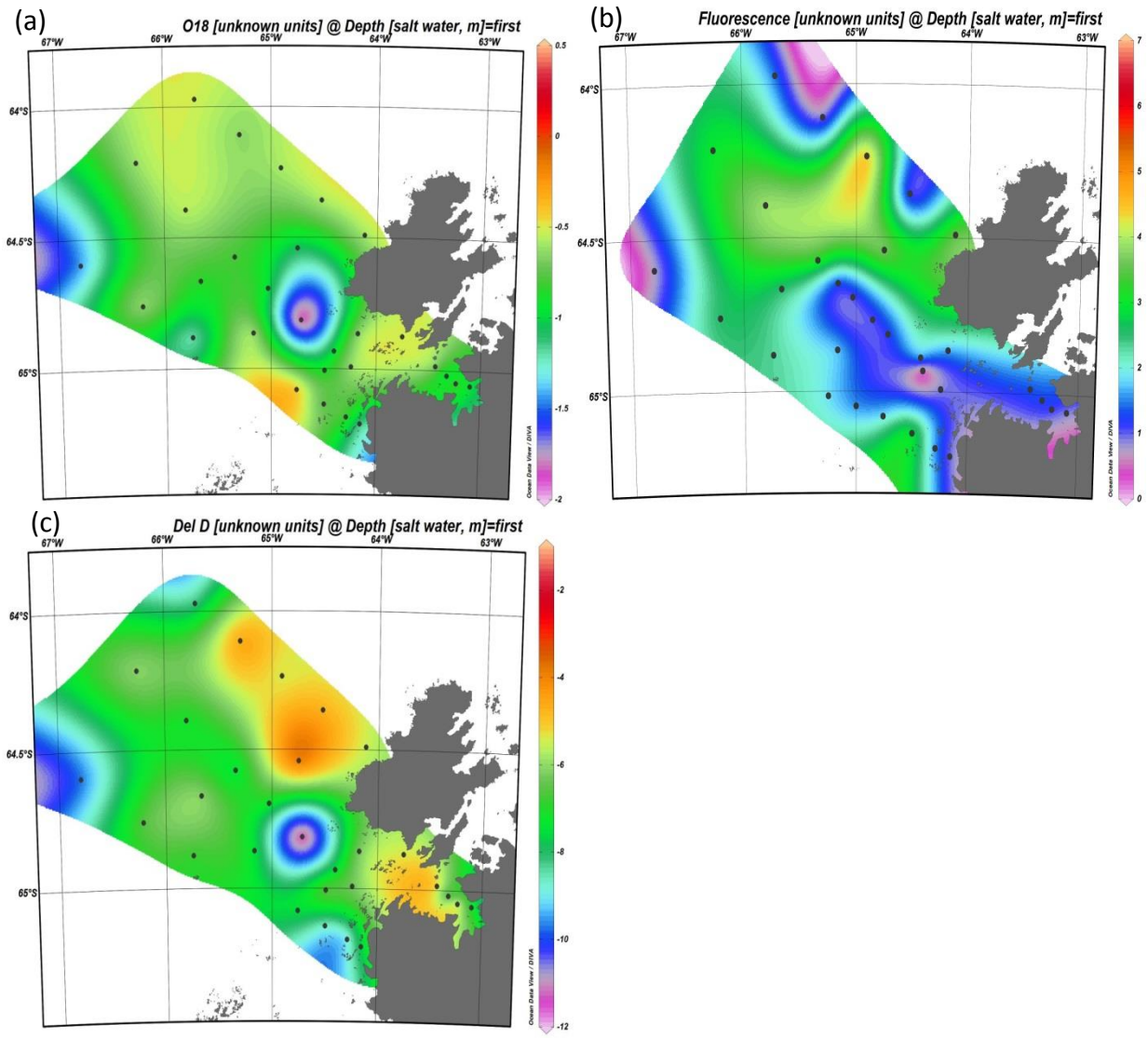

Figure 15. Surface water $\delta^{18}O$ (a), Fluorescence (b), and δD (c) along the 2012 cruise track.

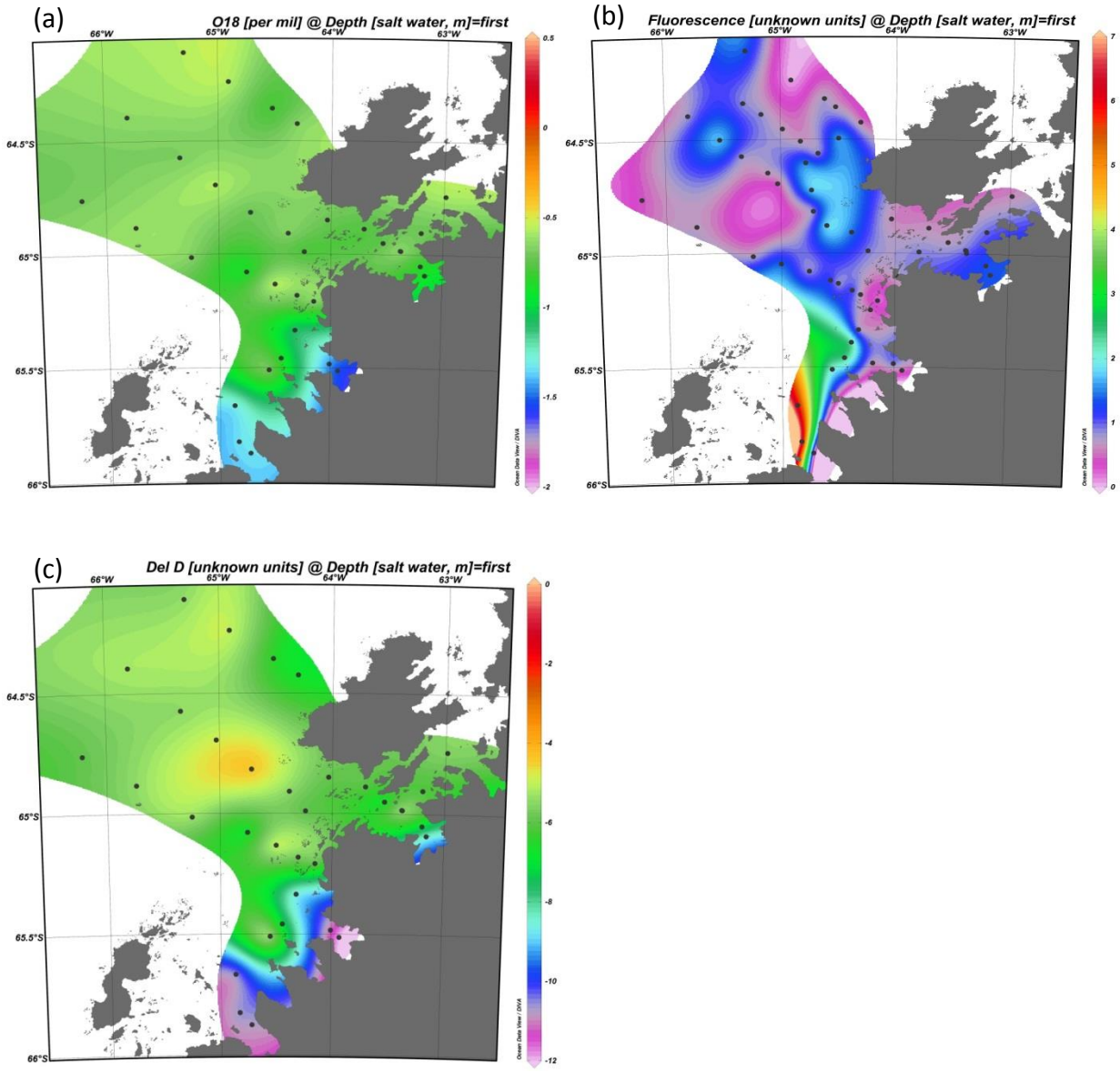

Figure 16. Surface water $\delta^{18}O$ (a), Fluorescence (b), and δD (c) along the 2014 cruise track.

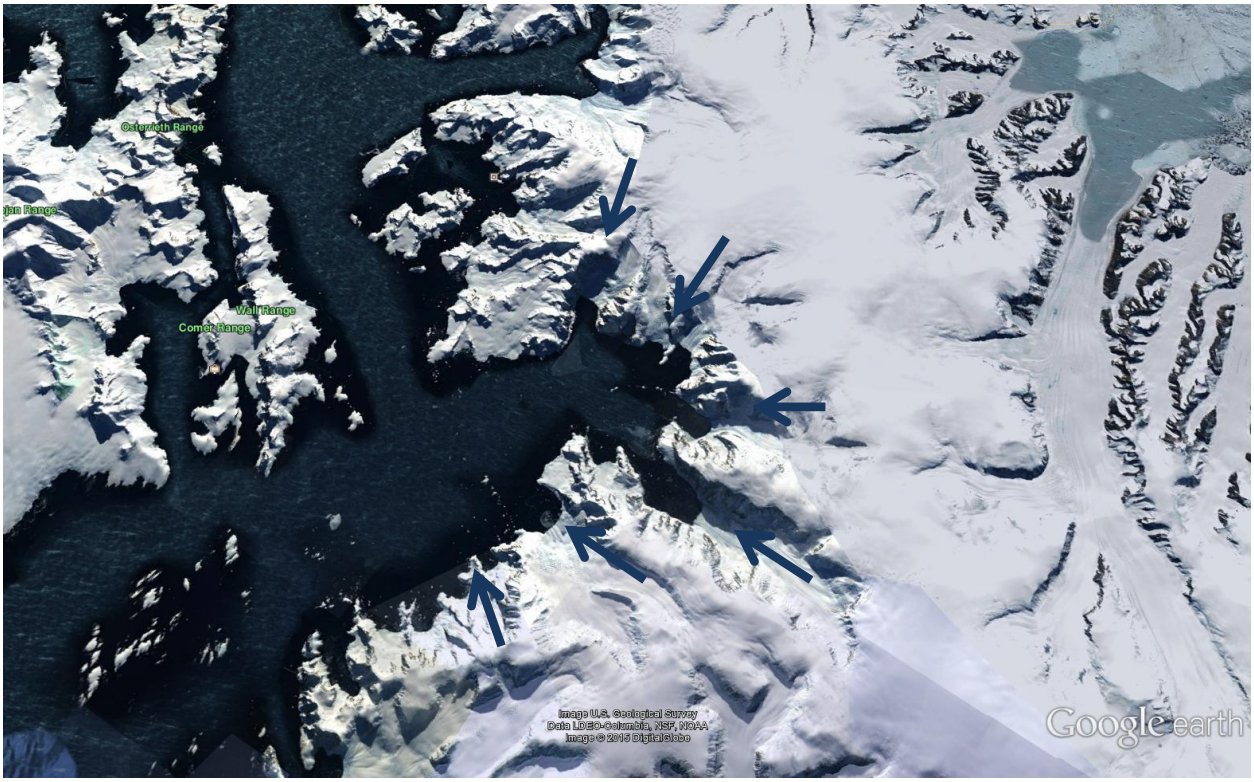

Figure 17: Aerial photograph of Flandres Bay. Arrows show potential flow paths of freshwater inputs along the fjord. (Google earth)

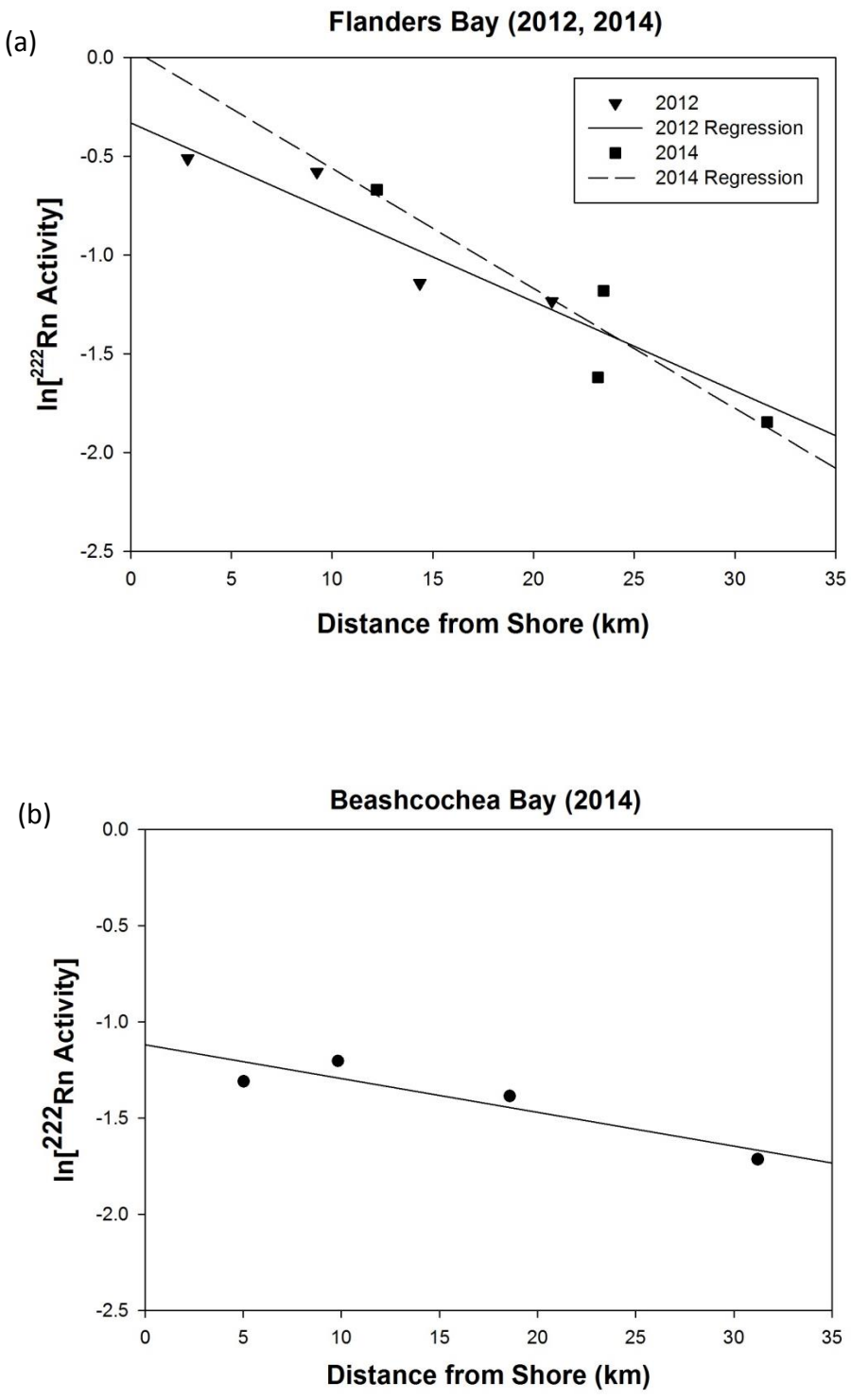

Figure 18: Plots of Ln ^{222}Rn with distance from the shoreline in (a) Flandres Bay and (b) Beascochea Bay to calculate horizontal mixing rates.

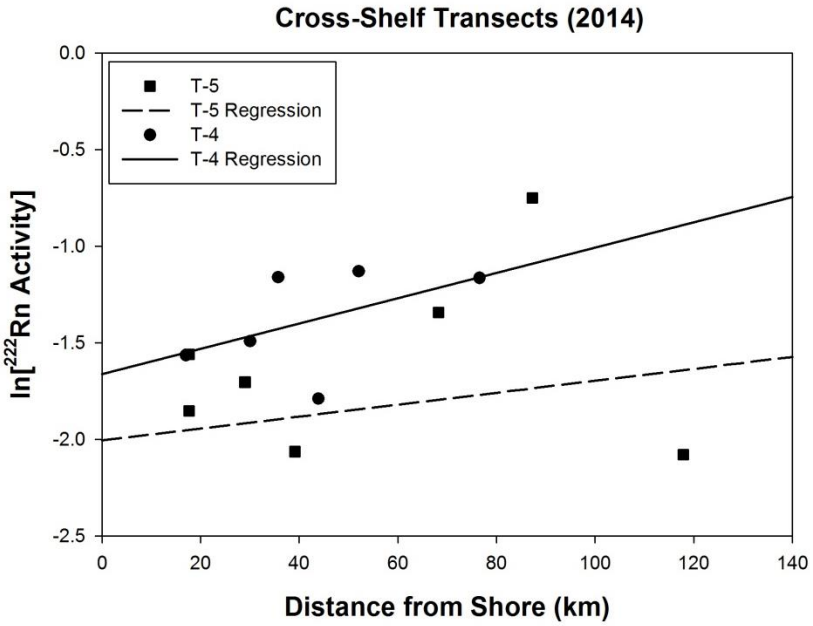

Figure 19: Ln ^{222}Rn with distance from the shore along T-4 and T-5 as a means of calculating horizontal mixing rates. Note the positive slope suggests sources of tracers beyond the coast.

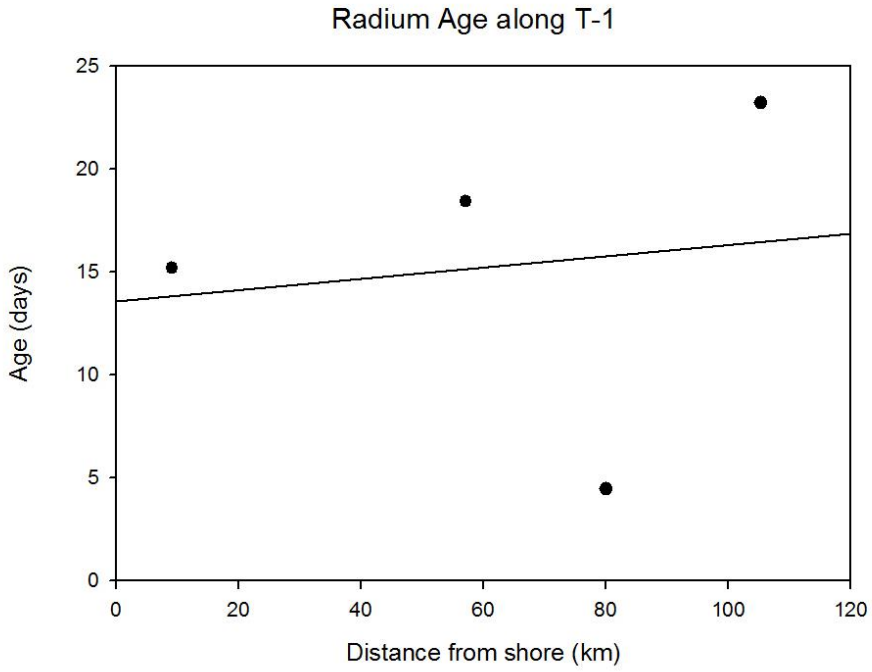

Figure 20: Radium age with distance from the shoreline along T-1.

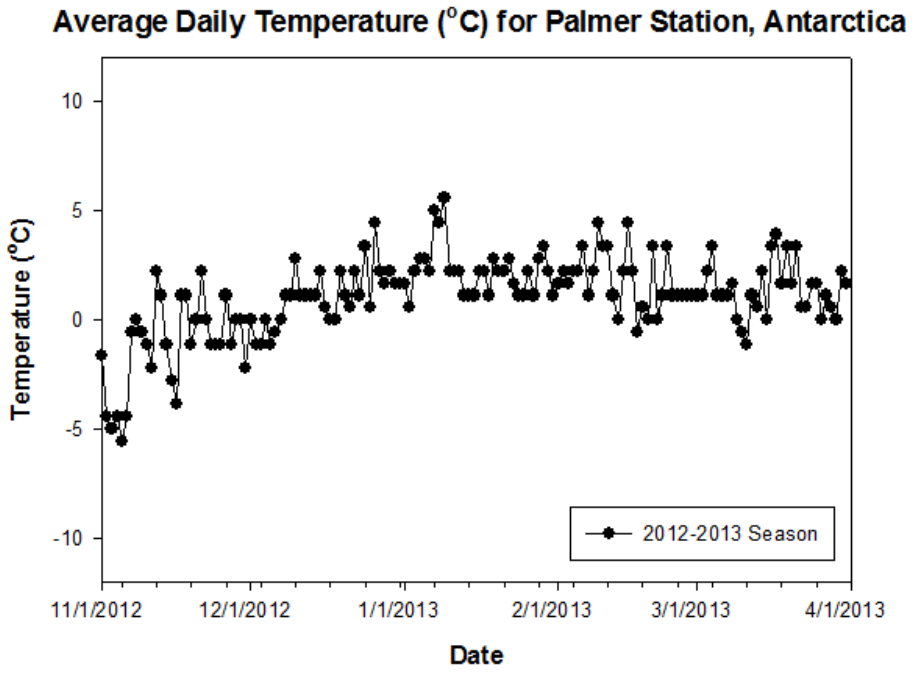

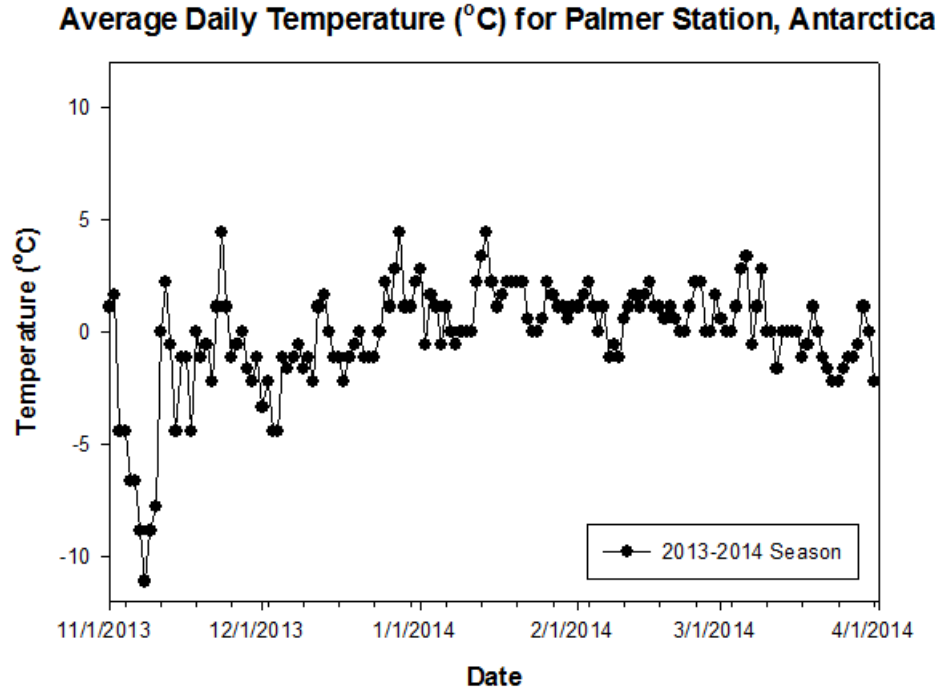

Figure 21. Average temperatures at Palmer Station during both field seasons.

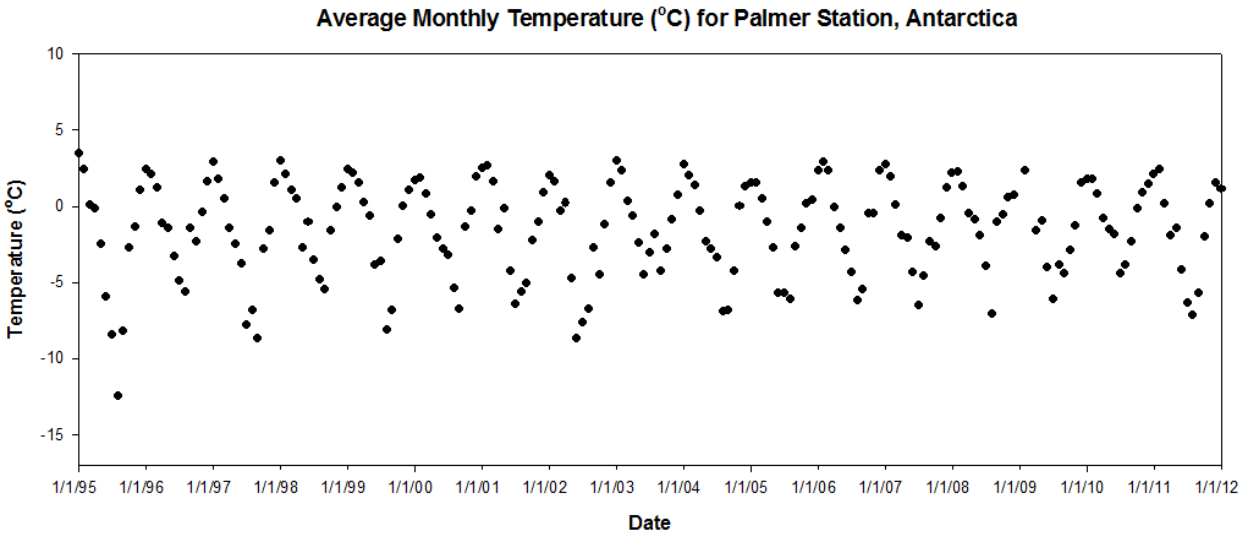

Figure 22. Average monthly temperatures at Palmer Station from 1995-2012 (LTER, 2014).

Table 1. Radium activities along the WAP and in other coastal environments

Study	Environment	Range - ^{224}Ra (dpm/m^3)	Range - ^{223}Ra (dpm/m^3)
This Study	Antarctic	bdl – 16.1	bdl – 1.7
Annett et al., 2012	Marguerite Bay	0.06 – 14.6	bdl – 0.6
Dulaiova et al., 2008	South Shetland Islands	0 - 17	
Moore, 2000	Temperate environments	0-11.7	0.01-0.3

Table 2. Comparison of nearshore and offshore parameters during both field seasons.

	2013		2014	
	Nearshore	**Offshore**	**Nearshore**	**Offshore**
Salinity	33.9±0.0	33.7±0.1	32.7±0.1	33.1±0.0
Temp (°C)	0.5±0.1	-0.1±0.1	0.7±0.2	0.9±0.0
δ^{18}O (‰)	-0.9±0.2	-0.8±0.1	-1.0±0.1	-0.7±0.0
δD (‰)	-6.1±1.2	-6.7±0.3	-8.1±0.6	-5.6±0.2
^{224}Ra(dpm/m^3)	1.7±1.0	1.2±0.4	3.6±0.7	2.1±0.5
^{223}Ra (dpm/m^3)	0.3±0.2	0.3±0.0	0.5±0.0	0.3±0.0
^{222}Rn (dpm/m^3)	0.4±0.1	0.3±0.0	0.3±0.0	0.2±0.0
N+N (uM)	3.6±0.6	5.0±0.3	2.5±0.4	4.3±0.3
NH_4 (uM)	4.3±0.6	1.2±0.2	0.9±0.1	1.8±0.2
HPO_4 (uM)	0.5±0.0	0.5±0.0	0.2±0.0	0.4±0.0

Table 3. Sea-Air Flux of ^{222}Rn along the WAP.

Site	Wind speed Knots (24hr average)	Air-Sea Flux dpm/m2/min	Min	Max
Beab 6	6.83	0.07	0.01	0.15
Beab 7	6.91	0.08	0.01	0.18
Flab 19	7.79	0.17	0.01	0.42
Flab 20	7.71	0.06	0.01	0.13
Flab 21	8.80	0.06	0.02	0.11
Flab 22	15.55	0.29	0.05	0.66
Flab 23	13.52	0.18	0.03	0.4
grand 33	7.74	0.06	0.01	0.12
T4-30	22.00	0.38	0.21	0.57
T4-31	22.12	0.55	0.31	0.85
T4-32	22.31	0.53	0.3	0.64
T5-10	16.87	0.32	0.09	0.59
T6-11	17.97	0.18	0.07	0.32
T6-12	17.94	0.43	0.17	0.73
T5-13	17.43	0.16	0.07	0.29
T5-14	17.22	0.27	0.11	0.49
T5-15	17.68	0.28	0.11	0.48
T5-16	19.12	0.53	0.22	0.93
T6-24	15.50	0.16	0.03	0.37
T6-25	15.37	0.03	0	0.06

Table 4. Average end member values for surface seawater and possible terrestrial inputs

Source	223-Ra (dpm/m^3)	224-Ra (dpm/m^3)	$\delta^{18}O$	δD
Porewaters	1.8	58.4	-11.87	-93.04
Glacial Ice	1.6	21.4	-10.96	-85.11
Stream	7.9	38.1	-10.7	-83.22
Surface seawater	0.4	2.8	-0.7	-6.89
Bottom Waters	9.8	7.0	-0.5	-4.11

References

Annett, A., Henley, S., van Beek, P., Souhaut, M., Ganeshram, R., Venebles, H., Meredith, M., Geibert, W., 2012. Use of radium isotopes to estimate mixing rates and trace sediment inputs to surface waters in northern Marguerite Bay, Antarctic Peninsula. Antarctic Science 24.

Ardelan, M.V., Holm-Hansen, O.O., Hewes, C.D., Reiss, C.S., Silva, N.S., Dulaiova, H.H., Sakshaug, E.E., 2009. Natural iron enrichment around the Antarctic Peninsula in the Southern Ocean. Biogeosciences Discussions 6 (4), 7481-7515.

Bhatia, M., Kujawinski, E., Das, S., Breier, F., Henderson, P., Charette, M., 2013. Greenland meltwater as a significant and potentially bioavailable source of iron to the ocean. Nature Geoscience 6, 274-278.

Boyd, P., Watson, A., Law, C., Abraham, E., Trull, T., Murdoch, R., Bakker, D., Bowie, A., Buesseler, K., Chang, H., Charette, M., Croot, P., Downing, K., Frew, R., Gall, M., Hadfield, M., Hall, J., Harvey, M., Jameson, G., LaRoche, J., Liddicoat, M., Ling, R., Maldonado, M., McKay, R., Nodder, S., Pickmere, S., Pridmore, R., Rintoul, S., Safi, K., Sutton, P., Strzepek, R., Tanneberger, K., Turner, S., Waite, A., Zeldis, J., 2000. A mesoscale phytoplankton bloom in the polar Southern Ocean stimulated by iron fertilization. Nature 407, 695-702.

Bugna, G.C., Chanton, J.P., Cable, J.E., Burnett, W.C., Cable, P.H., 1996. The importance of groundwater discharge to the methane budgets of nearshore and continental shelf waters of the northeastern Gulf of Mexico. Geochim. Cosmochim. Acta 60, 4735-4746.

Burnett, W.C., Aggarwal, P.K., Aureli, A., Bokuniewicz, H., Cable, J.E., Charette, M.A., Kontar, E., Krupa, S., Kulkarni, K.M., Loveless, A., Moore, W.S., Oberdorfer, J.A., Oliveira, J., Ozyurt, N., Povinec, P., Privitera, A.M.G., Rajar, R., Ramessur, R.T., Scholten, J., Stieglitz, T., Taniguchi, M., Turner, J.V., 2006. Quantifying submarine groundwater discharge in the coastal zone via multiple methods. Sci. Total Environ. 367, 498-543.

Burnett, W.C., Dulaiova, H., 2003. Estimating the dynamics of groundwater input into the coastal zone via continuous radon-222 measurements. Journal of Environmental Radioactivity 69, 21-35.

Cassar, N., Bender, M.L., Barnett, B.A., Fan, S., Moxim, W.J., II, H.L., Tilbrook, B., 2007. The Southern Ocean Biological Response to Aeolian Iron Deposition. Science 317, 1067-1070.

Charette, M., Buesseler, K., 2004. Submarine groundwater discharge of nutrients and copper to an urban subestuary of Chesapeake Bay (Elizabeth River). Limnology and Oceanography 49 (2), 376-385.

Charette, M., Buesseler, K., Andrews, J., 2001. Utility of radium isotopes for evaluating the input and transport of groundwater-derived nitrogen to a Cape Cod estuary. Limnology and Oceanography 46 (2), 465-470.

Charette, M.A., Gonneea, M.E., Morris, P.J., Statham, P., Fones, G., Planquette, H., Salter, I., Garabato, A.N., 2007. Radium isotopes as tracers of iron sources fueling a Southern Ocean phytoplankton bloom. Deep Sea Research Part II: Topical Studies in Oceanography 54, 1989-1998.

Charette, M.A., Sholkovitz, E.R., 2006. Trace element cycling in a subterranean estuary: Part 2. Geochemistry of the pore water. Geochim. Cosmochim. Acta 70, 811-826.

Cook, A.J., Fox, A.J., Vaughan, D.G., Ferrigno, J.G., 2005. Retreating Glacier Fronts on the Antarctic Peninsula over the Past Half-Century. Science 308, 541-4.

Corbett, D.R., Chanton, J., Burnett, W., Dillon, K., Rutkowski, C., 1999. Patterns of groundwater discharge into Florida Bay. Limnology and Oceanography 44 (4), 1045-1055.

Corbett, D.R., Dillon, K., Burnett, W., Chanton, J., 2000. Estimating the Groundwater Contribution into Florida Bay via Natural Tracers, 222Rn and CH4. Limnol. Oceanogr. 45, pp. 1546-1557.

Depoorter, M.A., Bamber, J.L., Griggs, J.A., Lenaerts, J.T.M., Ligtenberg, S.R.M., van, d.B., Moholdt, G., 2013. Calving fluxes and basal melt rates of Antarctic ice shelves. Nature 502, 89-92.

Dierssen, H., Smith, R., Vernet, M., 2002. Glacial meltwater dynamics in coastal waters west of the Antarctic peninsula. Proceedings of the National Academy of Science of the United States of America 99, 1790-1795.

Domack, E., Amblàs, D., Gilbert, R., Brachfeld, S., Camerlenghi, A., Rebesco, M., Canals, M., Urgeles, R., 2006. Subglacial morphology and glacial evolution of the Palmer deep outlet system, Antarctic Peninsula. Geomorphology 75, 125-142.

Ducklow, H.W., Baker, K., Martinson, D.G., Langdon B. Quetin, Ross, R.M., Smith, R.C., Sharon E. Stammerjohn, Vernet, M., Fraser, W., 2007. Marine Pelagic Ecosystems: The West Antarctic Peninsula. Philosophical Transactions: Biological Sciences 362, 67-94.

Dulaiova, H., Arldelan, M.V., Henderson, P.V., Charette, M.A., 2009.
Shelf-derived iron inputs drive biological productivityin the southern Drake Passage Global Biogeochemical Cycles 23.

Dulaiova, H., Burnett, W.C., 2004. An efficient method for gamma spectrometric determination of radium-226,228 via manganese fibers. Limnology and Oceanography-Methods 2, 256-261.

Edwards, R., Sedwick, P., 2001. Iron in East Antarctic snow: Implications for atmospheric iron deposition and algal production in Antarctic waters. Geophysical Research Letters 28 (20), 3907-3910.

Google earth V 6.2.9200.0 (January 15, 2014) Flandres Bay, Western Antarctic Peninsula. -65.099798° N, -63.099798° W, Eye alt 51.76 mi. http://www.earth.google.com [April 9, 2015]

Hakkinen, S., Rhines, P.B., 2004. Decline of Subpolar North Atlantic Circulation During the 1990s. Science 23-304, 555-559.

Hancock, G., Webster, I., Stieglitz, T., 2006. Horizontal mixing of Great Barrier Reef waters: Offshore diffusivity determined from radium isotope distribution. Journal of Geophysical Research-Oceans 111 (C12).

Hawkings, J.R., Wadham, J.L., Tranter, M., Raiswell, R., Benning, L.G., Statham, P.J., Tedstone, A., Nienow, P., Lee, K., Telling, J., 2014. Ice sheets as a significant source of highly reactive nanoparticulate iron to the oceans. Nat Commun 5.

Heywood, K., Naveira, G., Stevens, D., Muench, R., 2004. On the fate of the Antarctic Slope Front and the Origin of the Weddell Front. Journal of Geophysical Research-Oceans 109, 1978-2012.

Holm-Hansen, O.O., Kahru, M., Hewes, C.D., 2005. Deep chlorophyll *a* maxima (DCMs) in pelagic Antarctic waters. II. Relation to bathymetric features and dissolved iron concentrations. Marine Ecology Progress Series 297, 71-81.

Hopkinson, B.M., Mitchell, B.G., Reynolds, R.A., Wang, H., Selph, K.E., Measures, C.I., 2007. Iron limitation across chlorophyll gradients in the southern Drake Passage: phytoplankton responses to iron addition and photosynthetic indicators of iron stress. Limnology and Oceanography 52, 2540-2554.

Hwang, D., Kim, G., Lee, Y., Yang, H., 2005. Estimating submarine inputs of groundwater and nutrients to a coastal bay using radium isotopes. Mar. Chem. 96, 61-71.

Jacobs, S.S., 1991. On the nature and significance of the Antarctic Slope Front. Marine Chemistry 35, 9-24.

Johannes, R.E., 1980. The ecological significance of the submarine discharge of groundwater. Mar. Ecol. Prog. Ser. 3, 1937-1950.

Kim, G., Burnett, W., Dulaiova, H., Swarzenski, P., Moore, W., 2001. Measurement of Ra-224 and Ra-226 activities in natural waters using a radon-in-air monitor. Environmental Science & Technology 35, 4680-4683.

Kim, G., Ryu, J., Hwang, D., 2008. Radium tracing of submarine groundwater discharge (SGD) and associated nutrient fluxes in a highly-permeable bed coastal zone, Korea. Mar. Chem. 109, 307-317.

Klinck, J.M., Hofmann, E.E., Beardsley, R.C., Salihoglu, B., Howard, S., 2004. Water-mass properties and circulation on the west Antarctic Peninsula Continental Shelf in Austral Fall and Winter 2001. Deep Sea Research Part II: Topical Studies in Oceanography 51, 1925-1946.

Knee, K.L., Garcia-Solsona, E., Garcia-Orellana, J., Boehm, A.B., Paytan, A., 2011. Using radium isotopes to characterize water ages and coastal mixing rates: A sensitivity analysis. Limnology and Oceanography-Methods 9, 380-395.

Marinov, I., Gnanadesikan, A., Toggweiler, J.R., Sarmiento, J.L., 2006. The Southern Ocean biogeochemical divide. Nature 441, 964-7.

Martin, J.H., Gordon, R.M., Fitzwater, S.E., 1990. Iron in Antarctic Waters. Nature 345, 156.

Martinson, D.G., McKee, D.C., 2012. Transport of warm Upper Circumpolar Deep Water onto the western Antarctic Peninsula continental shelf. Ocean Science 8, 433-442.

Martinson, D.G., Stammerjohn, S.E., Iannuzzi, R.A., Smith, R.C., Vernet, M., 2008. Western Antarctic Peninsula physical oceanography and spatio–temporal variability. Deep Sea Research Part II: Topical Studies in Oceanography 55, 1964-1987.

McCoy, C.A., Corbett, D.R., Cable, J.E., Spruill, R.K., 2007. Hydrological characterization of southeast coastal plain aquifers and groundwater discharge to Onslow Bay, North Carolina (USA). Journal of Hydrology 339, 159-171.

McCoy, C., Viso, R., Peterson, R.N., Libes, S., Lewis, B., Ledoux, J., Voulgaris, G., Smith, E., Sanger, D., 2011. Radon as an indicator of limited cross-shelf mixing of submarine groundwater discharge along an open ocean beach in the South Atlantic Bight during observed hypoxia. Cont. Shelf Res. 31, 1306-1317.

Meredith, M.P., Brandon, M.A., Wallace, M.I., Clarke, A., Leng, M.J., Renfrew, I.A., van Lipzig, N.P.M., King, J.C., 2008. Variability in the freshwater balance of northern Marguerite Bay, Antarctic Peninsula: Results from δ18O. Deep Sea Research Part II: Topical Studies in Oceanography 55, 309-322.

Moffat, C., Beardsley, R.C., Owens, B., van Lipzig, N., 2008. A first description of the Antarctic Peninsula Coastal Current. Deep-Sea Res. Part II-Top. Stud. Oceanogr. 55, 277-293.

Moline, M.A., Karnovsky, N.J., Brown, Z., Divoky, G.J., Frazer, T.K., Jacoby, C.A., Torres, J.J., Fraser, W.R., 2008. High Latitude Changes in Ice Dynamics and Their Impact on Polar Marine Ecosystems. Ann. N. Y. Acad. Sci. 1134, 267-319.

Moore, W.S., Arnold, R., 1996. Measurement of 223Ra and 224Ra in coastal watersusing a delayed coincidence counter. Journal of Geophysical Research 101, 1321-1329.

Moore, W.S., 2007. Seasonal distribution and flux of radium isotopes on the southeastern U.S. continental shelf. Journal of Geophysical Research: Oceans 112, - C10013.

Moore, W.S., 2006. Radium isotopes as tracers of submarine groundwater discharge in Sicily. Cont. Shelf Res. 26, 852-861.

Moore, W.S., 2000. Determining coastal mixing rates using radium isotopes. Cont. Shelf Res. 20, 1993-2007.

Moore, W.S., 1996. Large groundwater inputs to coastal waters revealed by 226Ra enrichments. Nature 380, 612-614.

Moore, W.S., Astwood, H., Lindstrom, C., 1995. Radium isotopes in coastal waters on the Amazon shelf. Geochim. Cosmochim. Acta 59, 4285-4298.

Moore, W., 2003. Sources and fluxes of submarine groundwater discharge delineated by radium isotopes. Biogeochemistry 66, 75-93.

Moore, W., 2000. Ages of continental shelf waters determined from Ra-223 and Ra-224. Journal of Geophysical Research: Oceans 105, 22117-22122.

Moore, W., Reid, D., 1973. Extraction of Radium from Natural-Waters using Manganese-Impregnated Acrylic Fibers. Journal of Geophysical Research 78, 8880-8886.

Null, K., Dimova, N., Knee, K., Esser, B., Swarzenski, P., Singleton, M., Stacey, M., Paytan, A., 2012.
Submarine Groundwater Discharge-Derived Nutrient Loads to San Francisco Bay: Implications to Future
Ecosystem Changes Estuaries and Coasts 35, 1299-1315.

Palmer Station Antarctica LTER., 2014. Monthly averages of temperature, pressure and melted precipitation from Palmer Station (LTER). Combines legacy monthly average temperature timeseries (1974-1989) with full time series that includes pressure and melted precipitation (1989-ongoing). 1989-ongoing portion computed from the (Daily Averages time series). See the metadata for this dataset for measurement methods.. Palmer Station Antarctica LTER; Long Term Ecological Research Network.

Peterson, R., Burnett, W., Glenn, C., Johnson, A., 2009.
Quantification of point-source groundwater discharges to the ocean from the shoreline of the Big Island, Hawaii Limnology and Oceanography 54 (3), 890-904.

Peterson, R., Burnett, W., Taniguchi, M., Chen, J., Santos, I., Ishitobi, T., 2008. Radon and radium isotope assessment of submarine groundwater discharge in the Yellow River delta, China. Journal of Geophysical Research-Oceans 113 (C9).

Peterson, R.N., Burnett, W.C., Dimova, N., Santos, I.R., 2009. Comparison of measurement methods for radium-226 on manganese-fiber. Limnology and Oceanography-Methods 7, 196-205.

Pike, J., Swann, G.E.A., Leng, M.J., Snelling, A.M., 2013. Glacial discharge along the west Antarctic Peninsula during the Holocene. Nature Geosci 6, 199-202.

Savidge, D.K., Amft, J.A., 2009. Circulation on the West Antarctic Peninsula derived from 6 years of shipboard ADCP transects. Deep Sea Research Part I: Oceanographic Research Papers 56, 1633-1655.

Schlitzer, R., 2012. Ocean Data View. 4.

Schlosser, P., Bayer, R., Foldvik, A., Gammelsrød, T., Rohardt, G., Münnich, K.O., 1990. Oxygen 18 and helium as tracers of ice shelf water and water/ice interaction in the Weddell Sea. Journal of Geophysical Research: Oceans 95, 3253-3263.

Schofield, O., Ducklow, H., Martinson, D., Meredith, M.P., Moline, M., Fraser, W.R., 2010. How Do Polar Marine Ecosystems Respond to Rapid Climate Change? Science 328, 1520-1523.

Skvarca, P., Rack, W., Rott, H., Donángelo, T.I., 1999. Climatic trend and the retreat and disintegration of ice shelves on the Antarctic Peninsula: an overview. Polar Res. 18, 151-157.

Sun, Y., Torgersen, T., 1998. The effects of water content and Mn-fiber surface conditions on 224Ra measurement by 220Rn emanation. Marine Chemistry 62, 299-306.

Takahashi, T., Sweeney, C., Hales, B., Chipman, D.W., Newberger, T., Goddard, J.G., Iannnuzzi, R.A., Sutherland, S.C., 2012. The changing carbon cycle in the Southern Ocean. Oceanography 25-3, 26-37.

Turner, J., Lachlan-Cope, T.A., Colwell, S., Marshall, G.J., Connolley, W.M., 2006. Significant Warming of the Antarctic Winter Troposphere. Science 311, 1914-1917.

Viso, R., McCoy, C., Gayes, P., Quafisi, D., 2010. Geological controls on submarine groundwater discharge in Long Bay, South Carolina (USA). Cont. Shelf Res. 30, 335-341.

Waska, H., Kim, S., Kim, G., Peterson, R.N., Burnett, W.C., 2008. An efficient and simple method for measuring Ra-226 using the scintillation cell in a delayed coincidence counting system (RaDeCC). Journal of Environmental Radioactivity 99, 1859-1862.

Weiss, R.F., Östlund, H.G., Craig, H., 1979. Geochemical studies of the Weddell sea. Deep Sea Research Part A.Oceanographic Research Papers 26, 1093-1120.

Weppernig, R., Schlosser, P., Khatiwala, S., Fairbanks, R.G., 1996. Isotope data from Ice Station Weddell: Implications for deep water formation in the Weddell Sea. Journal of Geophysical Research: Oceans 101, 25723-25739.

Windom, H., Moore, W.S., Niencheski, L.F., Jahnke, R.,., 2006. Submarine groundwater discharge: a large, previously unrecognized source of dissolved iron to the South Atlantic Ocean. Marine Chemistry 102, 252-256.

Winton, V.H.L., Dunbar, G.B., Bertler, N.A.N., Millet, M.-., Delmonte, B., Atkins, C.B., Chewings, J.M., Andersson, P., 2014. The contribution of aeolian sand and dust to iron fertilization of phytoplankton blooms in southwestern Ross Sea, Antarctica. Global Biogeochem. Cycles 28, - 2013GB004574.

Zhou, M., Niiler, P.P., Hu, J., 2002. Surface currents in the Bransfield and Gerlache Straits, Antarctica. Deep Sea Research Part I: Oceanographic Research Papers 49, 267-280.

Appendix I Contour Plots of Geochemical and Physical Parameters from the 2012 Cruise

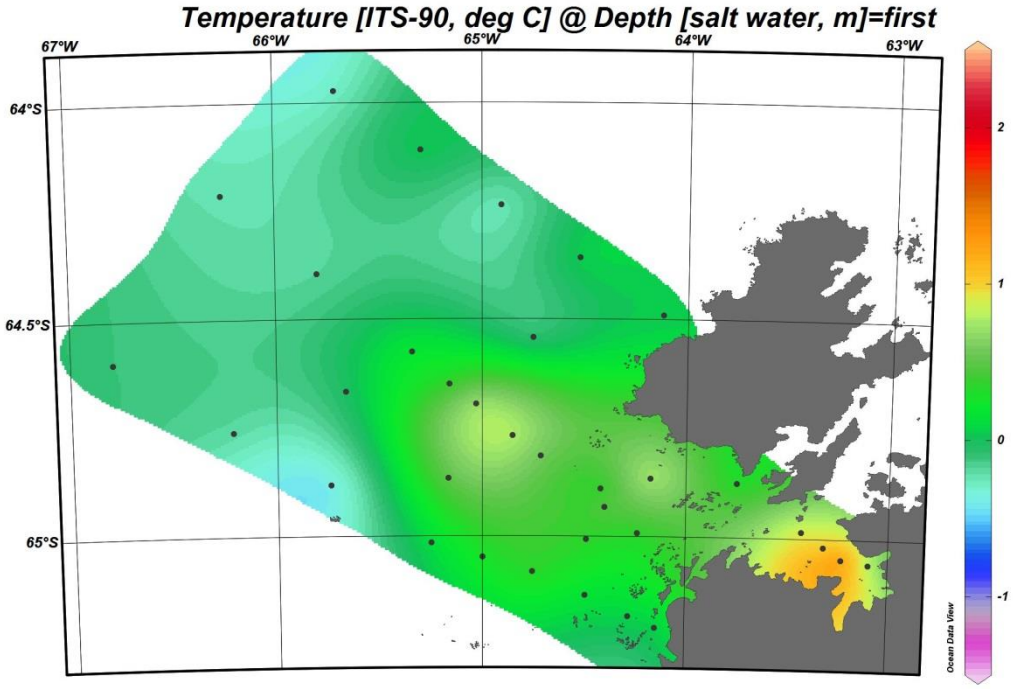
Temperature [ITS-90, deg C] @ Depth [salt water, m]=first
67°W
66°W
65°W
64°W
63°W
64°S
64.5°S
65°S
2
1
0
-1
Ocean Data View

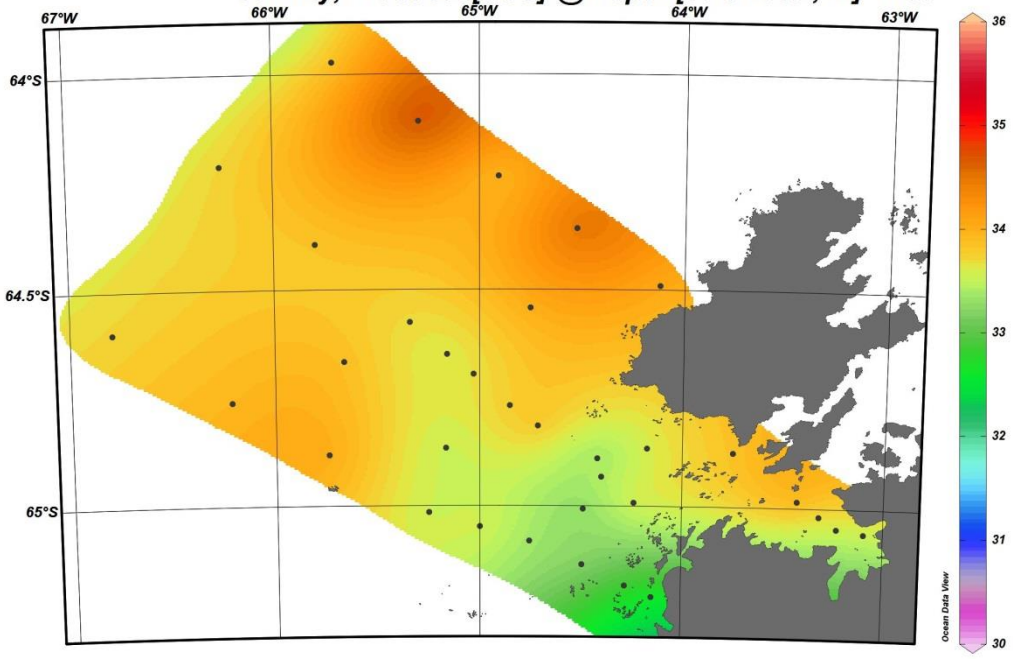
Salinity, Practical [PSU] @ Depth [salt water, m]=first
67°W
66°W
65°W
64°W
63°W
64°S
64.5°S
65°S
36
35
34
33
32
31
30
Ocean Data View

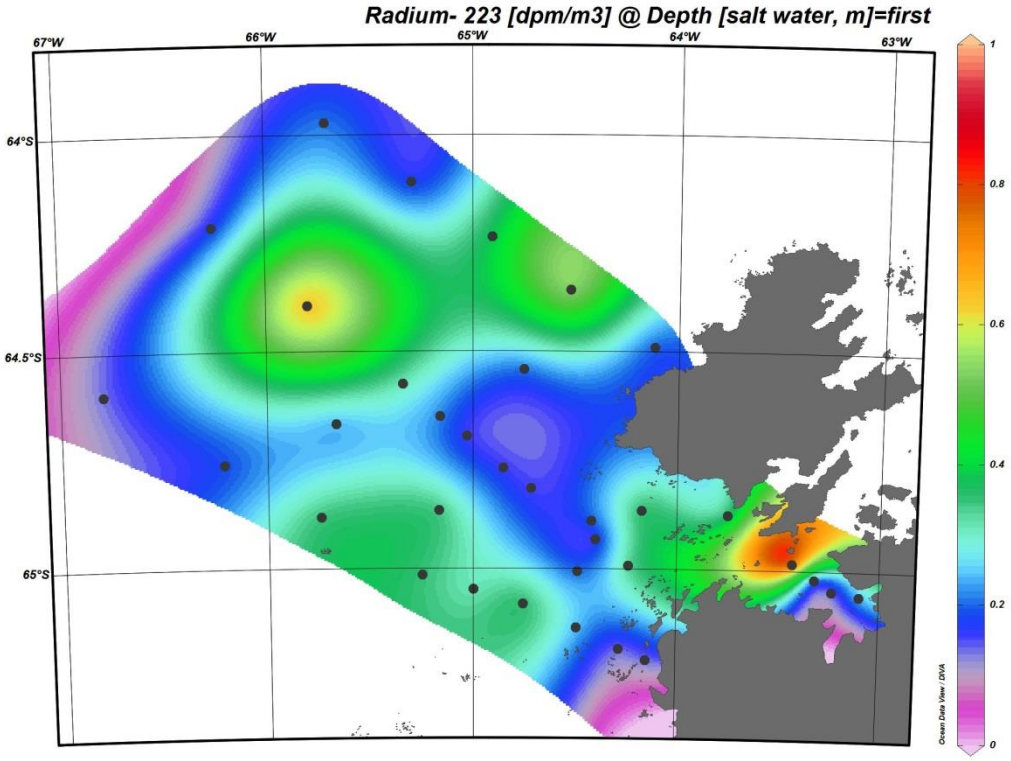
Radium- 223 [dpm/m3] @ Depth [salt water, m]=first
67°W
66°W
65°W
64°W
63°W
64°S
64.5°S
65°S
1
0.8
0.6
0.4
0.2
0
Ocean Data View / DIVA

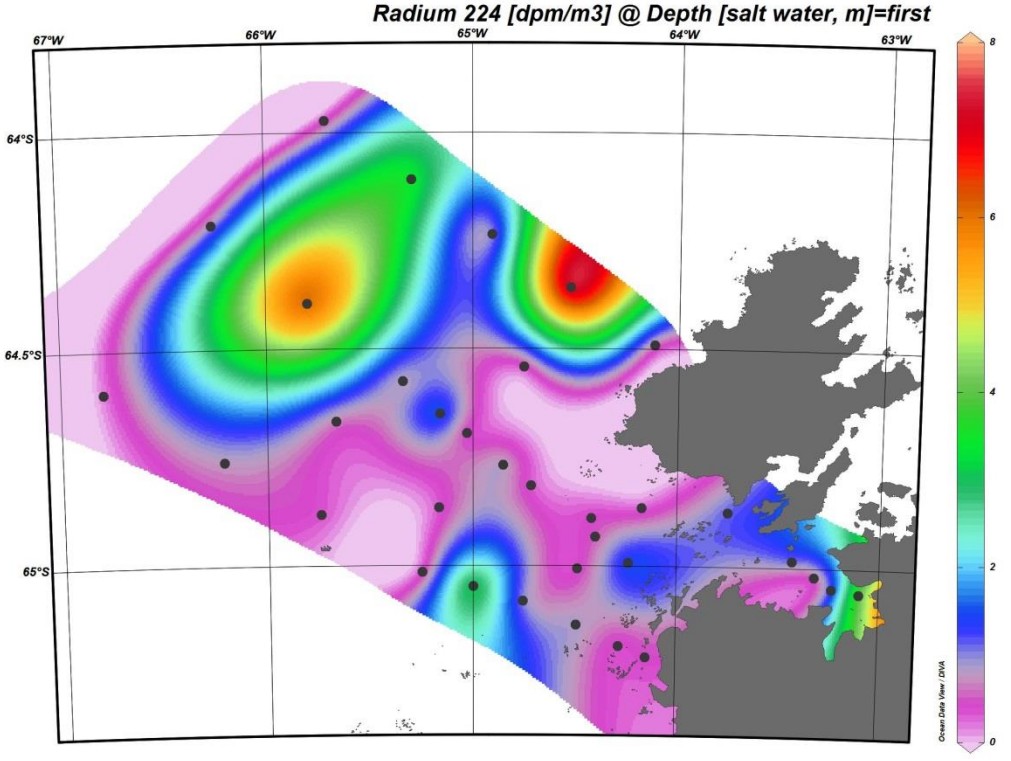
Radium 224 [dpm/m3] @ Depth [salt water, m]=first
67°W
66°W
65°W
64°W
63°W
64°S
64.5°S
65°S
8
6
4
2
0
Ocean Data View / DIVA

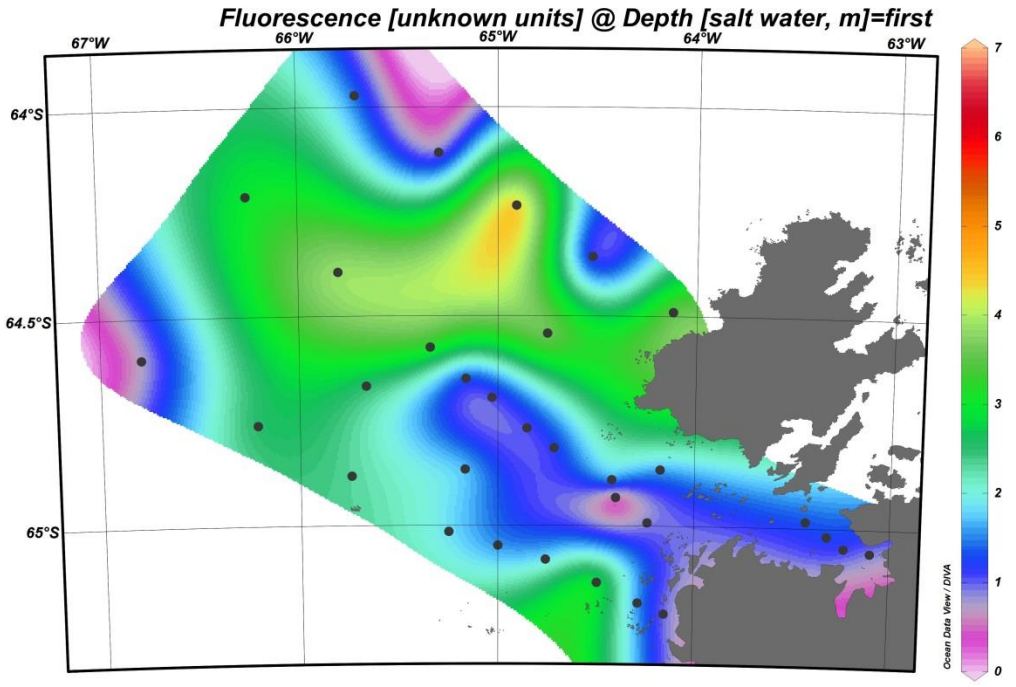
Fluorescence [unknown units] @ Depth [salt water, m]=first
67°W
66°W
65°W
64°W
63°W
64°S
64.5°S
65°S
7
6
5
4
3
2
1
0
Ocean Data View / DIVA

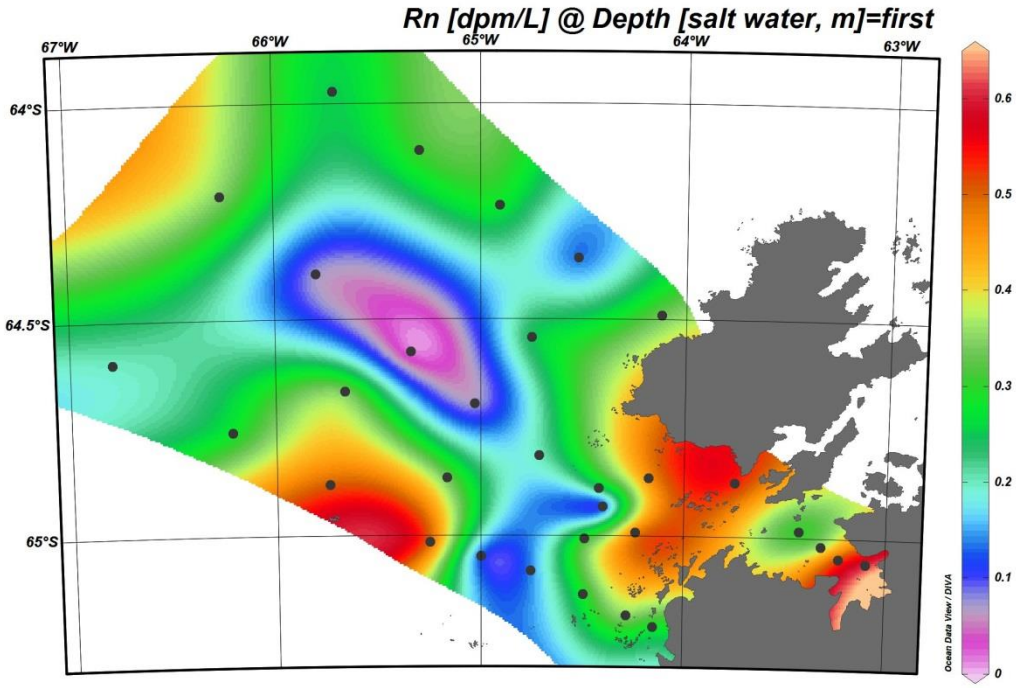
Rn [dpm/L] @ Depth [salt water, m]=first
67°W
66°W
65°W
64°W
63°W
64°S
64.5°S
65°S
0.6
0.5
0.4
0.3
0.2
0.1
0
Ocean Data View / DIVA

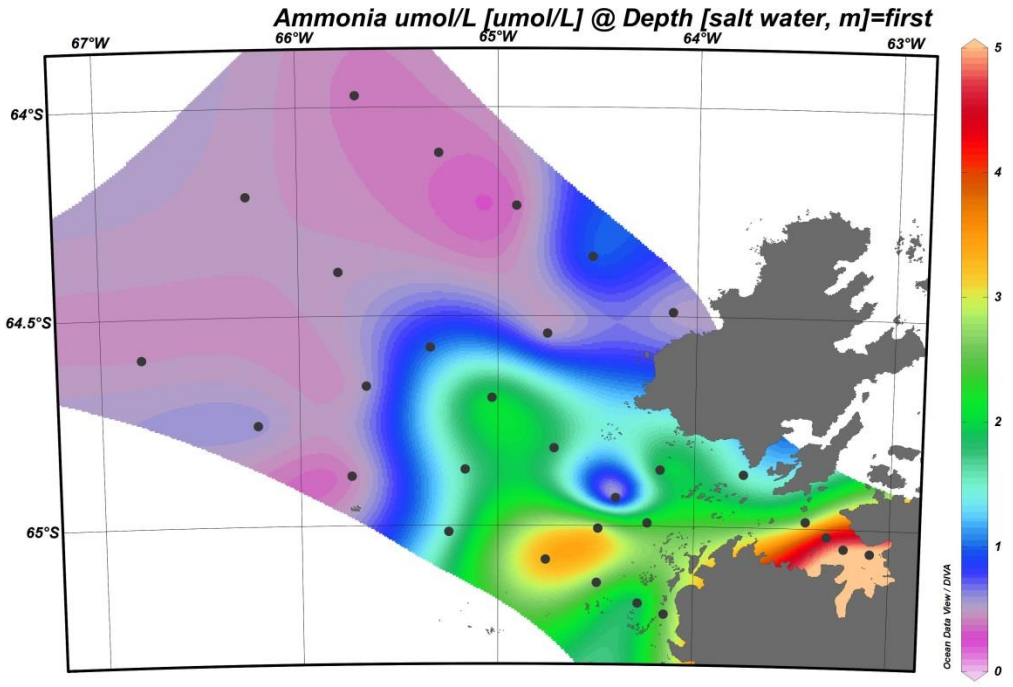
Ammonia umol/L [umol/L] @ Depth [salt water, m]=first
67°W
66°W
65°W
64°W
63°W
64°S
64.5°S
65°S
5
4
3
2
1
0
Ocean Data View / DIVA

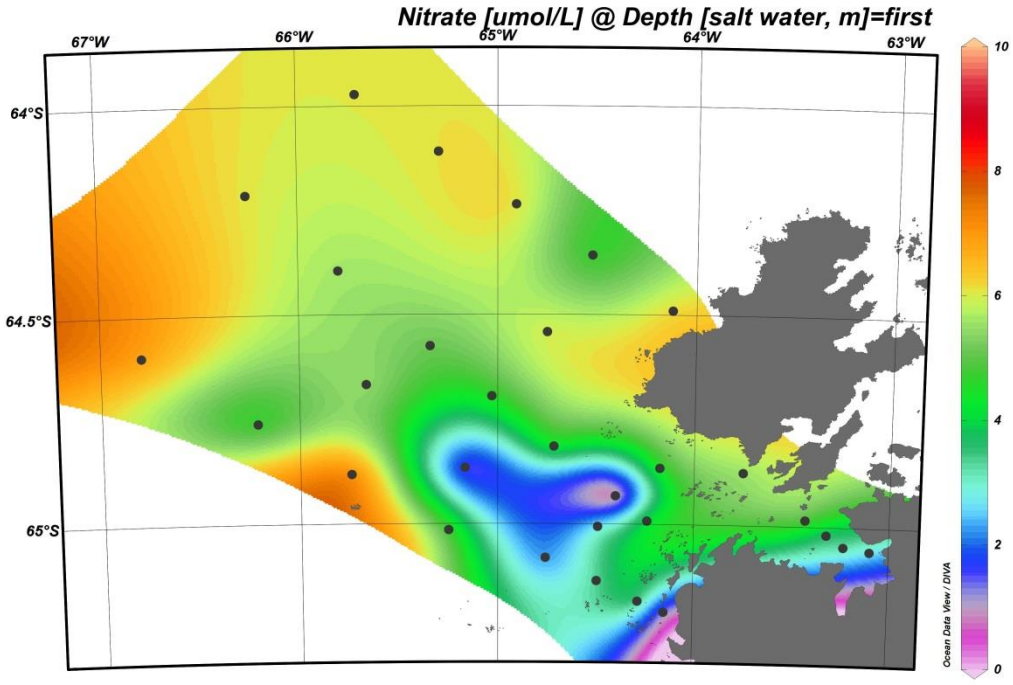
Nitrate [umol/L] @ Depth [salt water, m]=first
67°W
66°W
65°W
64°W
63°W
64°S
64.5°S
65°S
10
8
6
4
2
0
Ocean Data View / DIVA

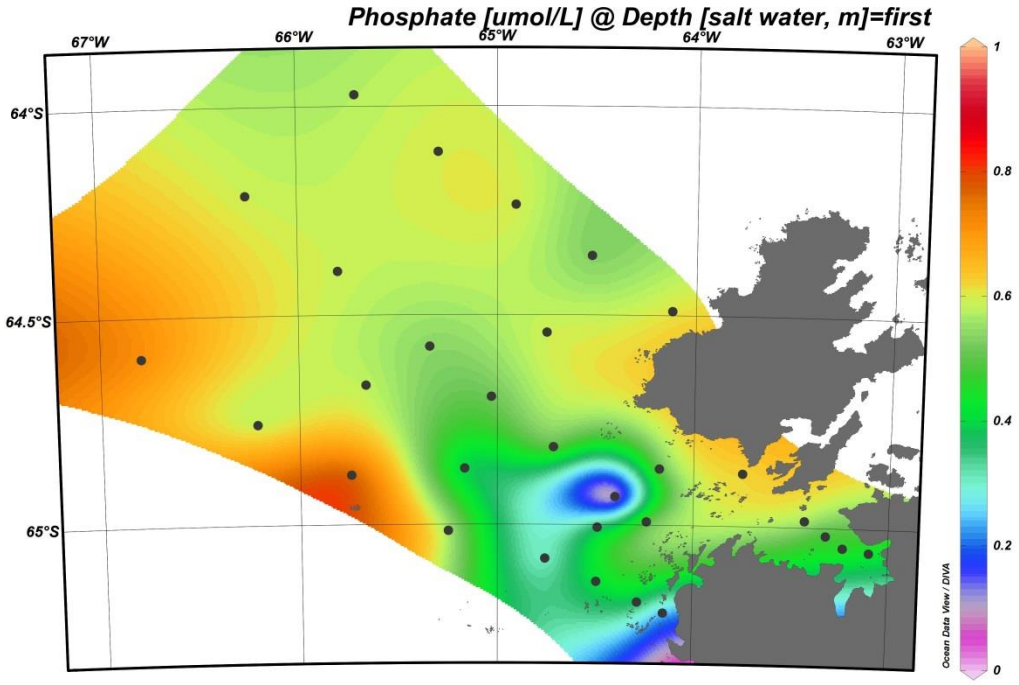
Phosphate [umol/L] @ Depth [salt water, m]=first
67°W
66°W
65°W
64°W
63°W
64°S
64.5°S
65°S
1
0.8
0.6
0.4
0.2
0
Ocean Data View / DIVA

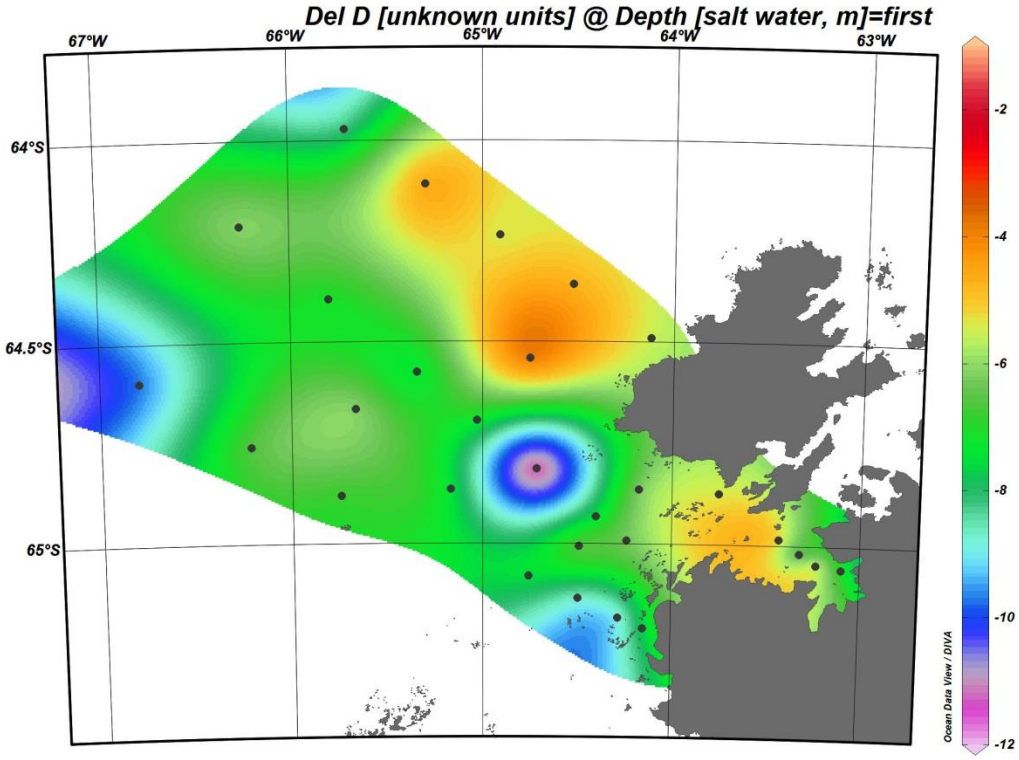
Del D [unknown units] @ Depth [salt water, m]=first
67°W
66°W
65°W
64°W
63°W
64°S
64.5°S
65°S
-2
-4
-6
-8
-10
-12
Ocean Data View / DIVA

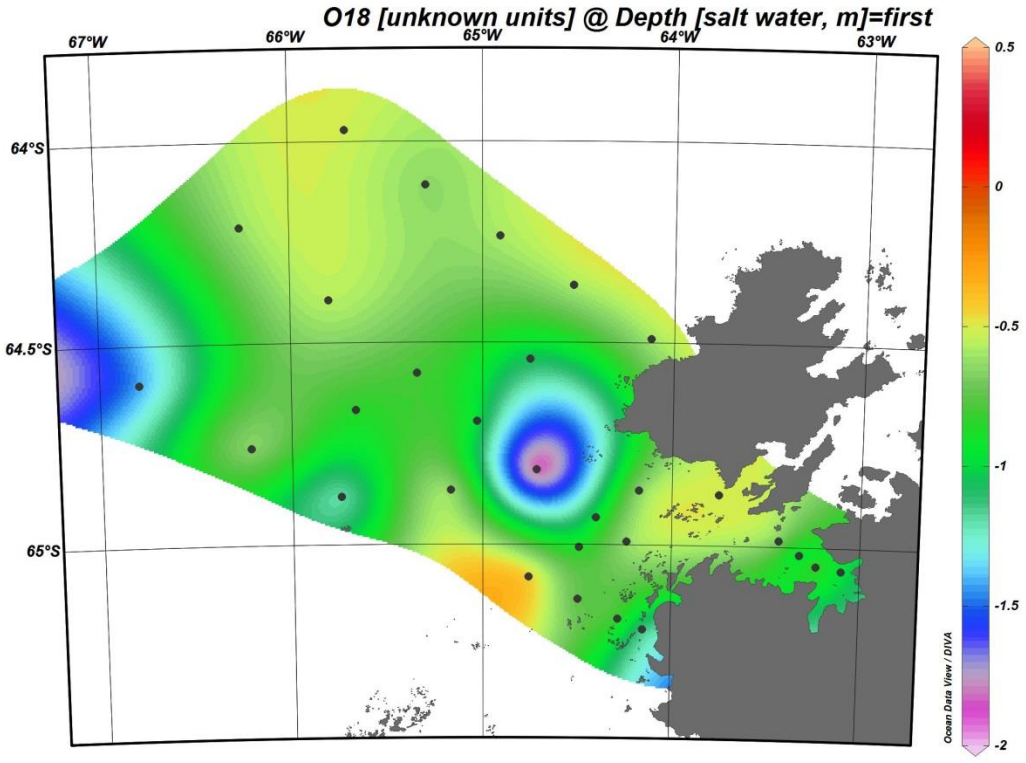
O18 [unknown units] @ Depth [salt water, m]=first
67°W
66°W
65°W
64°W
63°W
64°S
64.5°S
65°S
0.5
0
-0.5
-1
-1.5
-2
Ocean Data View / DIVA

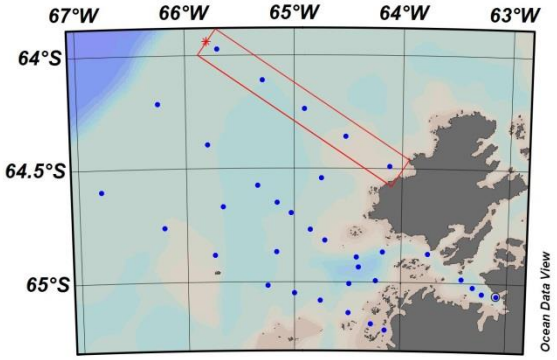
67°W
66°W
65°W
64°W
63°W
64°S
64.5°S
65°S
Ocean Data View

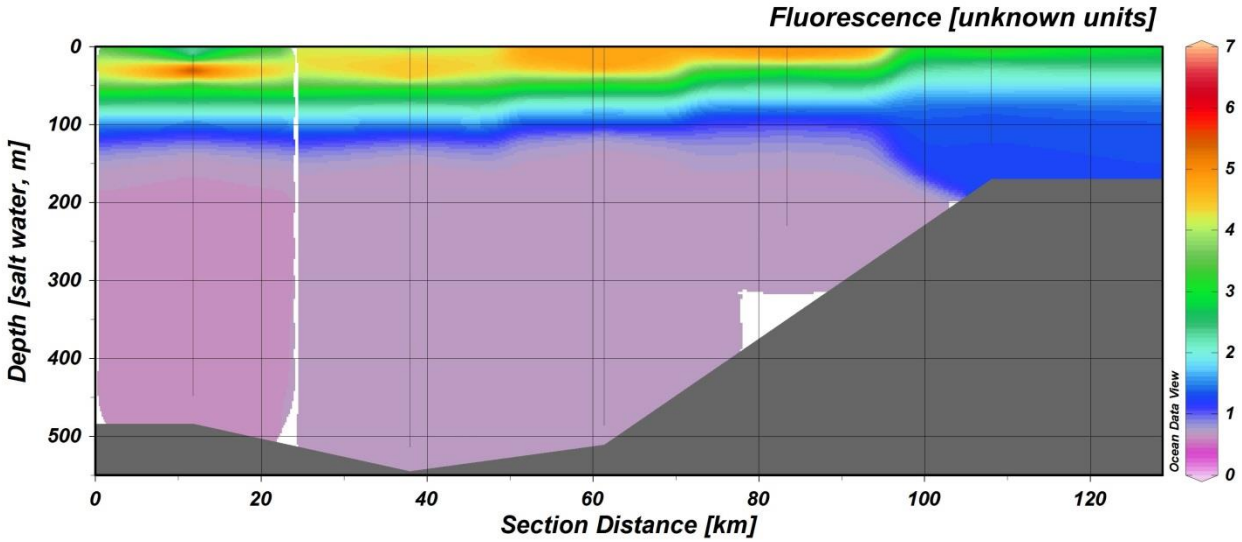
Fluorescence [unknown units]
Depth [salt water, m]
0
100
200
300
400
500
0
20
40
60
80
100
120
Section Distance [km]
7
6
5
4
3
2
1
0
Ocean Data View

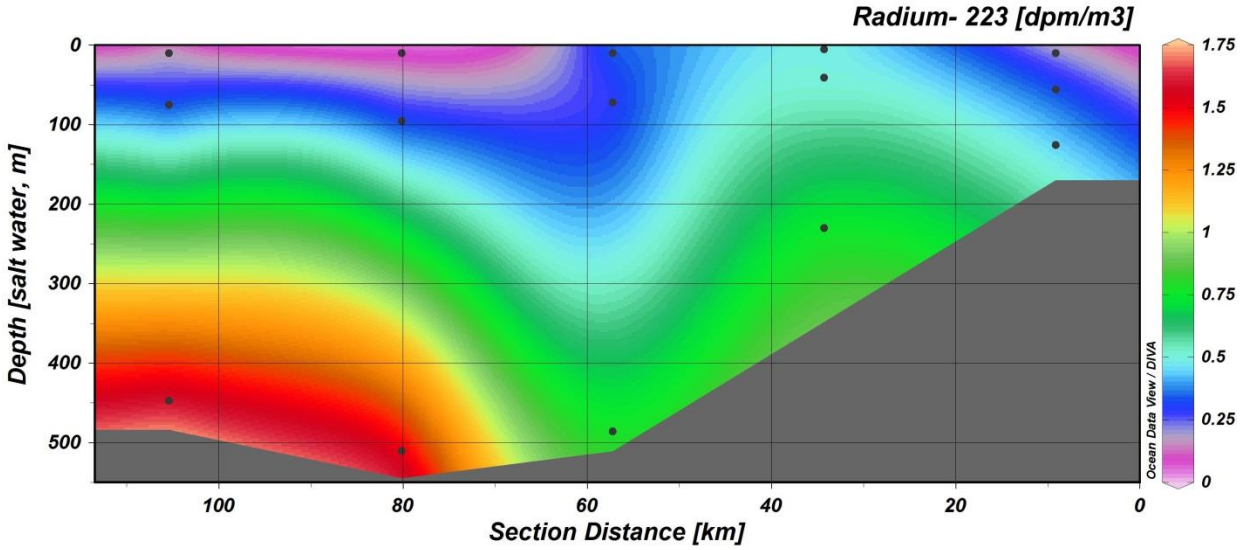
Radium- 223 [dpm/m3]
Depth [salt water, m]
0
100
200
300
400
500
100
80
60
40
20
0
Section Distance [km]
1.75
1.5
1.25
1
0.75
0.5
0.25
0
Ocean Data View / DIVA

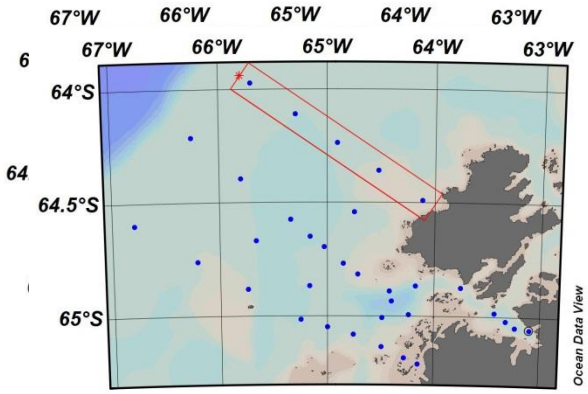
67°W
66°W
65°W
64°W
63°W
64°S
64.5°S
65°S
Ocean Data View

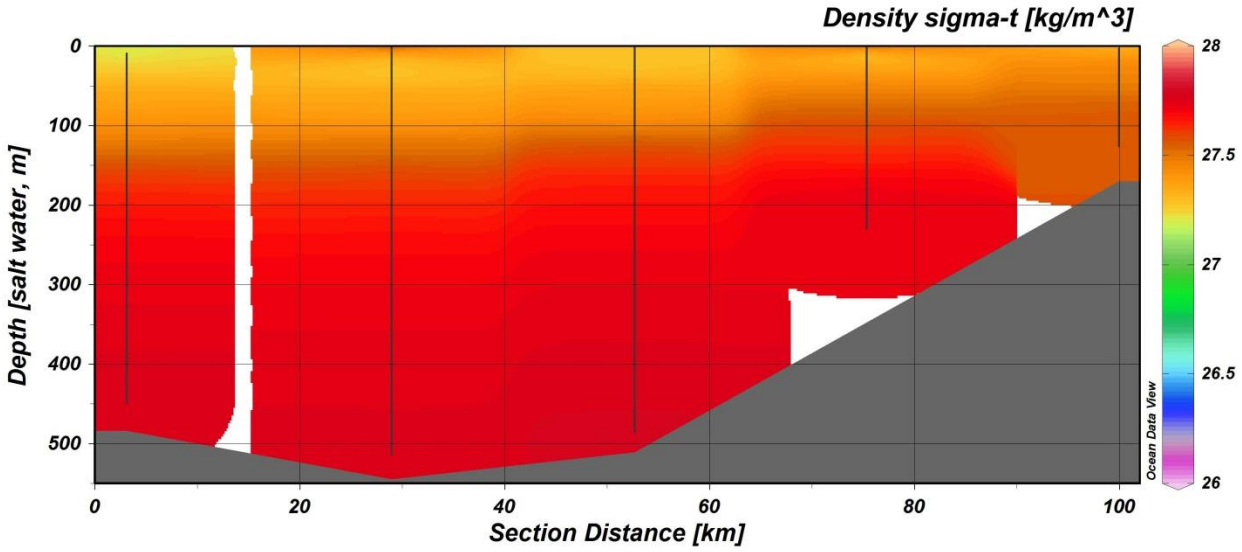
Density sigma-t [kg/m^3]
Depth [salt water, m]
Section Distance [km]
Ocean Data View
28
27.5
27
26.5
26

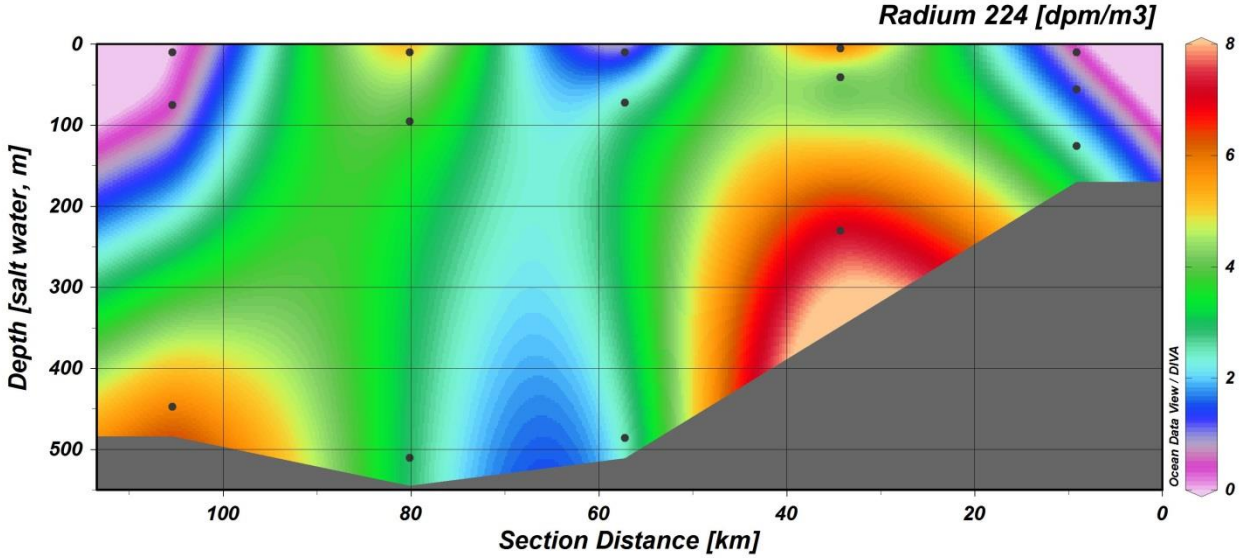
Radium 224 [dpm/m3]
Depth [salt water, m]
Section Distance [km]
Ocean Data View / DIVA

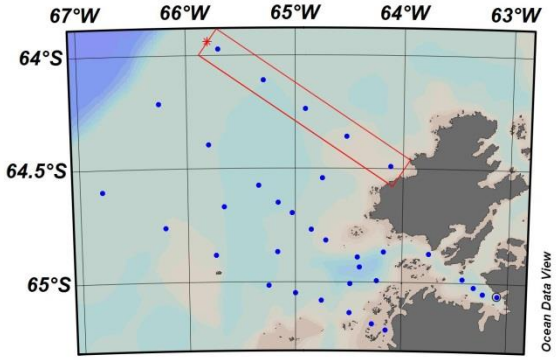
67°W
66°W
65°W
64°W
63°W
64°S
64.5°S
65°S
Ocean Data View

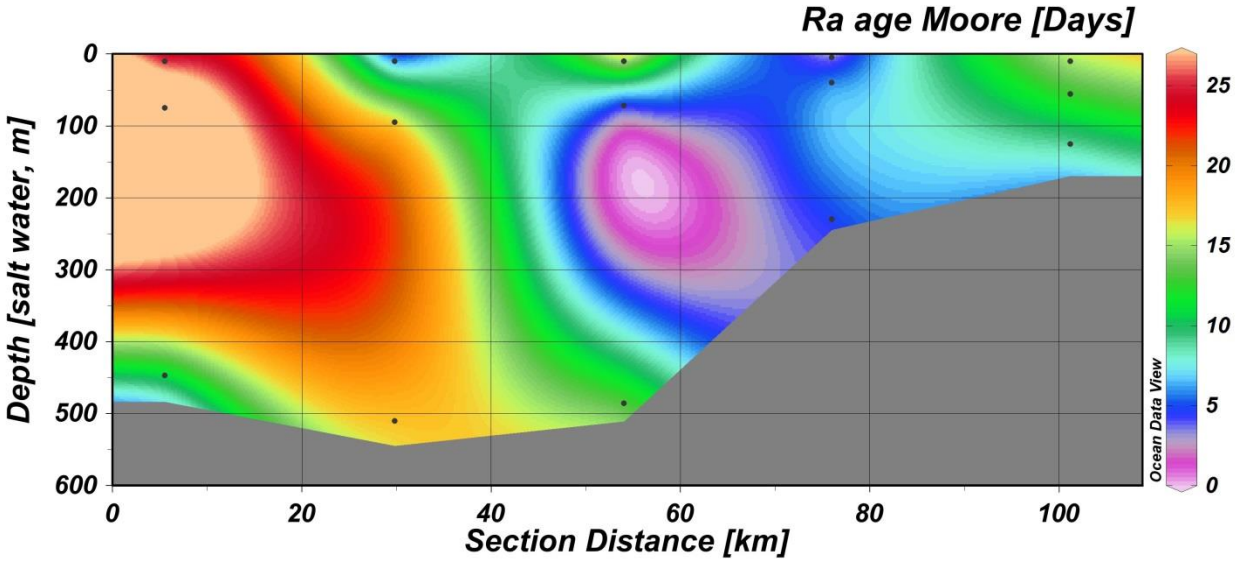
Ra age Moore [Days]
Depth [salt water, m]
0
100
200
300
400
500
600
0
20
40
60
80
100
Section Distance [km]
25
20
15
10
5
0
Ocean Data View

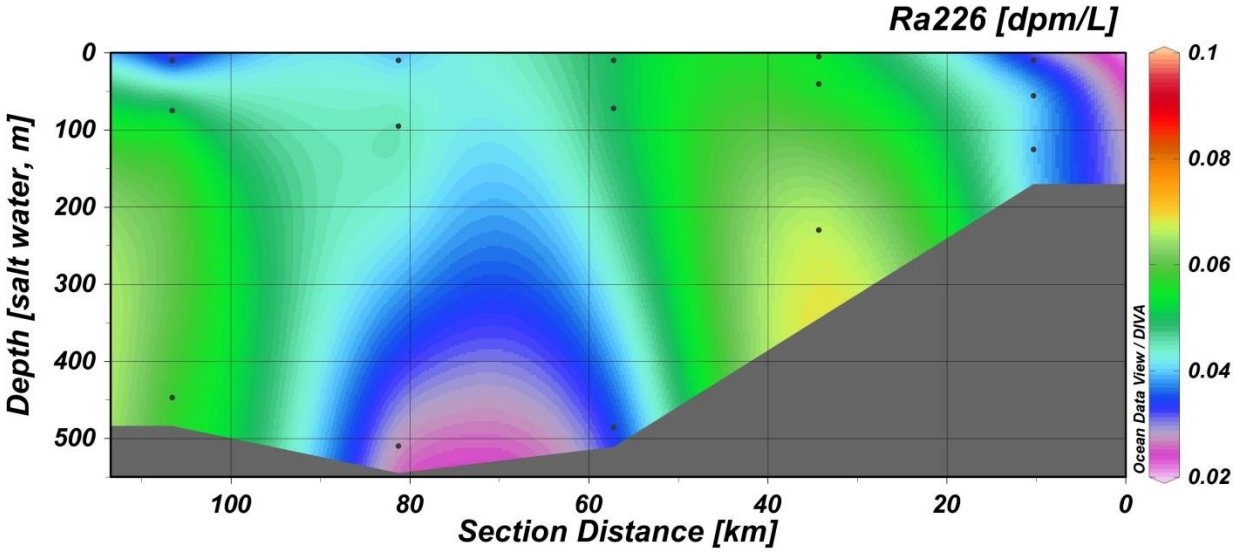
Ra226 [dpm/L]
Depth [salt water, m]
0
100
200
300
400
500
100
80
60
40
20
0
Section Distance [km]
0.1
0.08
0.06
0.04
0.02
Ocean Data View / DIVA

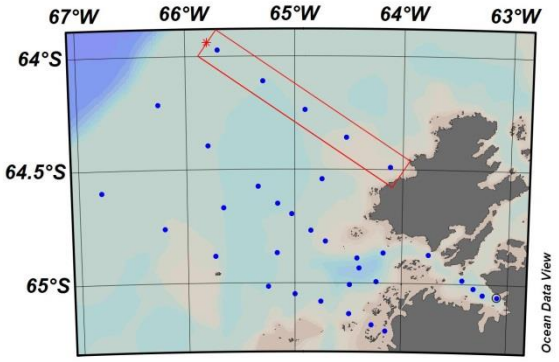
67°W
66°W
65°W
64°W
63°W
64°S
64.5°S
65°S
Ocean Data View

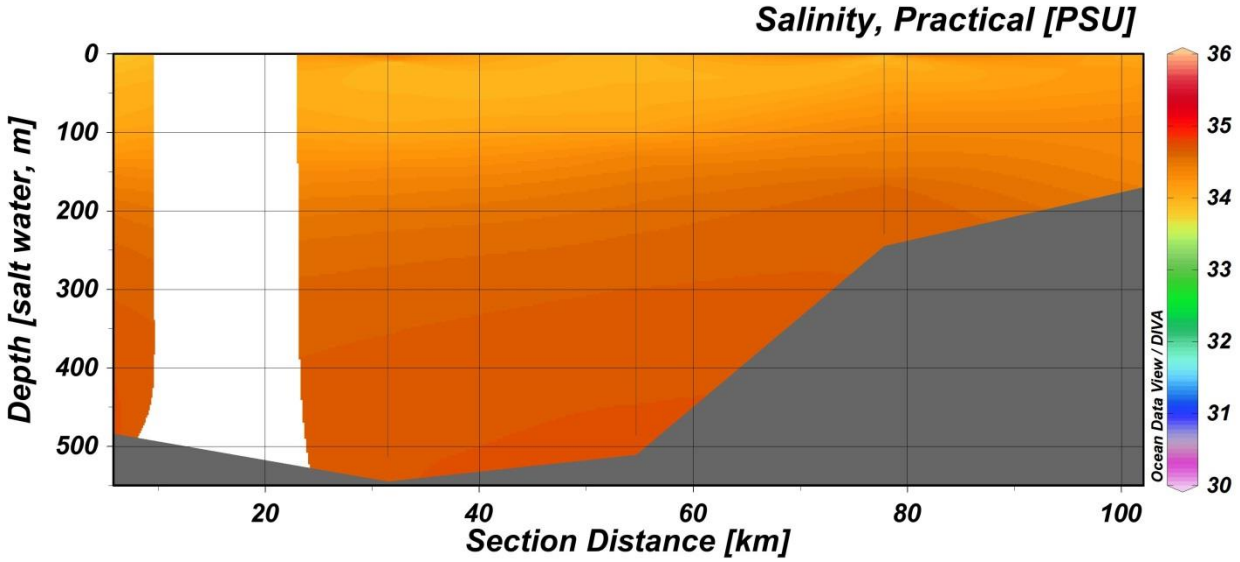
Salinity, Practical [PSU]
Depth [salt water, m]
0
100
200
300
400
500
20
40
60
80
100
Section Distance [km]
36
35
34
33
32
31
30
Ocean Data View / DIVA

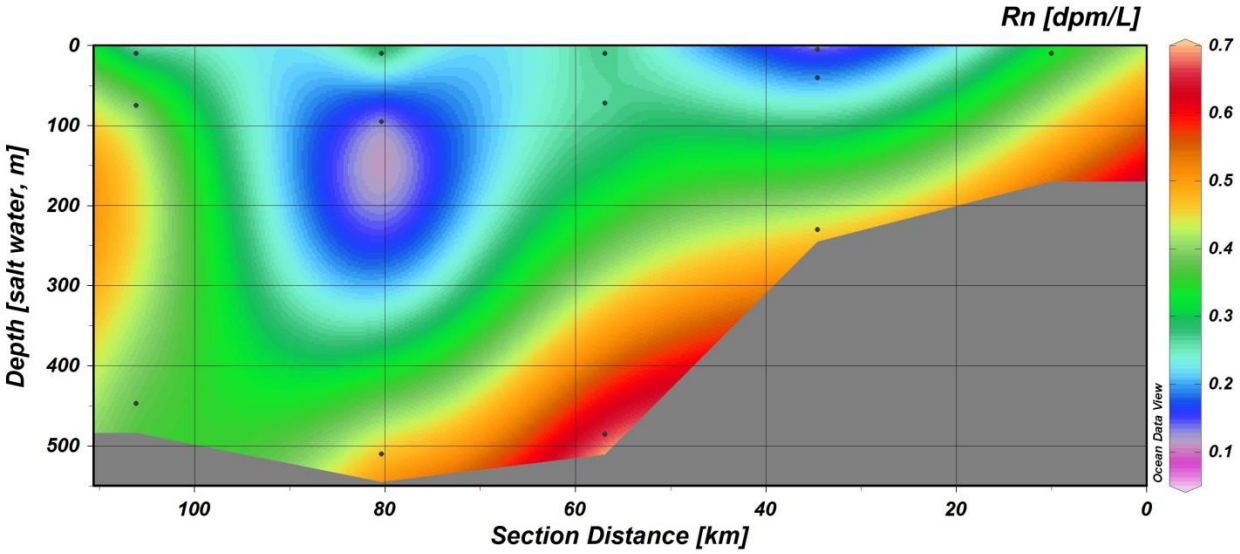
Rn [dpm/L]
Depth [salt water, m]
0
100
200
300
400
500
100
80
60
40
20
0
Section Distance [km]
0.7
0.6
0.5
0.4
0.3
0.2
0.1
Ocean Data View

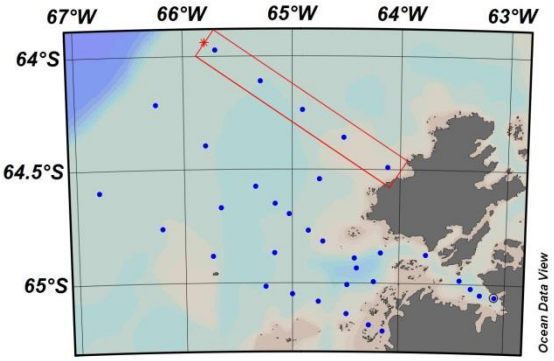
67°W
66°W
65°W
64°W
63°W
64°S
64.5°S
65°S
Ocean Data View

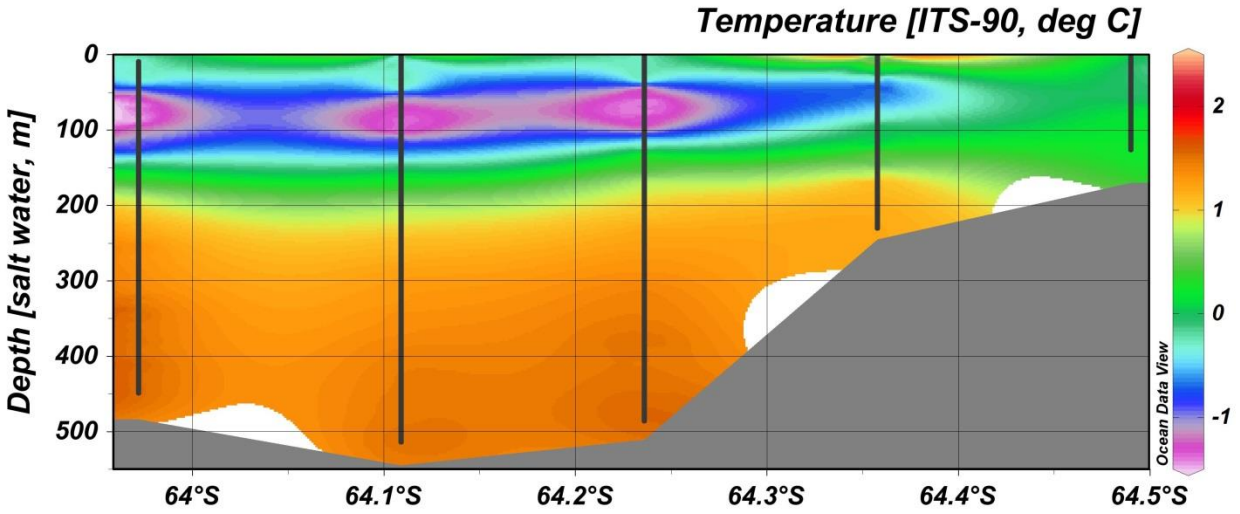
Temperature [ITS-90, deg C]
Depth [salt water, m]
0
100
200
300
400
500
64°S
64.1°S
64.2°S
64.3°S
64.4°S
64.5°S
2
1
0
-1
Ocean Data View

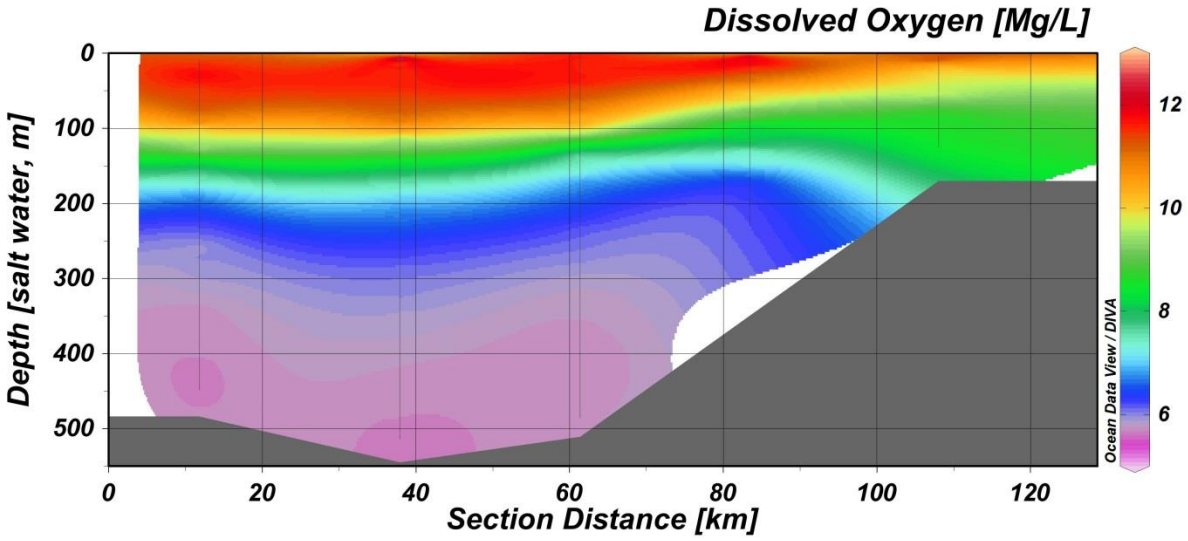
Dissolved Oxygen [Mg/L]
Depth [salt water, m]
0
100
200
300
400
500
0
20
40
60
80
100
120
Section Distance [km]
12
10
8
6
Ocean Data View / DIVA

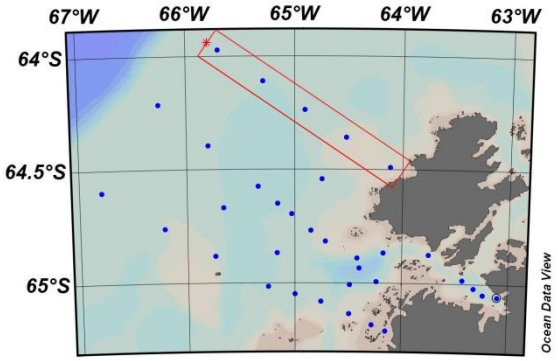
67°W
66°W
65°W
64°W
63°W
64°S
64.5°S
65°S
Ocean Data View

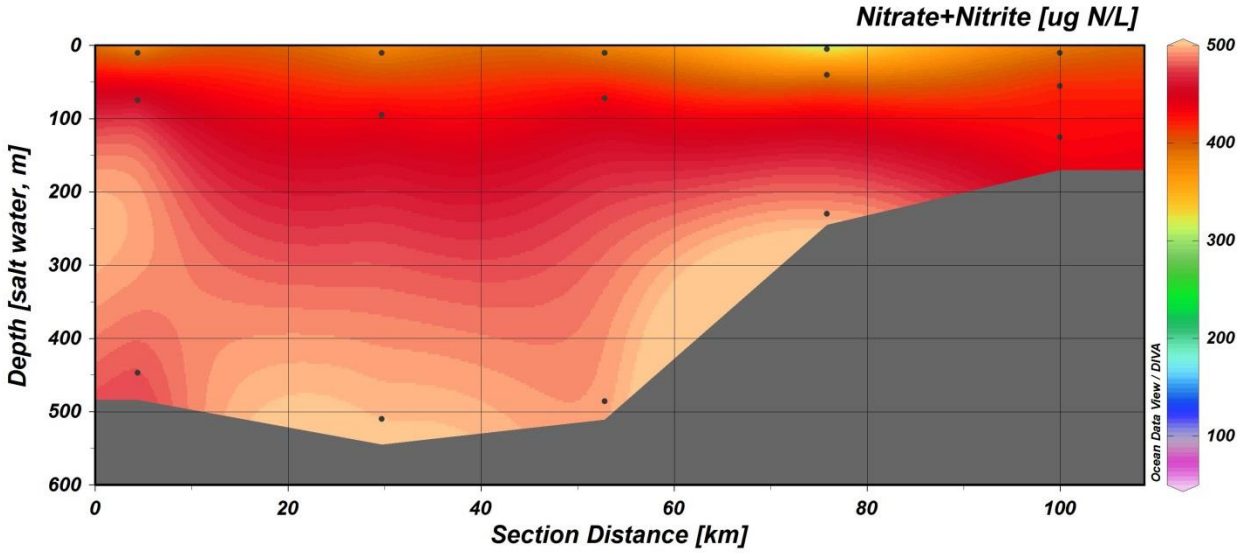
Nitrate+Nitrite [ug N/L]
Depth [salt water, m]
0
100
200
300
400
500
600
0
20
40
60
80
100
Section Distance [km]
500
400
300
200
100
Ocean Data View / DIVA

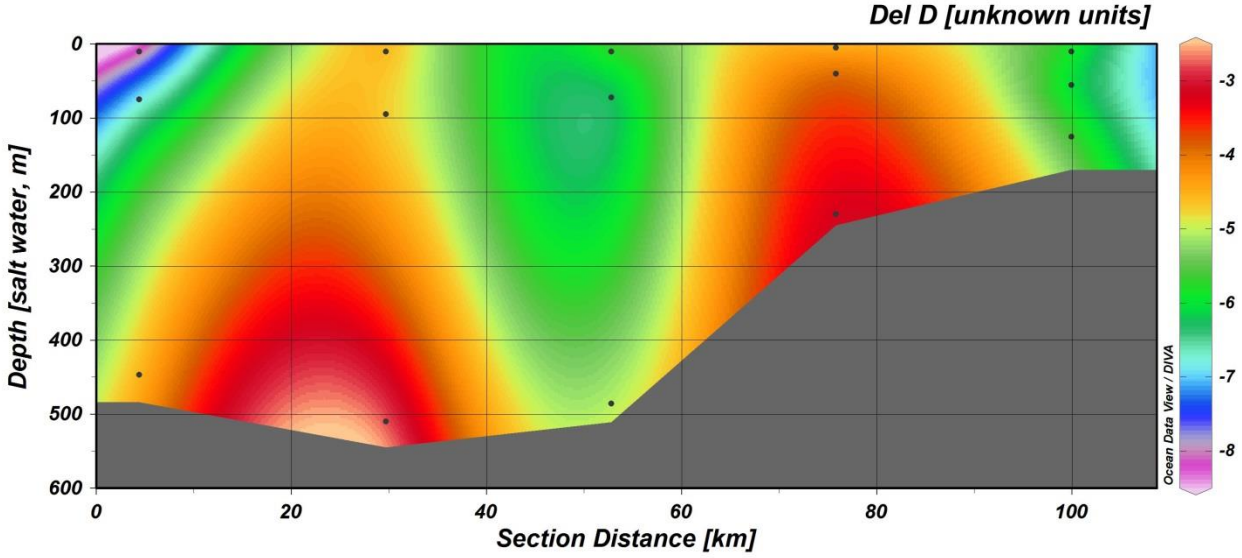
Del D [unknown units]
Depth [salt water, m]
0
100
200
300
400
500
600
0
20
40
60
80
100
Section Distance [km]
-3
-4
-5
-6
-7
-8
Ocean Data View / DIVA

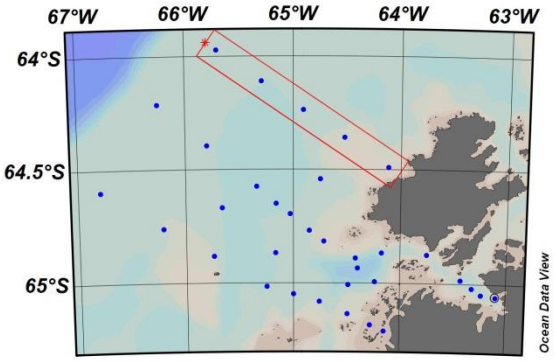
67°W
66°W
65°W
64°W
63°W
64°S
64.5°S
65°S
Ocean Data View

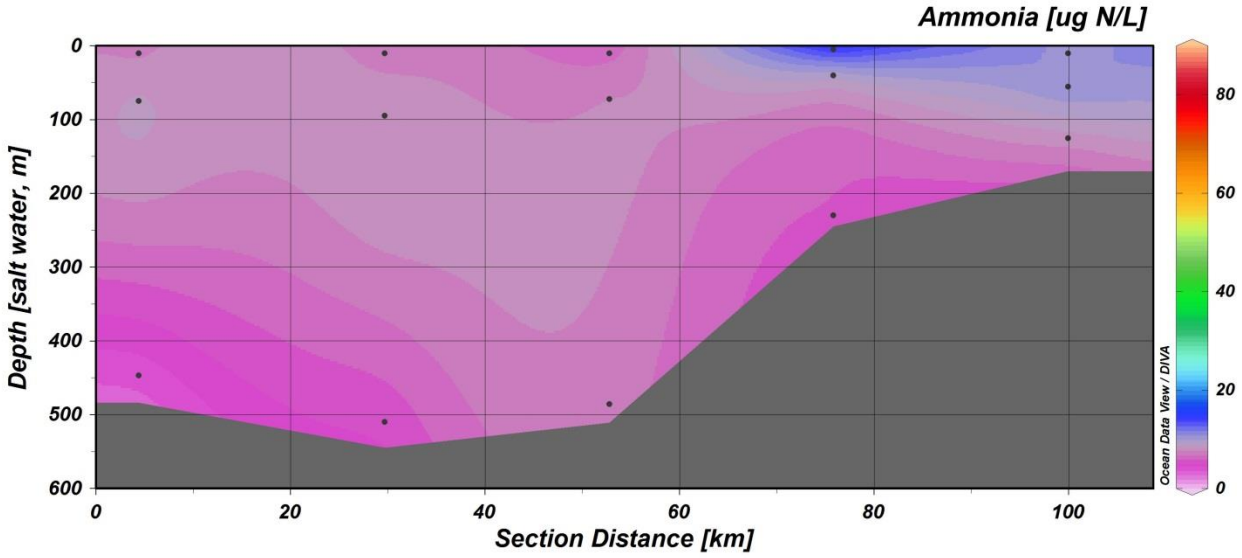
Ammonia [ug N/L]
Depth [salt water, m]
0
100
200
300
400
500
600
0
20
40
60
80
100
Section Distance [km]
Ocean Data View / DIVA
80
60
40
20
0

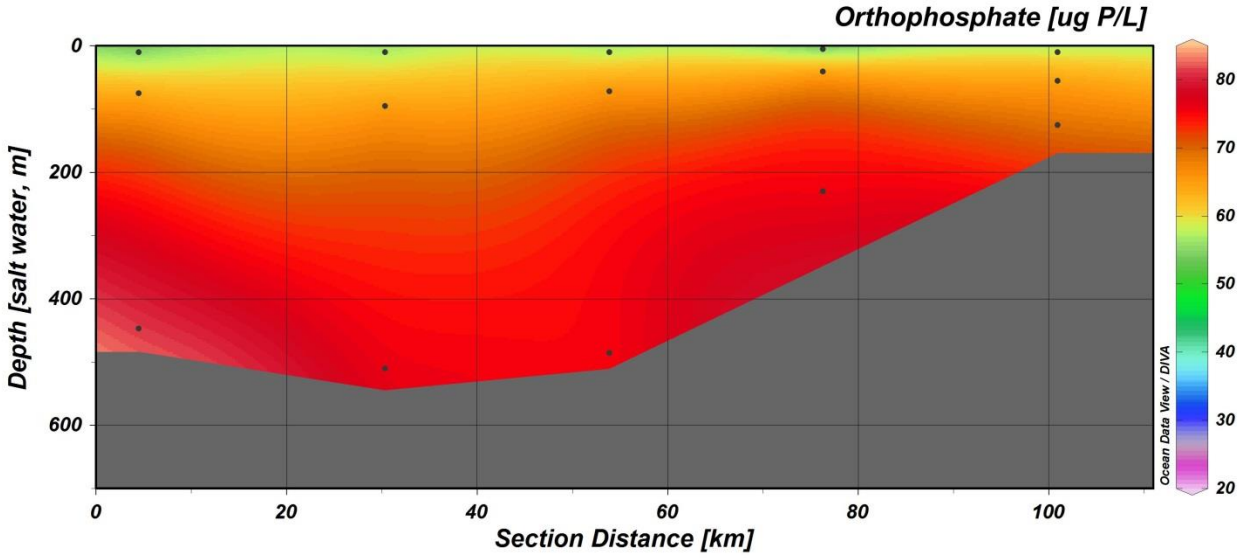
Orthophosphate [ug P/L]
Depth [salt water, m]
0
200
400
600
0
20
40
60
80
100
Section Distance [km]
Ocean Data View / DIVA
80
70
60
50
40
30
20

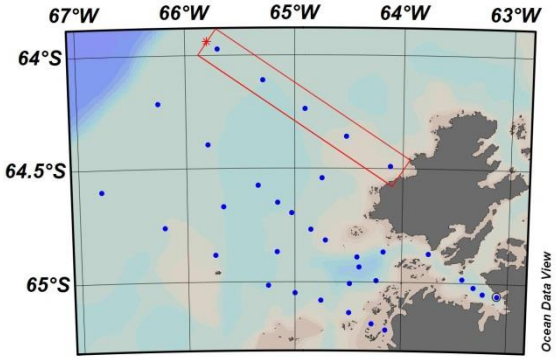
67°W
66°W
65°W
64°W
63°W
64°S
64.5°S
65°S
Ocean Data View

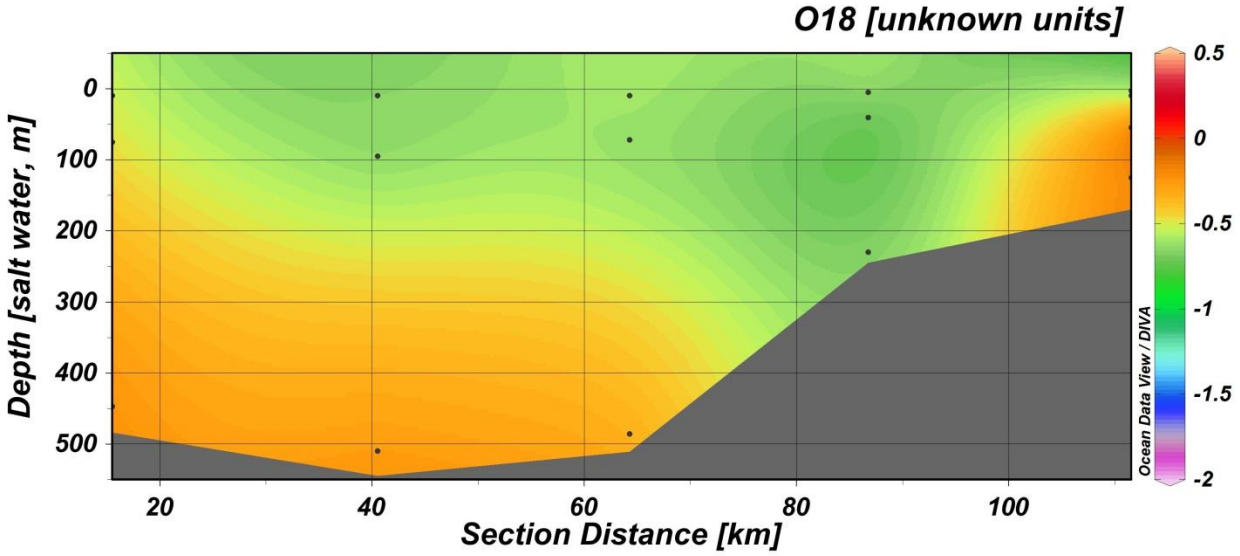
O18 [unknown units]
Depth [salt water, m]
0
100
200
300
400
500
20
40
60
80
100
Section Distance [km]
0.5
0
-0.5
-1
-1.5
-2
Ocean Data View / DIVA

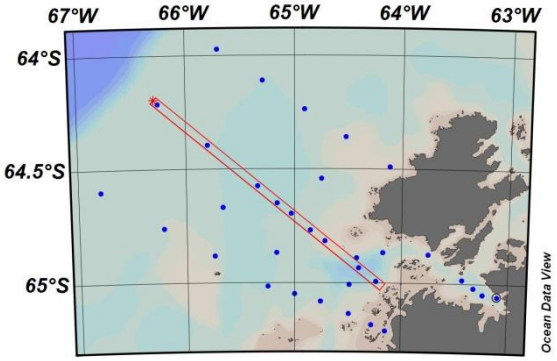
67°W
66°W
65°W
64°W
63°W
64°S
64.5°S
65°S
Ocean Data View

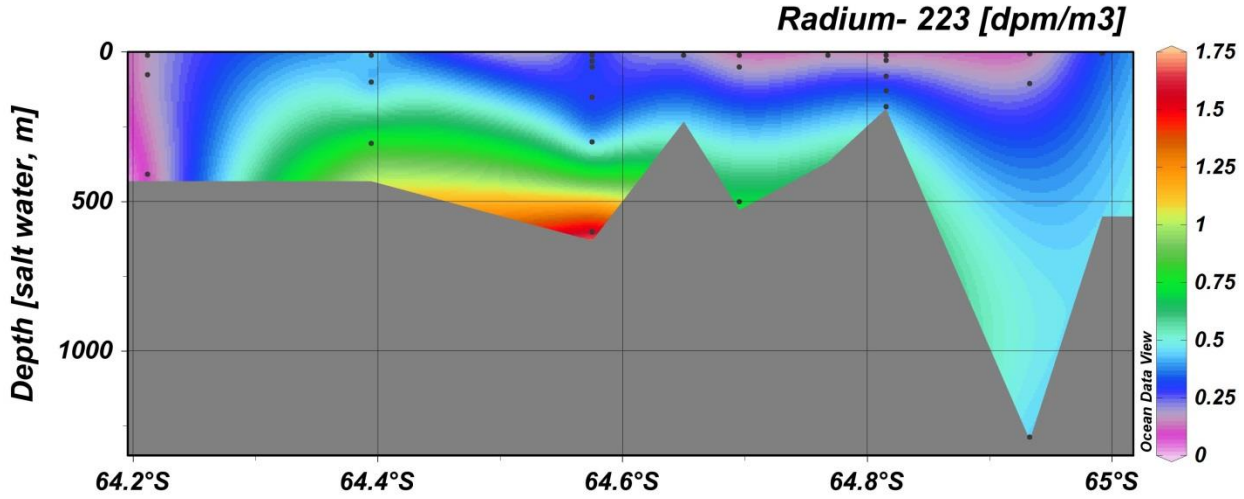
Radium- 223 [dpm/m3]
Depth [salt water, m]
0
500
1000
64.2°S
64.4°S
64.6°S
64.8°S
65°S
1.75
1.5
1.25
1
0.75
0.5
0.25
0
Ocean Data View

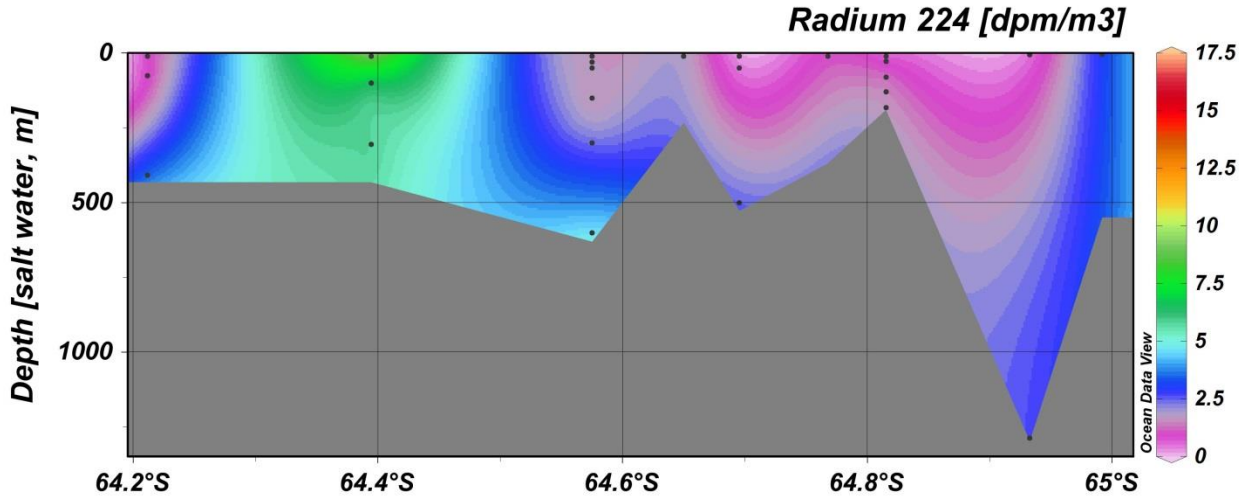
Radium 224 [dpm/m3]
Depth [salt water, m]
0
500
1000
64.2°S
64.4°S
64.6°S
64.8°S
65°S
17.5
15
12.5
10
7.5
5
2.5
0
Ocean Data View

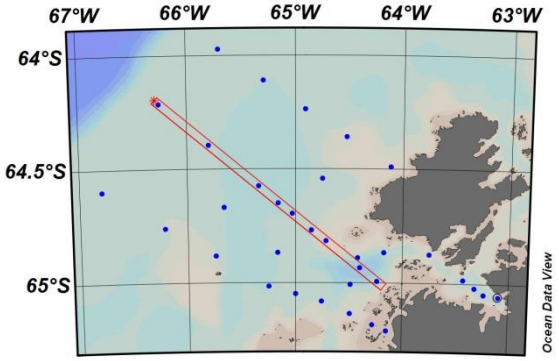
67°W
66°W
65°W
64°W
63°W
64°S
64.5°S
65°S
Ocean Data View

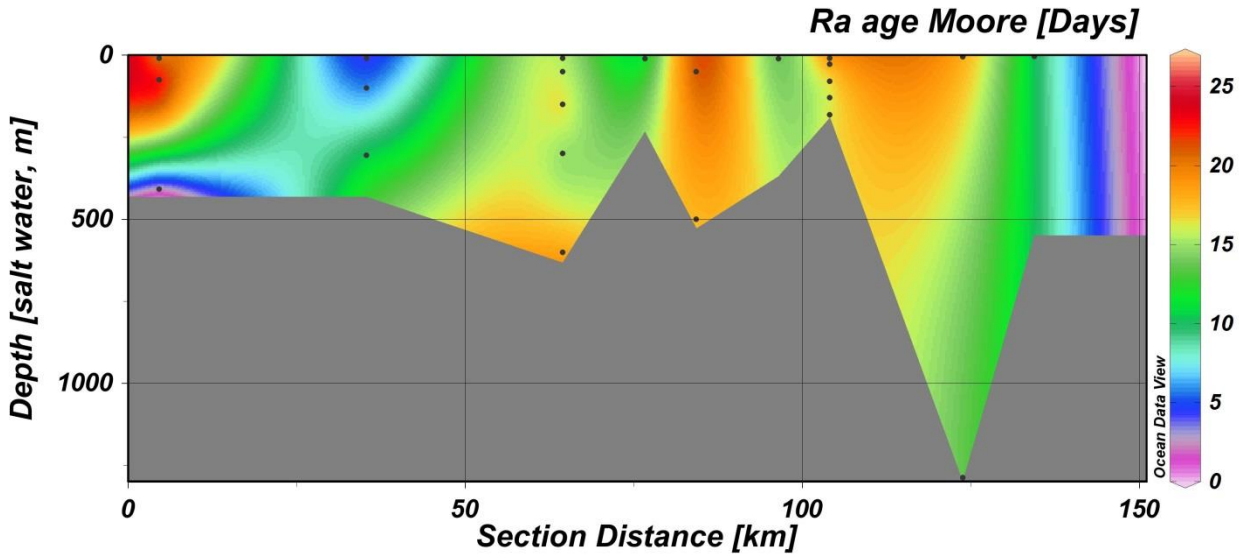
Ra age Moore [Days]
Depth [salt water, m]
0
500
1000
0
50
100
150
Section Distance [km]
25
20
15
10
5
0
Ocean Data View

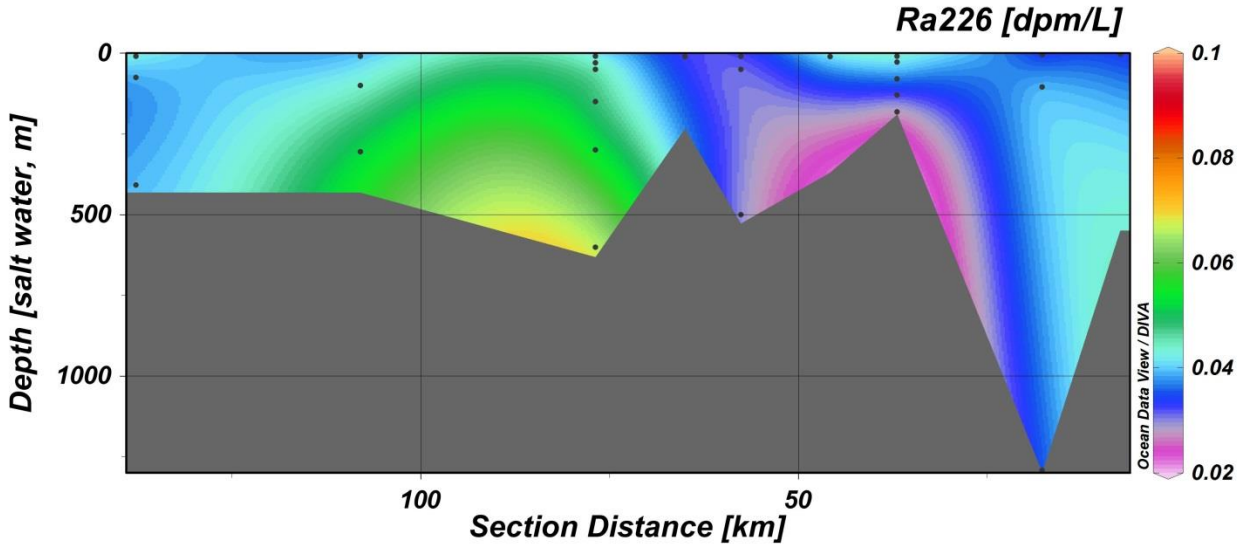
Ra226 [dpm/L]
Depth [salt water, m]
0
500
1000
100
50
Section Distance [km]
0.1
0.08
0.06
0.04
0.02
Ocean Data View / DIVA

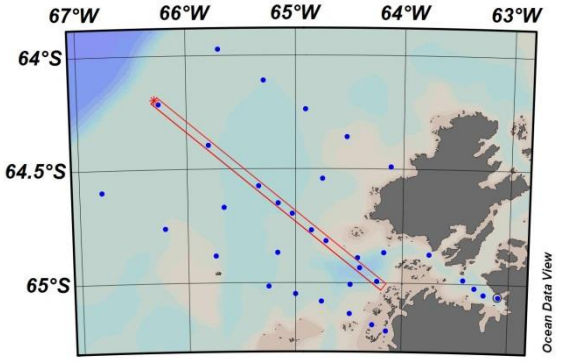
67°W
66°W
65°W
64°W
63°W
64°S
64.5°S
65°S
Ocean Data View

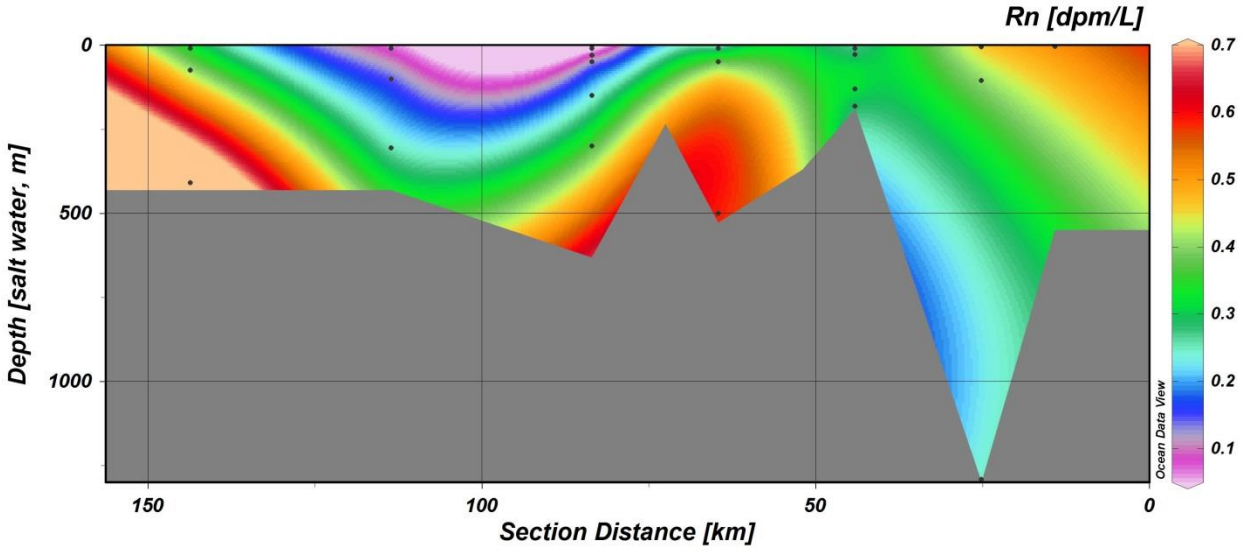
Rn [dpm/L]
Depth [salt water, m]
0
500
1000
150
100
50
0
Section Distance [km]
0.7
0.6
0.5
0.4
0.3
0.2
0.1
Ocean Data View

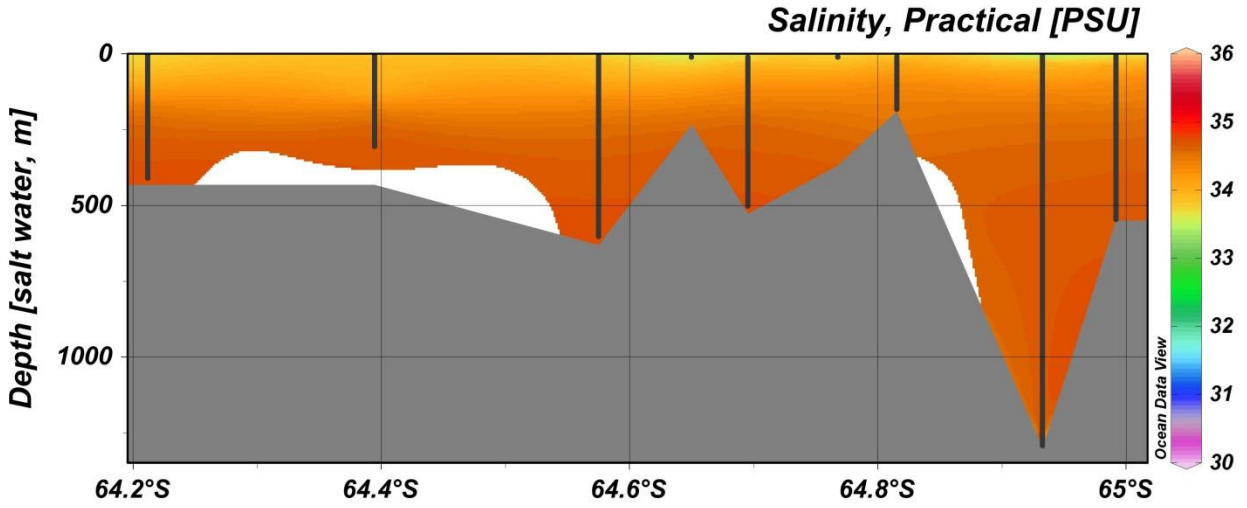
Salinity, Practical [PSU]
Depth [salt water, m]
0
500
1000
64.2°S
64.4°S
64.6°S
64.8°S
65°S
36
35
34
33
32
31
30
Ocean Data View

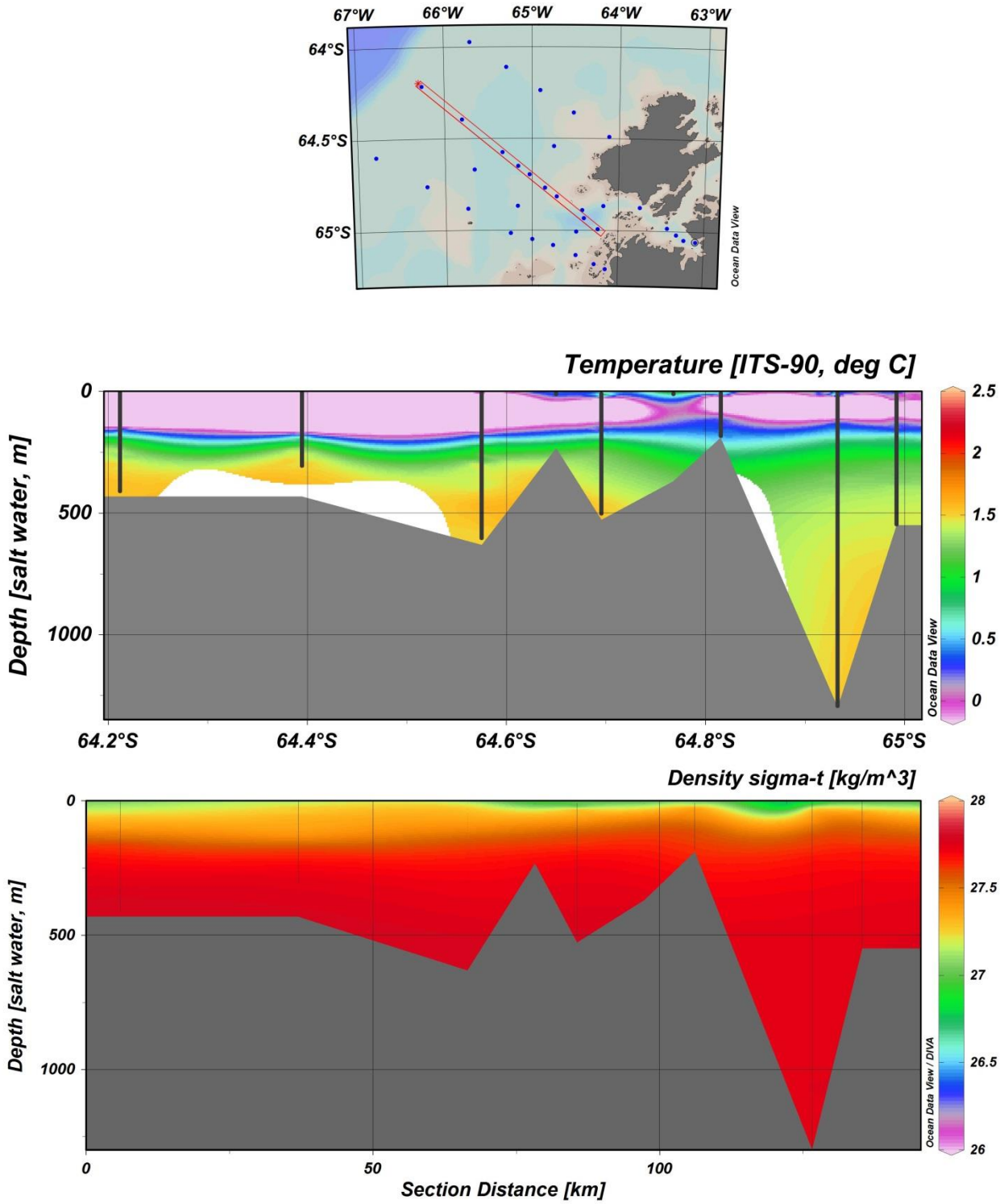
67°W
66°W
65°W
64°W
63°W
64°S
64.5°S
65°S
Ocean Data View
Temperature [ITS-90, deg C]
Depth [salt water, m]
0
500
1000
64.2°S
64.4°S
64.6°S
64.8°S
65°S
2.5
2
1.5
1
0.5
0
Ocean Data View
Density sigma-t [kg/m^3]
Depth [salt water, m]
0
500
1000
0
50
100
Section Distance [km]
28
27.5
27
26.5
26
Ocean Data View / DIVA

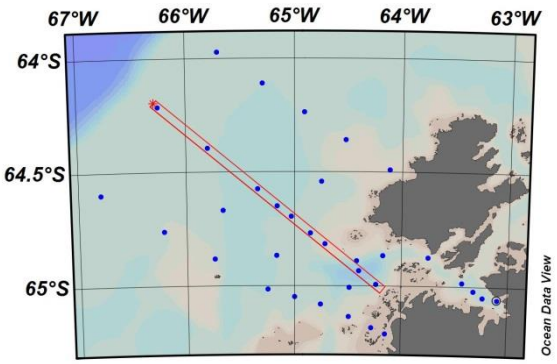
67°W
66°W
65°W
64°W
63°W
64°S
64.5°S
65°S
Ocean Data View

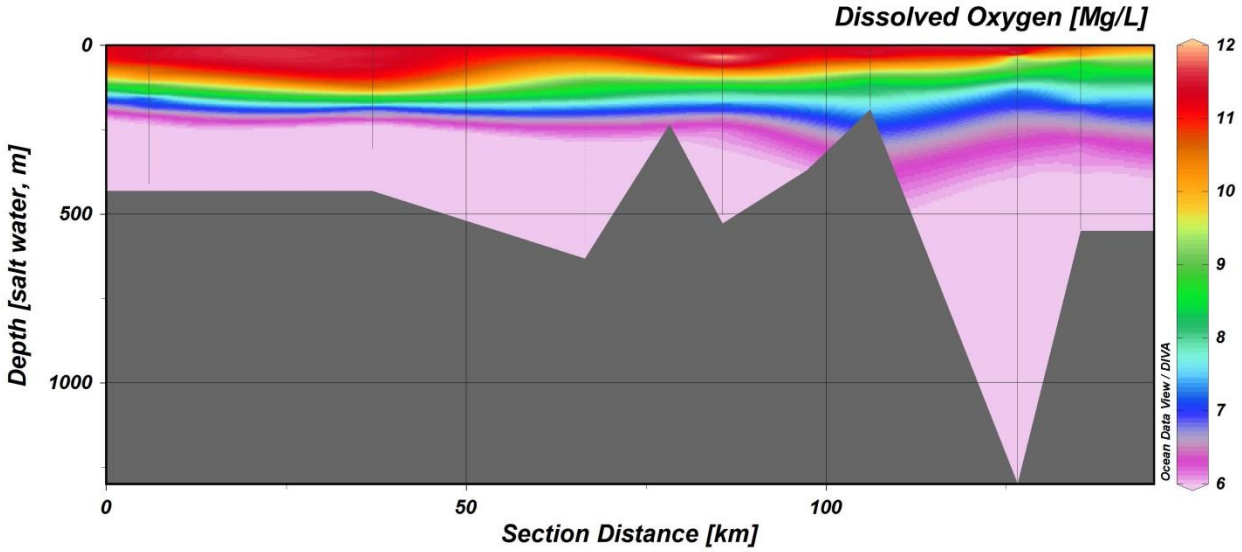
Dissolved Oxygen [Mg/L]
Depth [salt water, m]
0
500
1000
0
50
100
Section Distance [km]
12
11
10
9
8
7
6
Ocean Data View / DIVA

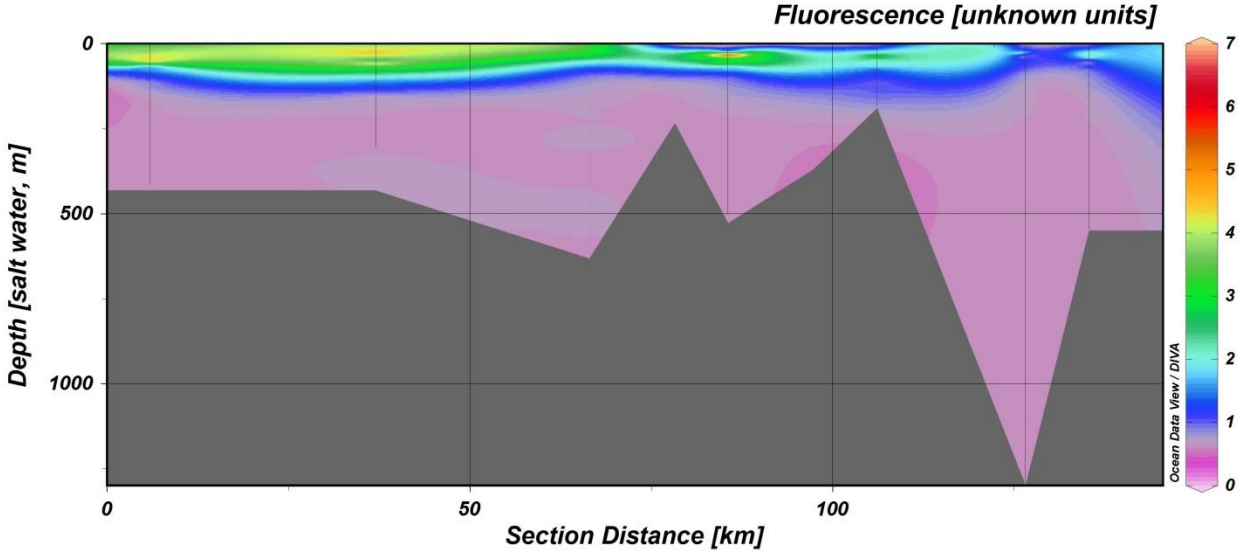
Fluorescence [unknown units]
Depth [salt water, m]
0
500
1000
0
50
100
Section Distance [km]
7
6
5
4
3
2
1
0
Ocean Data View / DIVA

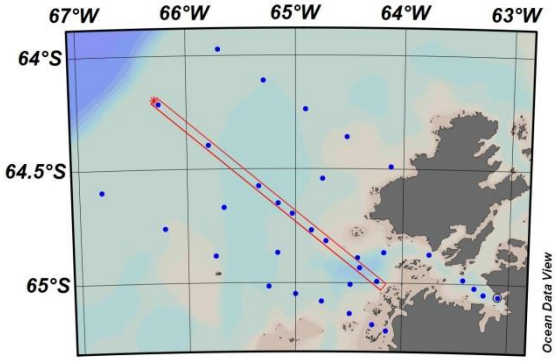
67°W
66°W
65°W
64°W
63°W
64°S
64.5°S
65°S
Ocean Data View

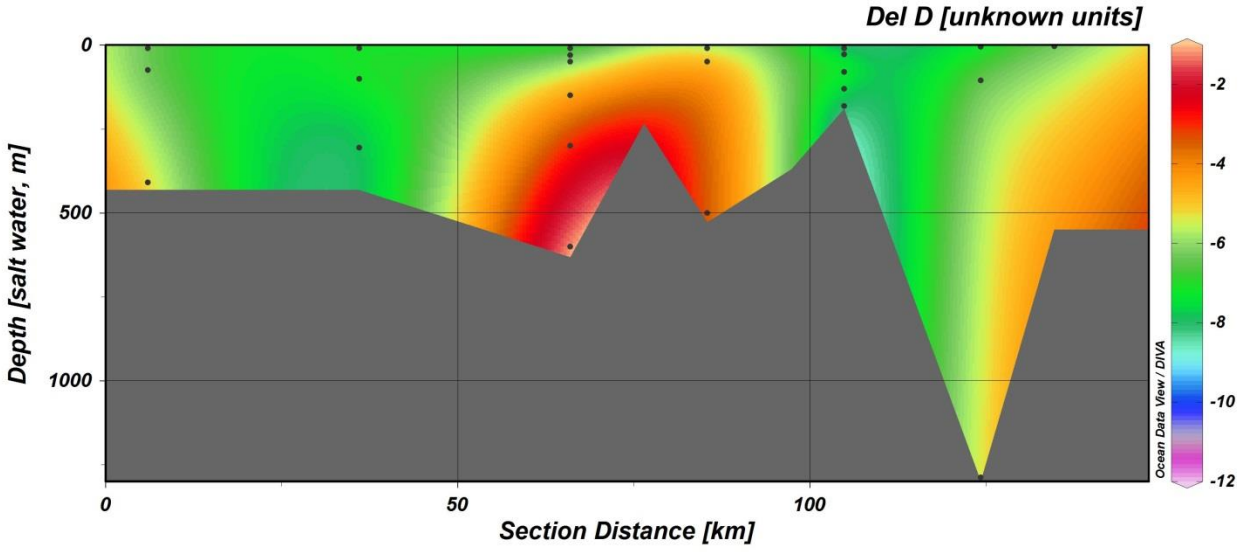
Del D [unknown units]
Depth [salt water, m]
0
500
1000
0
50
100
Section Distance [km]
-2
-4
-6
-8
-10
-12
Ocean Data View / DIVA

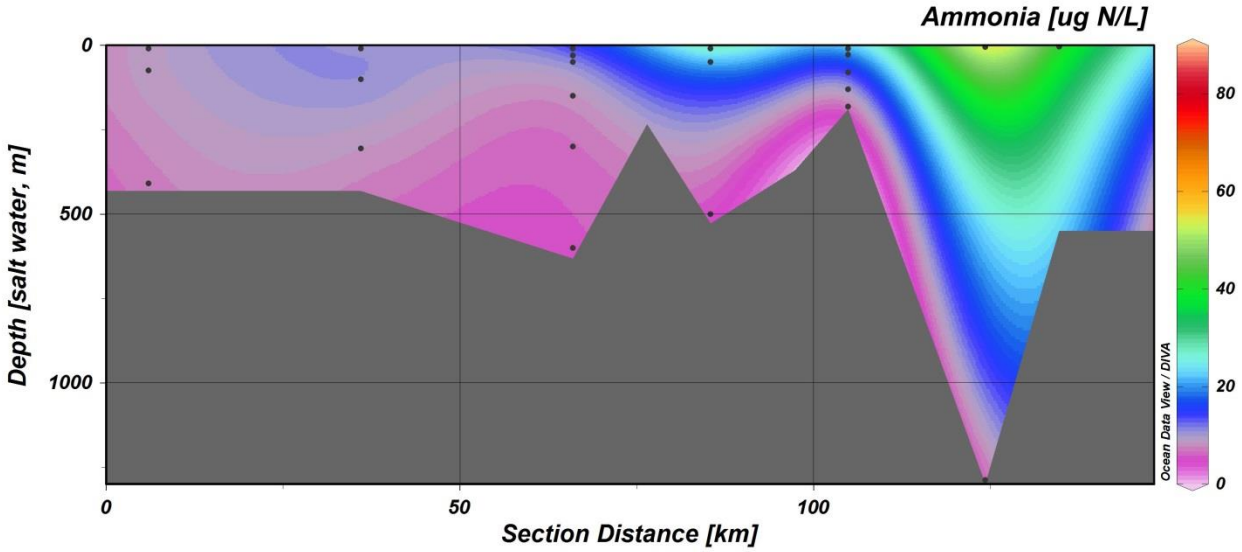
Ammonia [ug N/L]
Depth [salt water, m]
0
500
1000
0
50
100
Section Distance [km]
80
60
40
20
0
Ocean Data View / DIVA

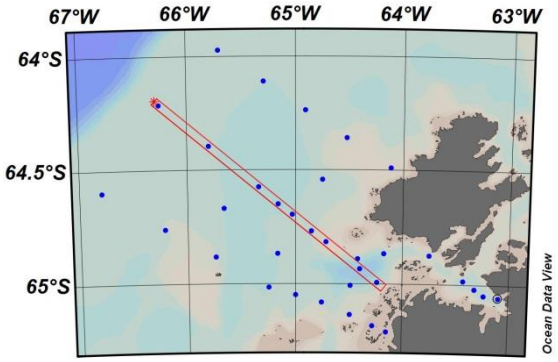
67°W
66°W
65°W
64°W
63°W
64°S
64.5°S
65°S
Ocean Data View

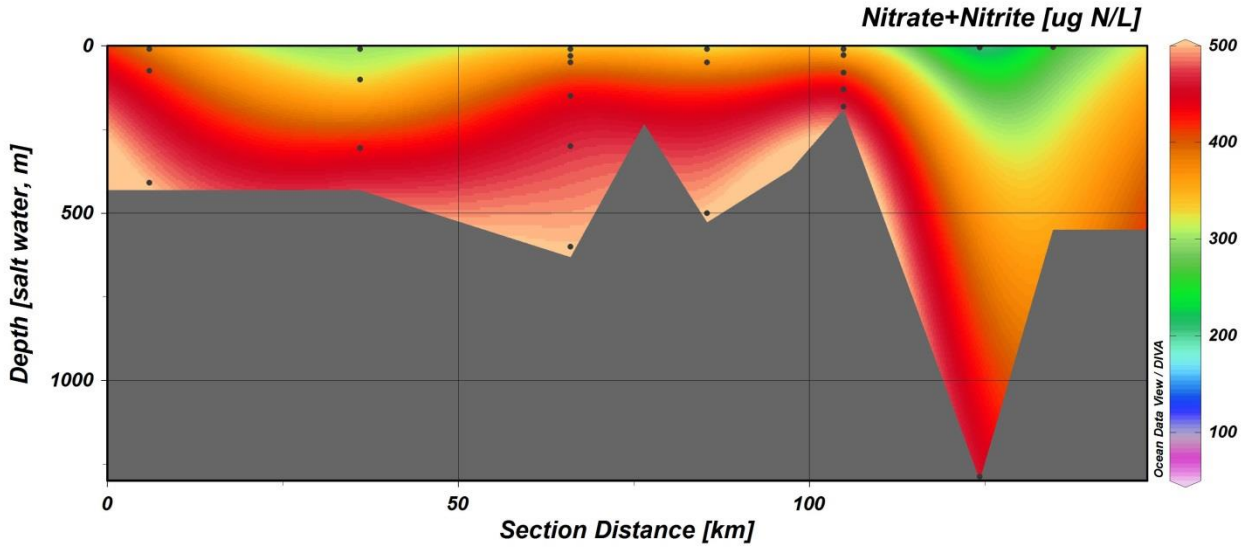
Nitrate+Nitrite [ug N/L]
Depth [salt water, m]
0
500
1000
0
50
100
Section Distance [km]
500
400
300
200
100
Ocean Data View / DIVA

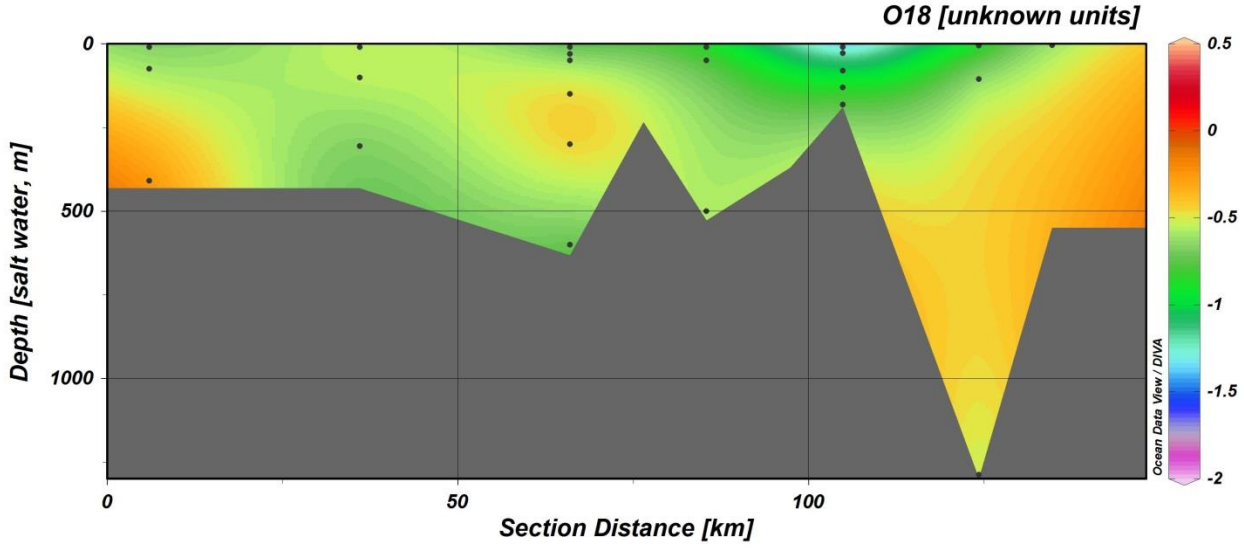
O18 [unknown units]
Depth [salt water, m]
0
500
1000
0
50
100
Section Distance [km]
0.5
0
-0.5
-1
-1.5
-2
Ocean Data View / DIVA

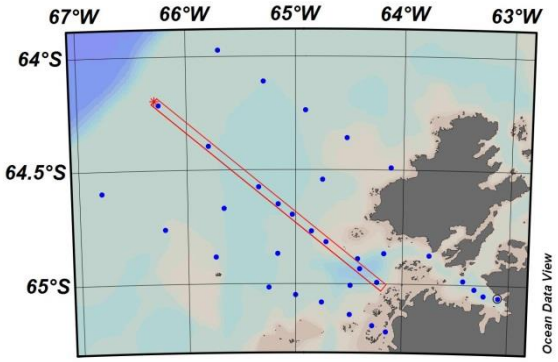
67°W
66°W
65°W
64°W
63°W
64°S
64.5°S
65°S
Ocean Data View

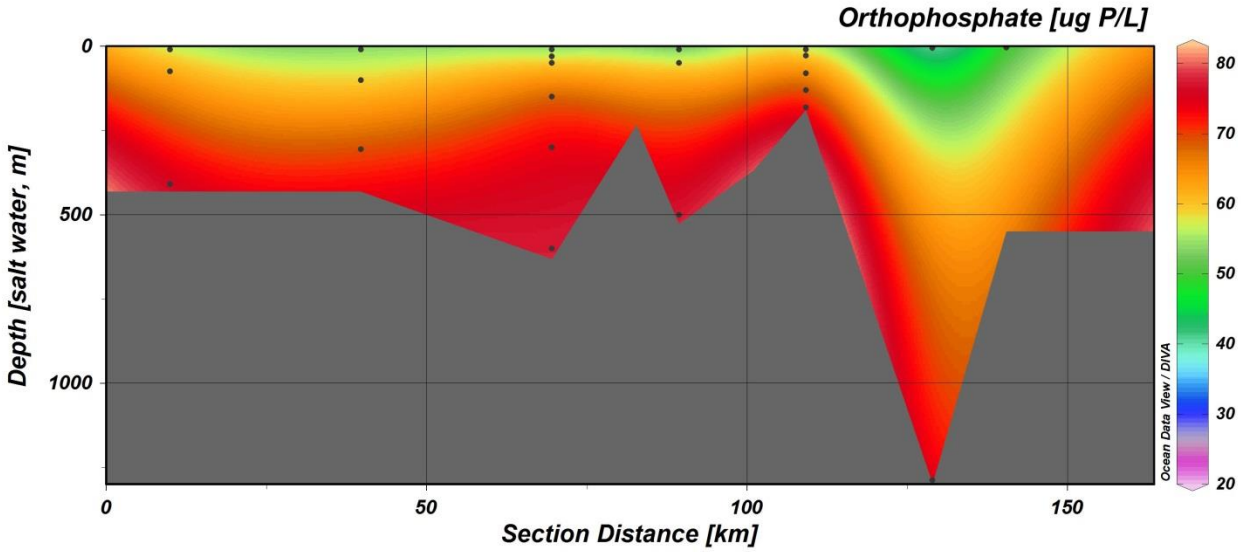
Orthophosphate [ug P/L]
Depth [salt water, m]
0
500
1000
0
50
100
150
Section Distance [km]
80
70
60
50
40
30
20
Ocean Data View / DIVA

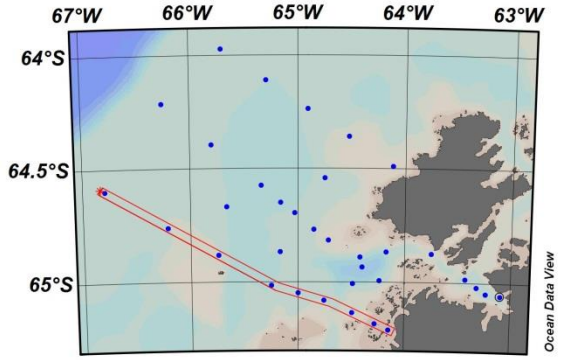
67°W
66°W
65°W
64°W
63°W
64°S
64.5°S
65°S
Ocean Data View

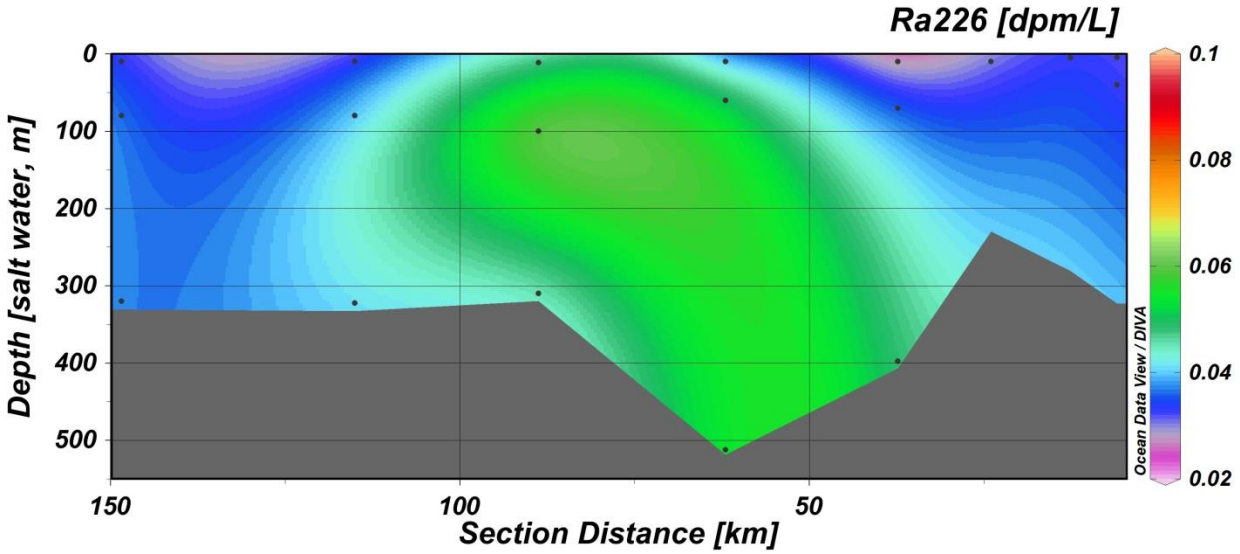
Ra226 [dpm/L]
Depth [salt water, m]
0
100
200
300
400
500
150
100
50
Section Distance [km]
0.1
0.08
0.06
0.04
0.02
Ocean Data View / DIVA

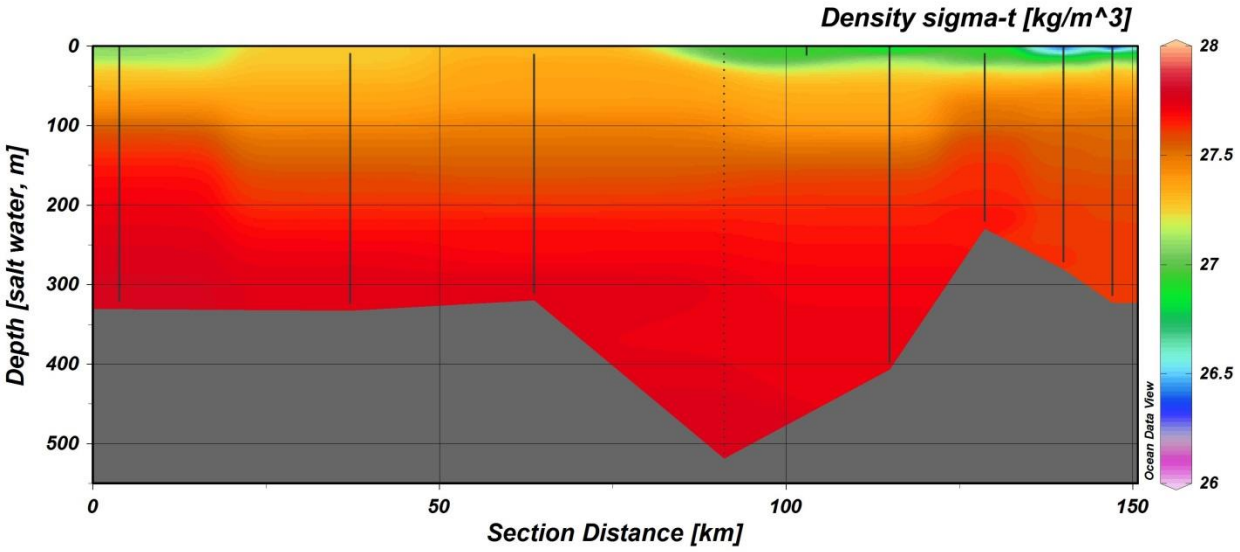
Density sigma-t [kg/m^3]
Depth [salt water, m]
0
100
200
300
400
500
0
50
100
150
Section Distance [km]
28
27.5
27
26.5
26
Ocean Data View

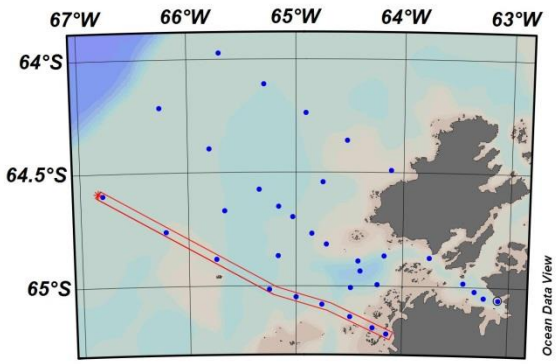
67°W
66°W
65°W
64°W
63°W
64°S
64.5°S
65°S
Ocean Data View

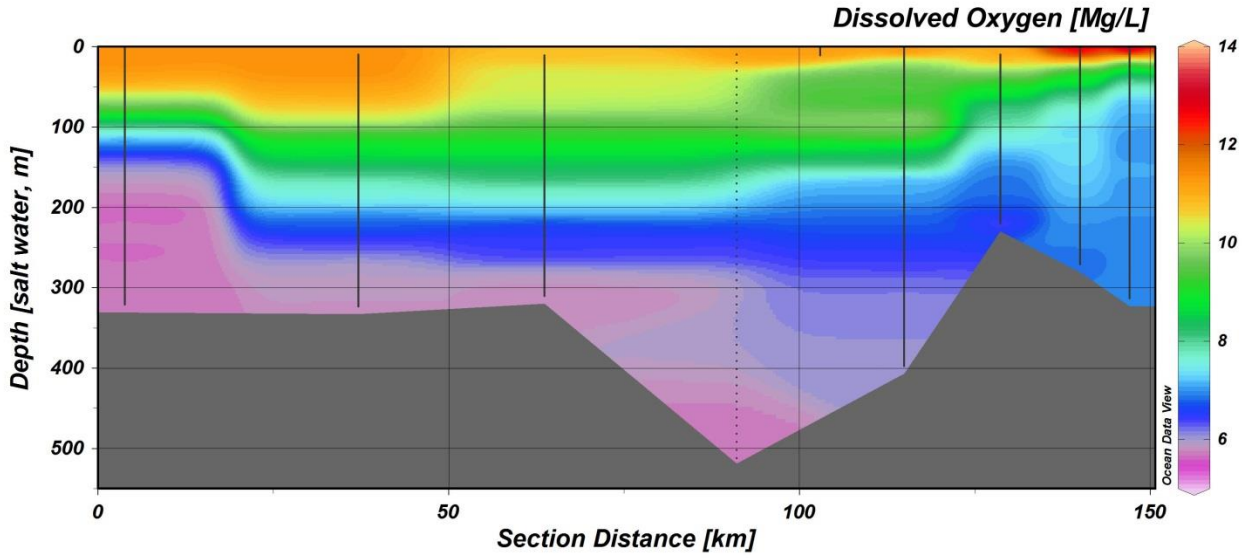
Dissolved Oxygen [Mg/L]
Depth [salt water, m]
0
100
200
300
400
500
0
50
100
150
Section Distance [km]
14
12
10
8
6
Ocean Data View

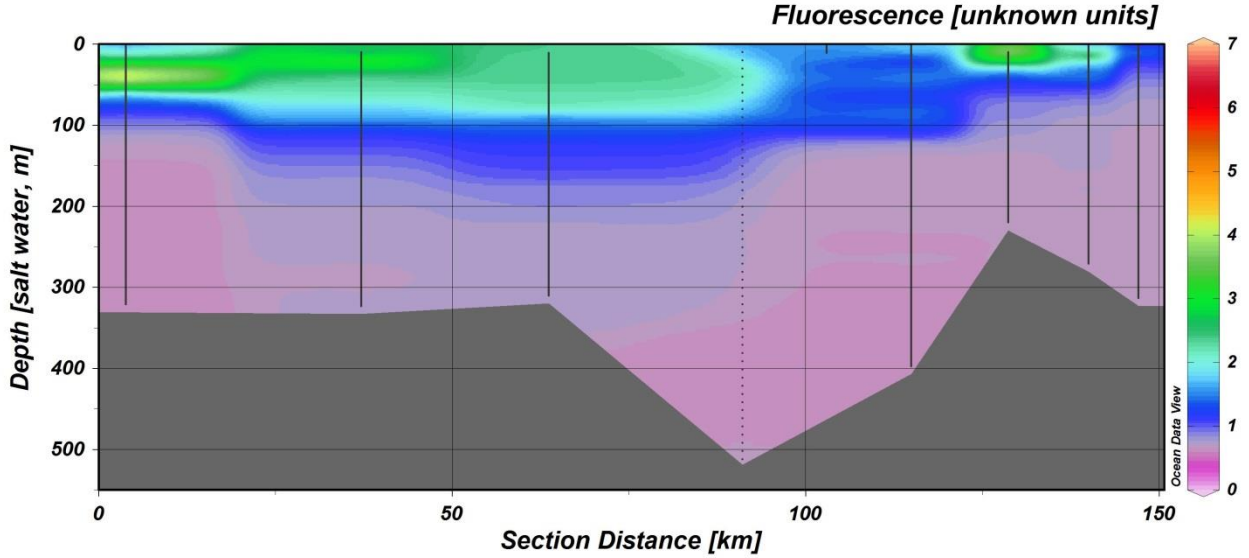
Fluorescence [unknown units]
Depth [salt water, m]
0
100
200
300
400
500
0
50
100
150
Section Distance [km]
7
6
5
4
3
2
1
0
Ocean Data View

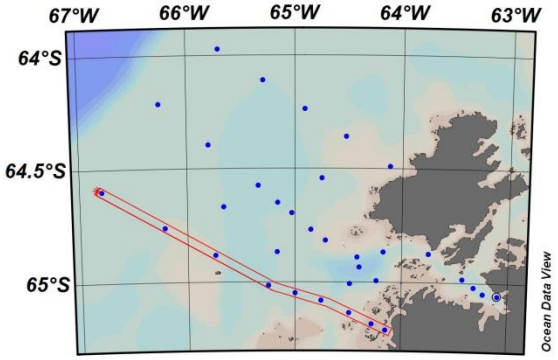
67°W
66°W
65°W
64°W
63°W
64°S
64.5°S
65°S
Ocean Data View

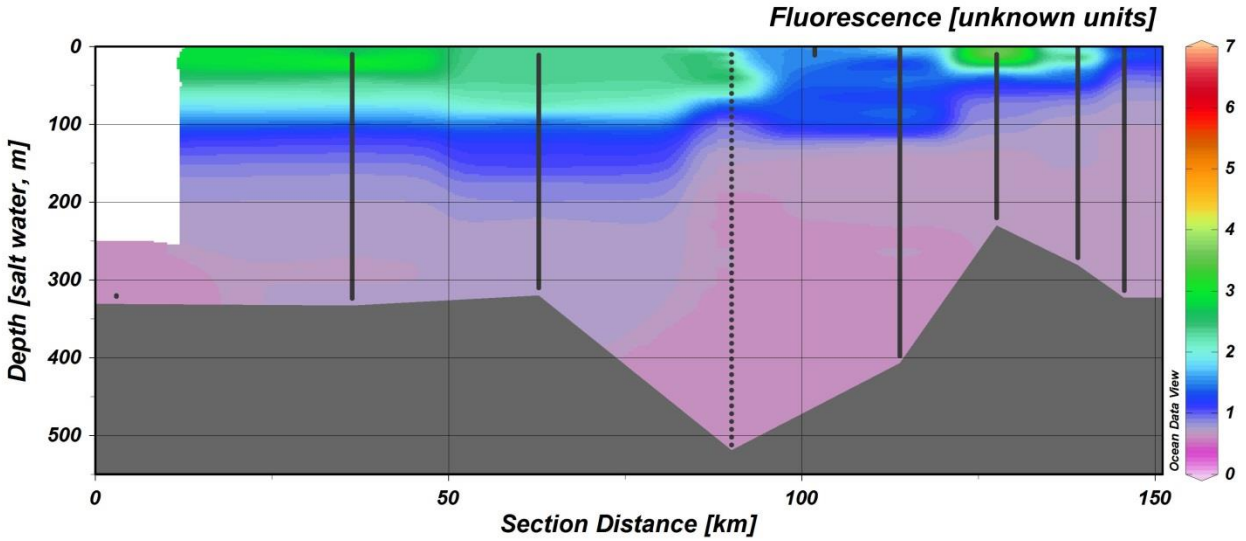
Fluorescence [unknown units]
Depth [salt water, m]
0
100
200
300
400
500
0
50
100
150
Section Distance [km]
7
6
5
4
3
2
1
0
Ocean Data View

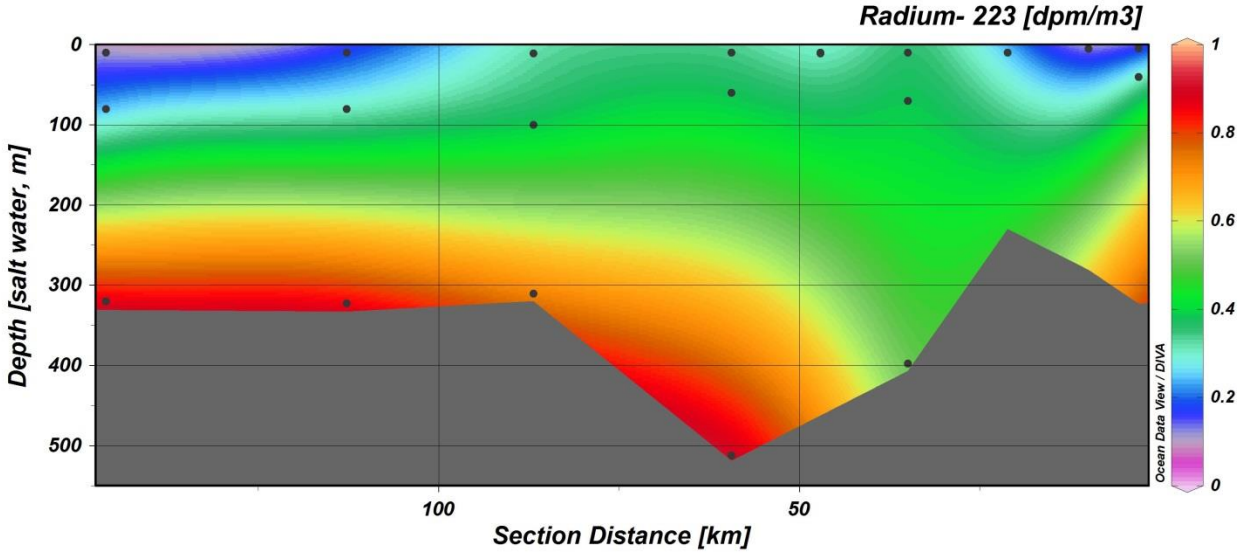
Radium- 223 [dpm/m3]
Depth [salt water, m]
0
100
200
300
400
500
100
50
Section Distance [km]
1
0.8
0.6
0.4
0.2
0
Ocean Data View / DIVA

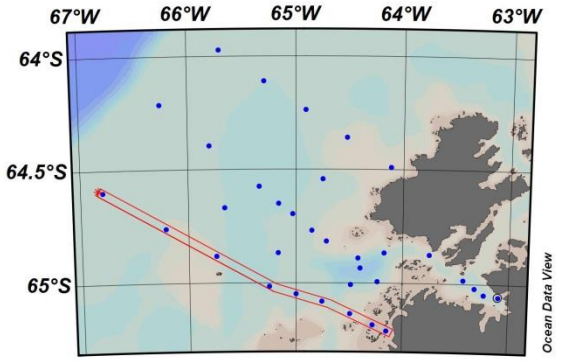
67°W
66°W
65°W
64°W
63°W
64°S
64.5°S
65°S
Ocean Data View

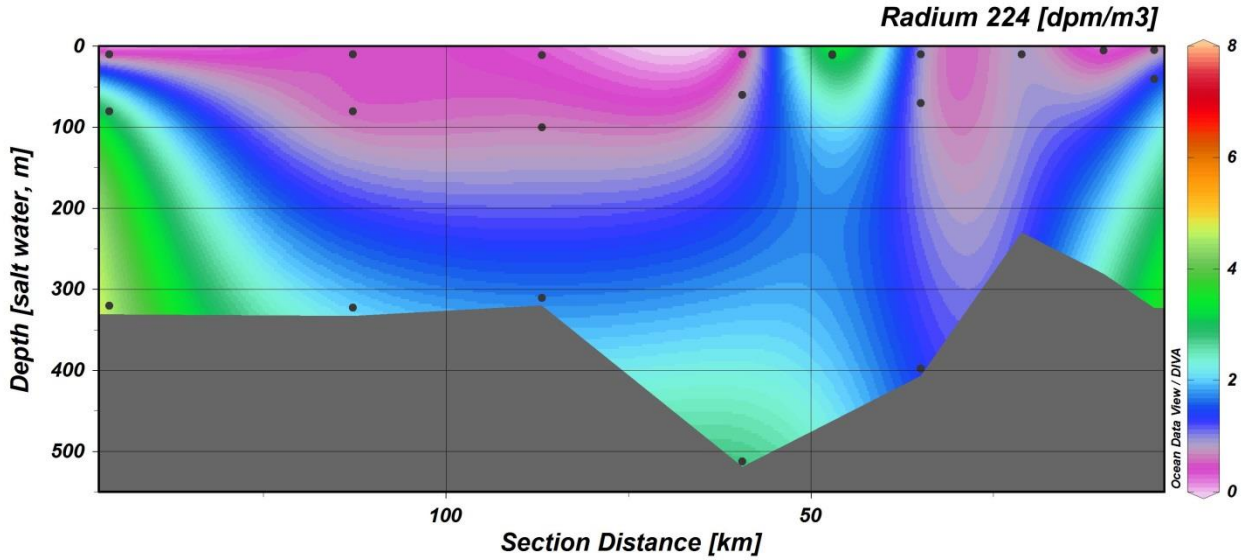
Radium 224 [dpm/m3]
Depth [salt water, m]
0
100
200
300
400
500
100
50
Section Distance [km]
8
6
4
2
0
Ocean Data View / DIVA

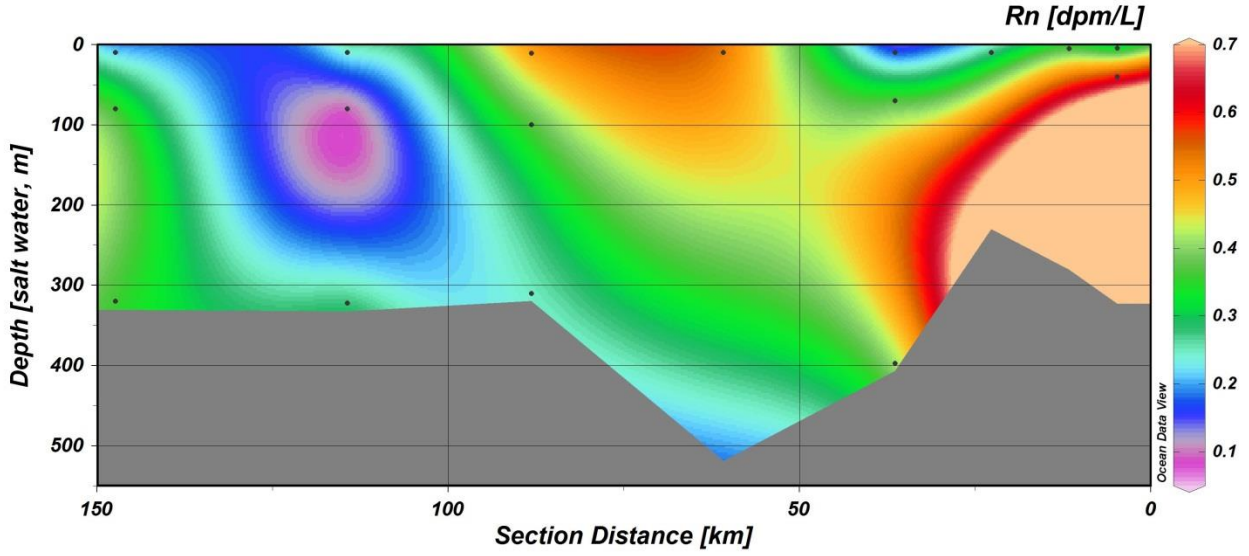
Rn [dpm/L]
Depth [salt water, m]
0
100
200
300
400
500
150
100
50
0
Section Distance [km]
0.7
0.6
0.5
0.4
0.3
0.2
0.1
Ocean Data View

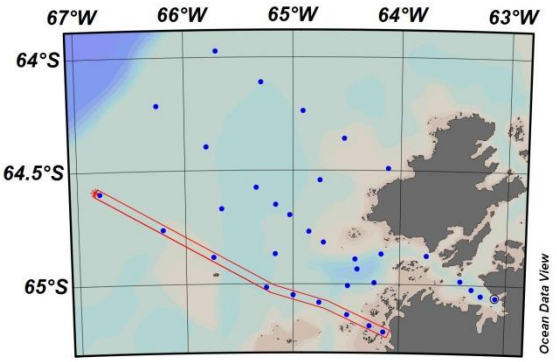
67°W
66°W
65°W
64°W
63°W
64°S
64.5°S
65°S
Ocean Data View

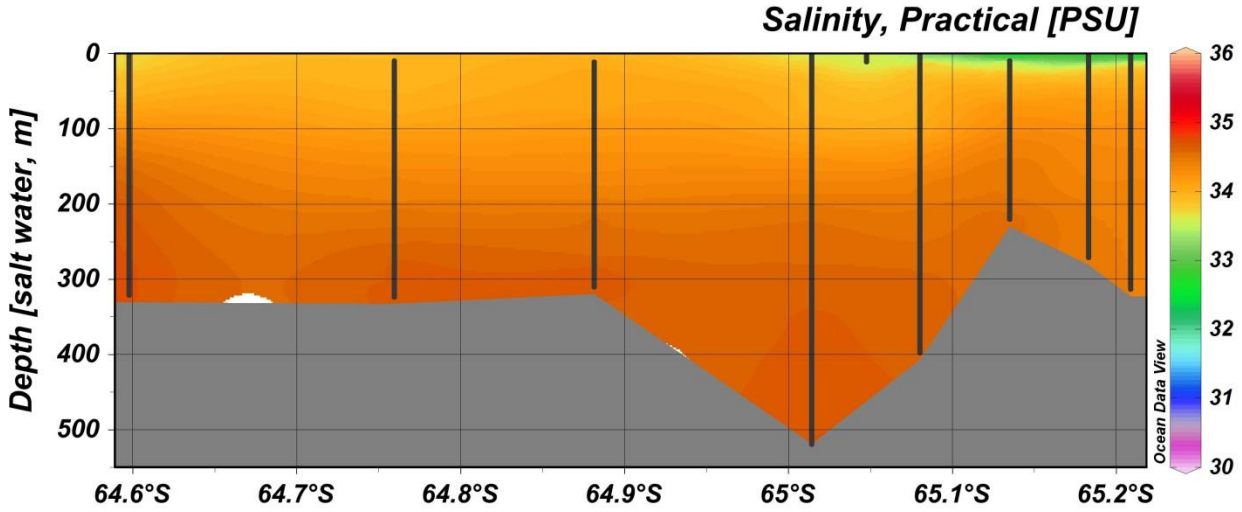
Salinity, Practical [PSU]
Depth [salt water, m]
0
100
200
300
400
500
64.6°S
64.7°S
64.8°S
64.9°S
65°S
65.1°S
65.2°S
36
35
34
33
32
31
30
Ocean Data View

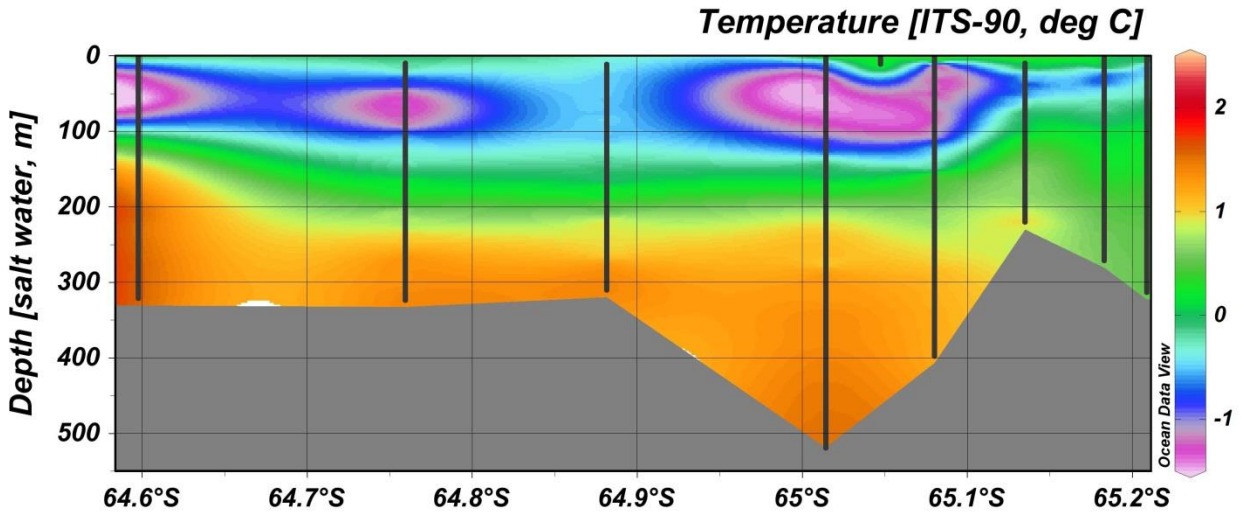
Temperature [ITS-90, deg C]
Depth [salt water, m]
0
100
200
300
400
500
64.6°S
64.7°S
64.8°S
64.9°S
65°S
65.1°S
65.2°S
2
1
0
-1
Ocean Data View

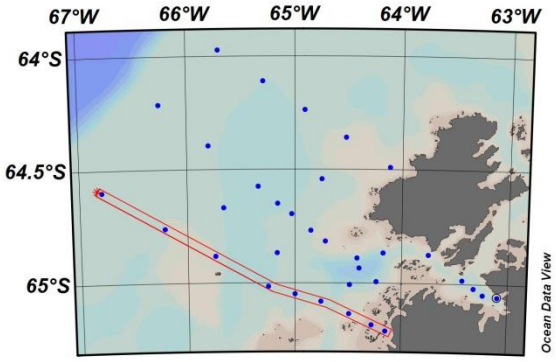
67°W
66°W
65°W
64°W
63°W
64°S
64.5°S
65°S
Ocean Data View

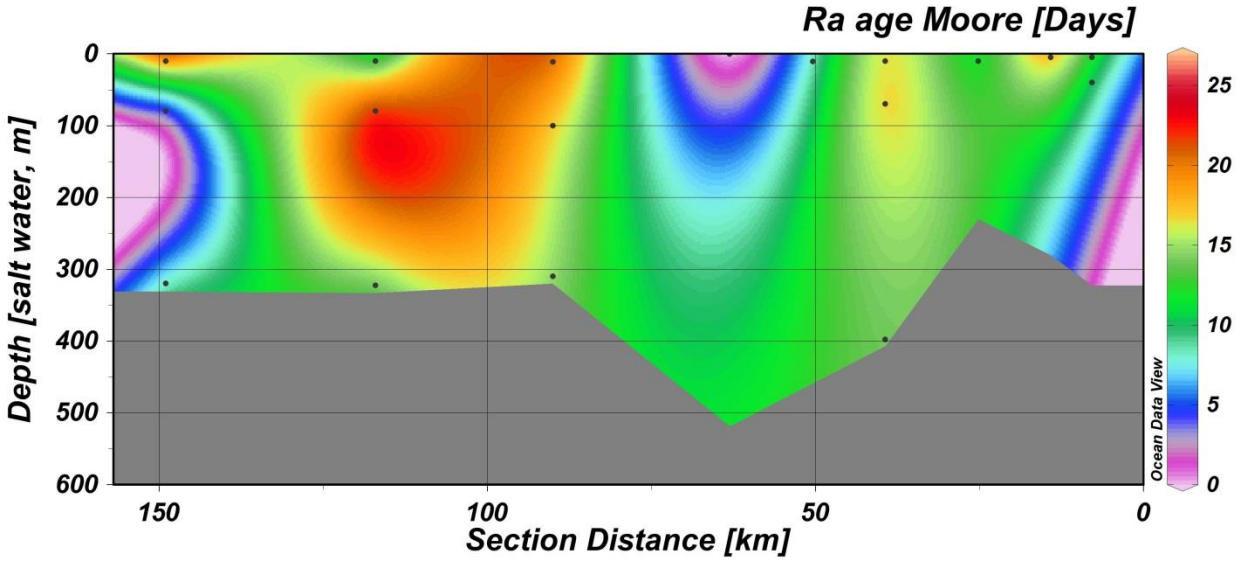
Ra age Moore [Days]
Depth [salt water, m]
0
100
200
300
400
500
600
150
100
50
0
Section Distance [km]
25
20
15
10
5
0
Ocean Data View

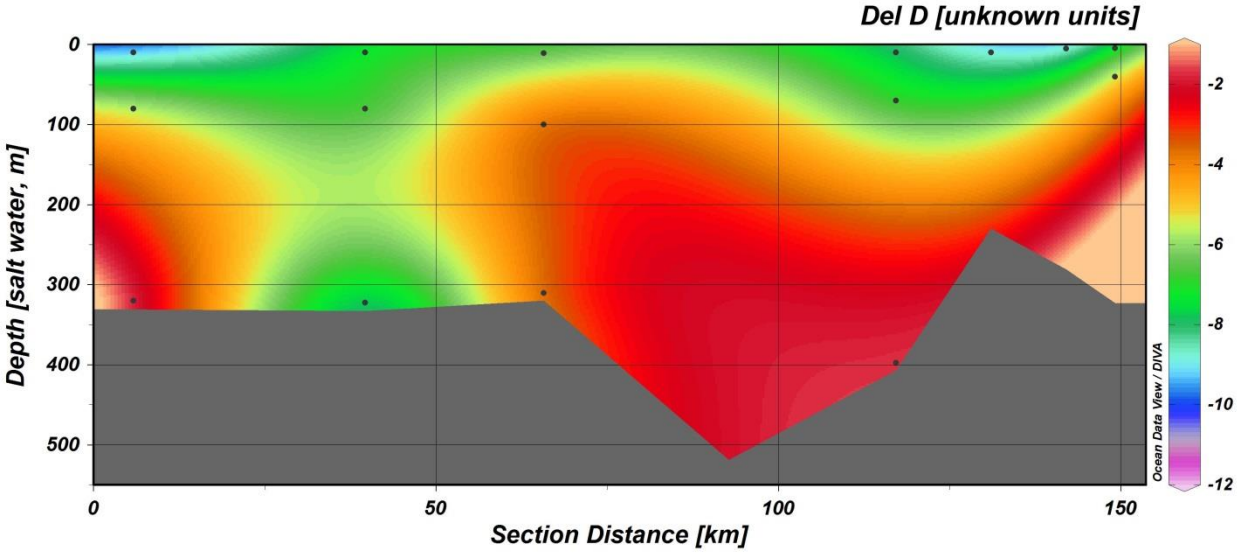
Del D [unknown units]
Depth [salt water, m]
0
100
200
300
400
500
0
50
100
150
Section Distance [km]
-2
-4
-6
-8
-10
-12
Ocean Data View / DIVA

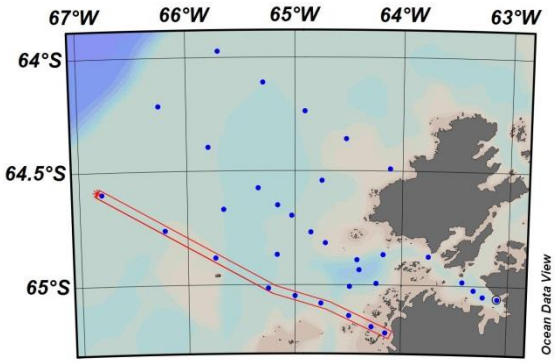
67°W
66°W
65°W
64°W
63°W
64°S
64.5°S
65°S
Ocean Data View

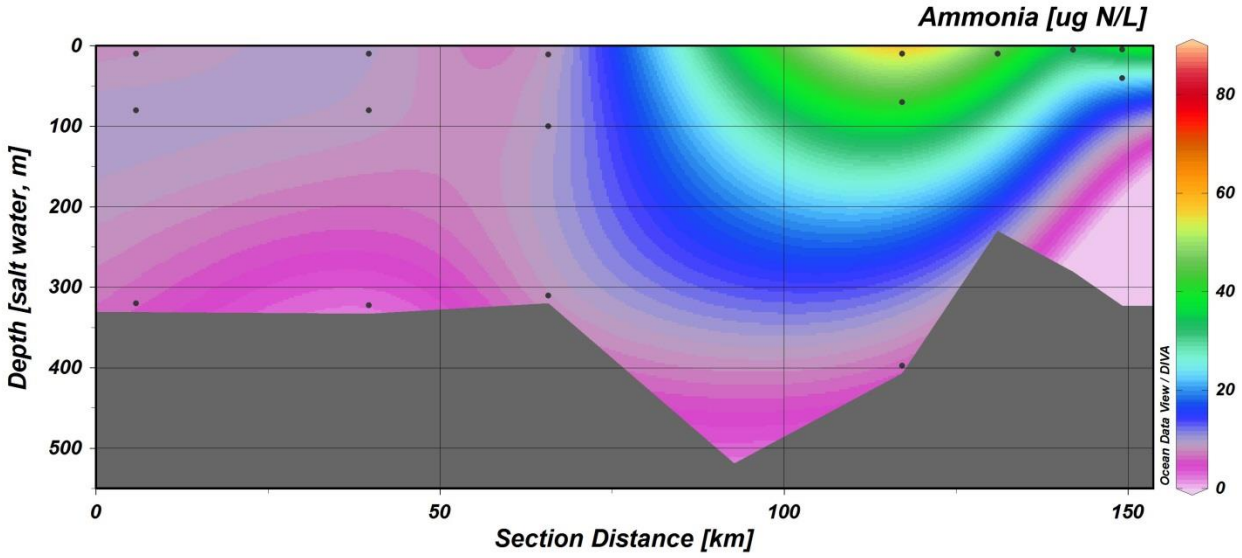
Ammonia [ug N/L]
Depth [salt water, m]
0
100
200
300
400
500
0
50
100
150
Section Distance [km]
80
60
40
20
0
Ocean Data View / DIVA

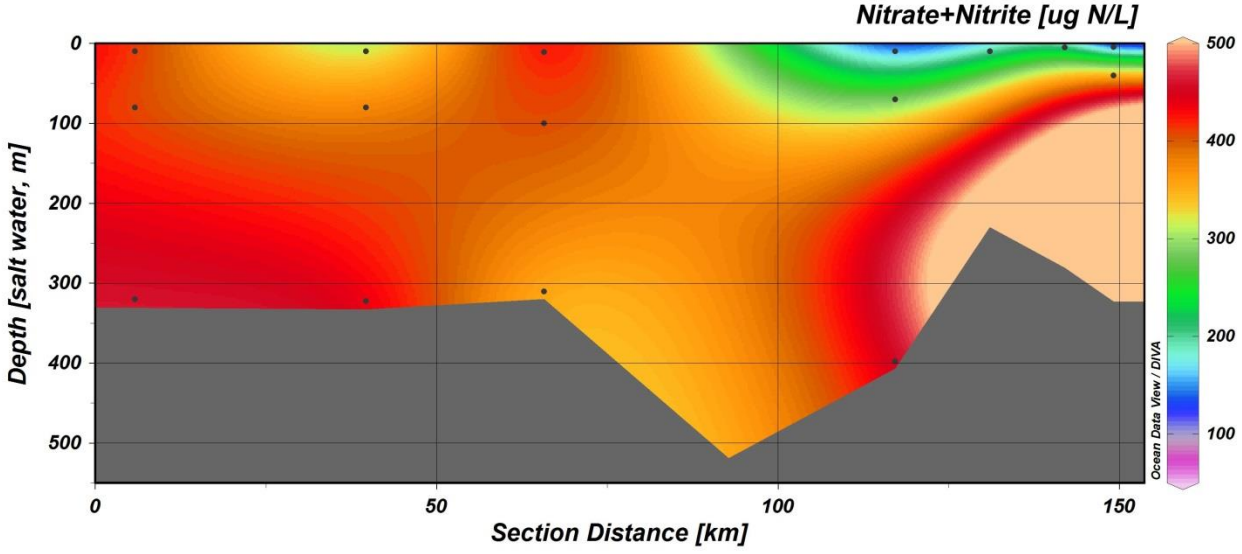
Nitrate+Nitrite [ug N/L]
Depth [salt water, m]
0
100
200
300
400
500
0
50
100
150
Section Distance [km]
500
400
300
200
100
Ocean Data View / DIVA

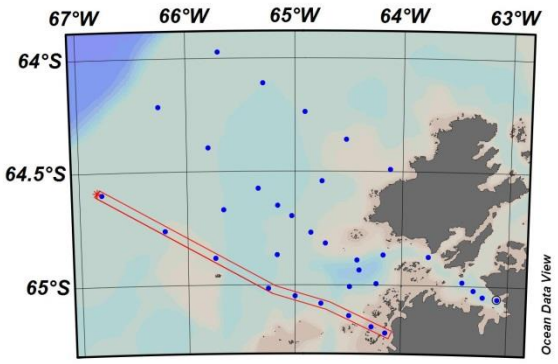
67°W
66°W
65°W
64°W
63°W
64°S
64.5°S
65°S
Ocean Data View

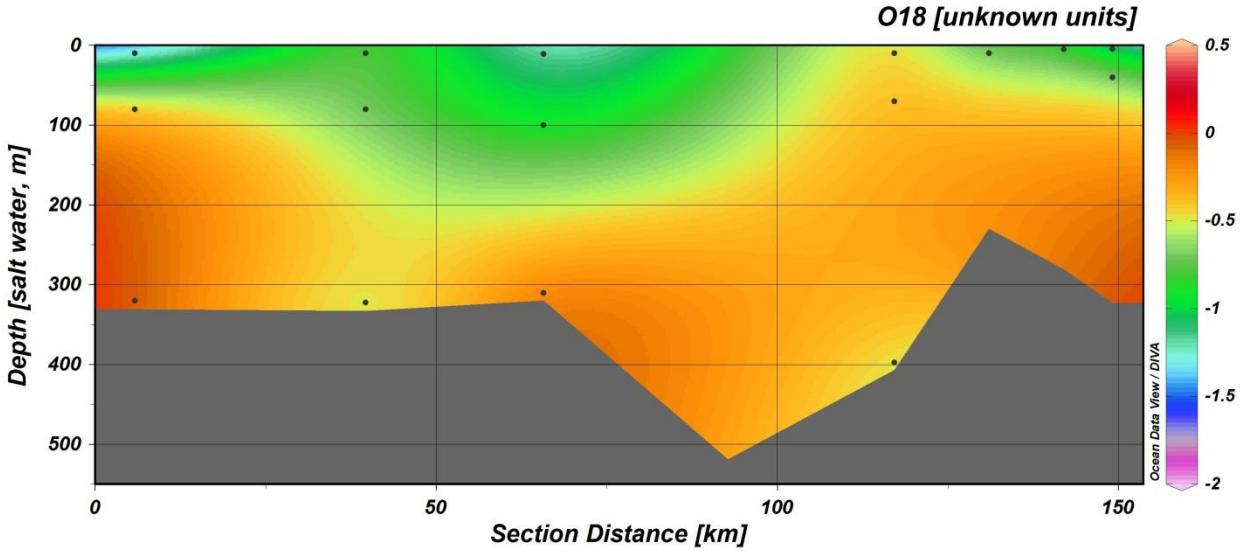
O18 [unknown units]
Depth [salt water, m]
0
100
200
300
400
500
0
50
100
150
Section Distance [km]
0.5
0
-0.5
-1
-1.5
-2
Ocean Data View / DIVA

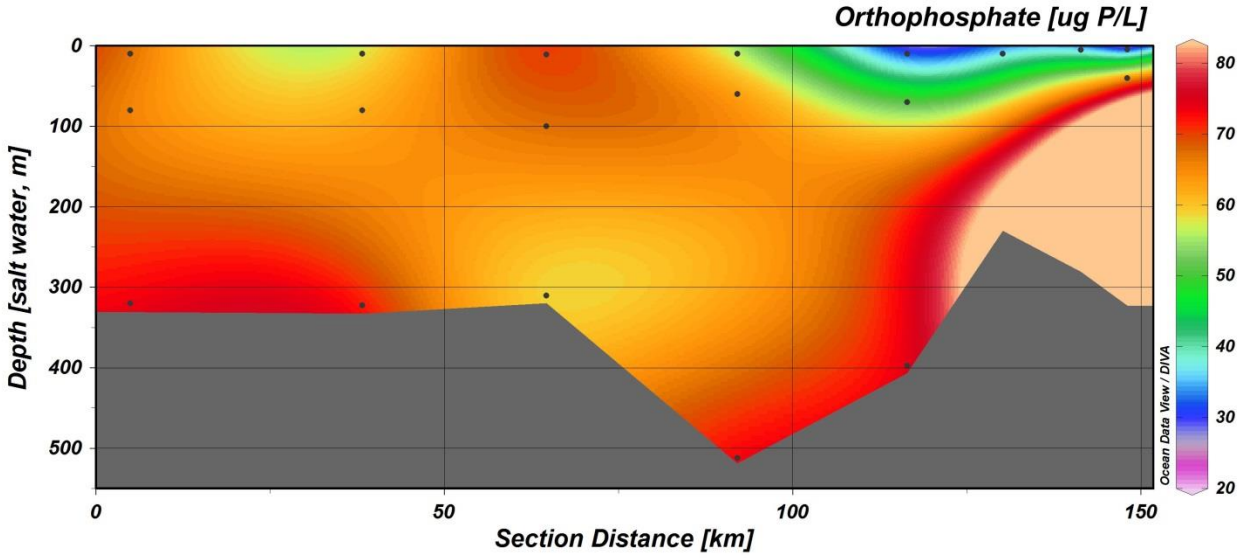
Orthophosphate [ug P/L]
Depth [salt water, m]
0
100
200
300
400
500
0
50
100
150
Section Distance [km]
80
70
60
50
40
30
20
Ocean Data View / DIVA

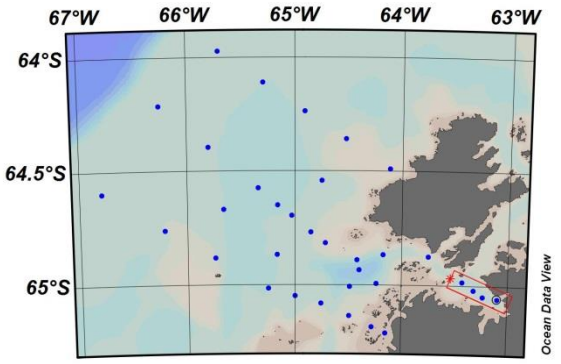
67°W
66°W
65°W
64°W
63°W
64°S
64.5°S
65°S
Ocean Data View

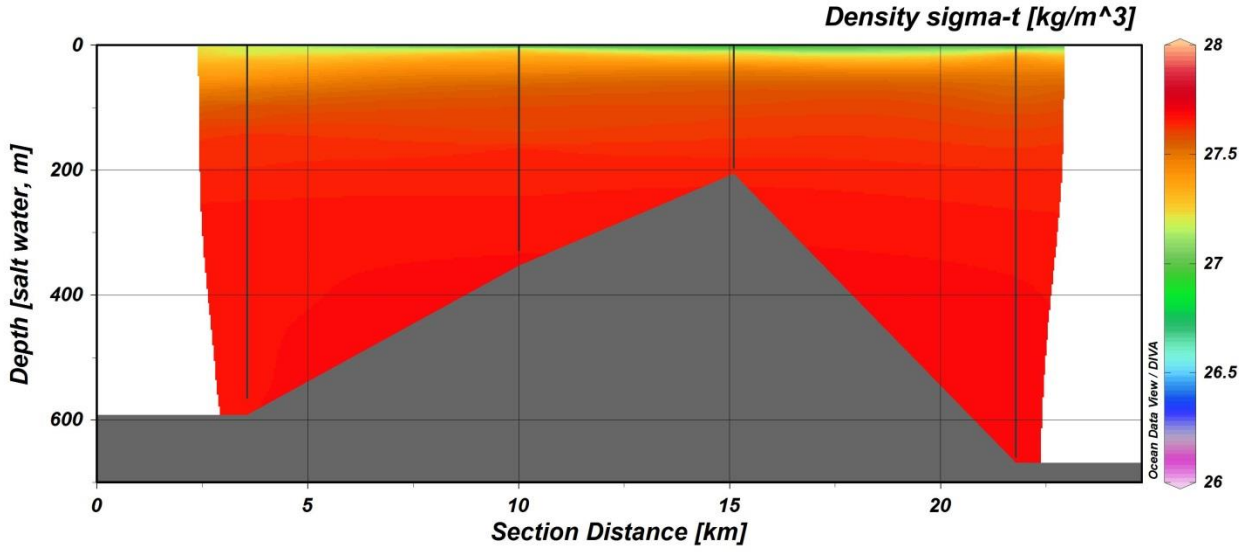
Density sigma-t [kg/m^3]
Depth [salt water, m]
0
200
400
600
0
5
10
15
20
Section Distance [km]
28
27.5
27
26.5
26
Ocean Data View / DIVA

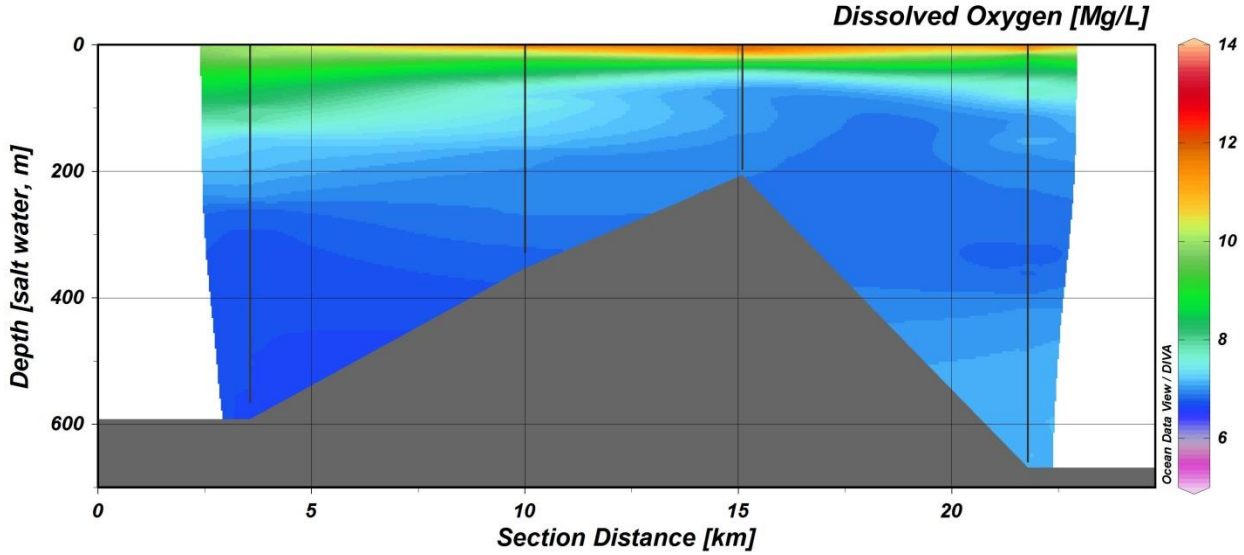
Dissolved Oxygen [Mg/L]
Depth [salt water, m]
0
200
400
600
0
5
10
15
20
Section Distance [km]
14
12
10
8
6
Ocean Data View / DIVA

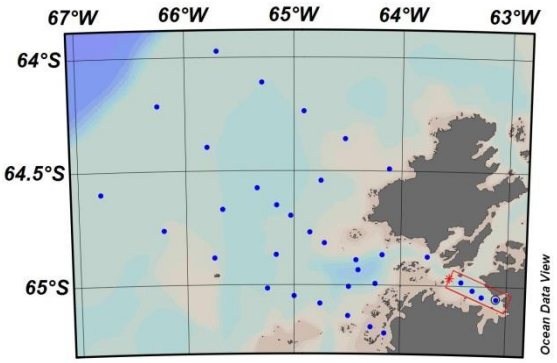
67°W
66°W
65°W
64°W
63°W
64°S
64.5°S
65°S
Ocean Data View

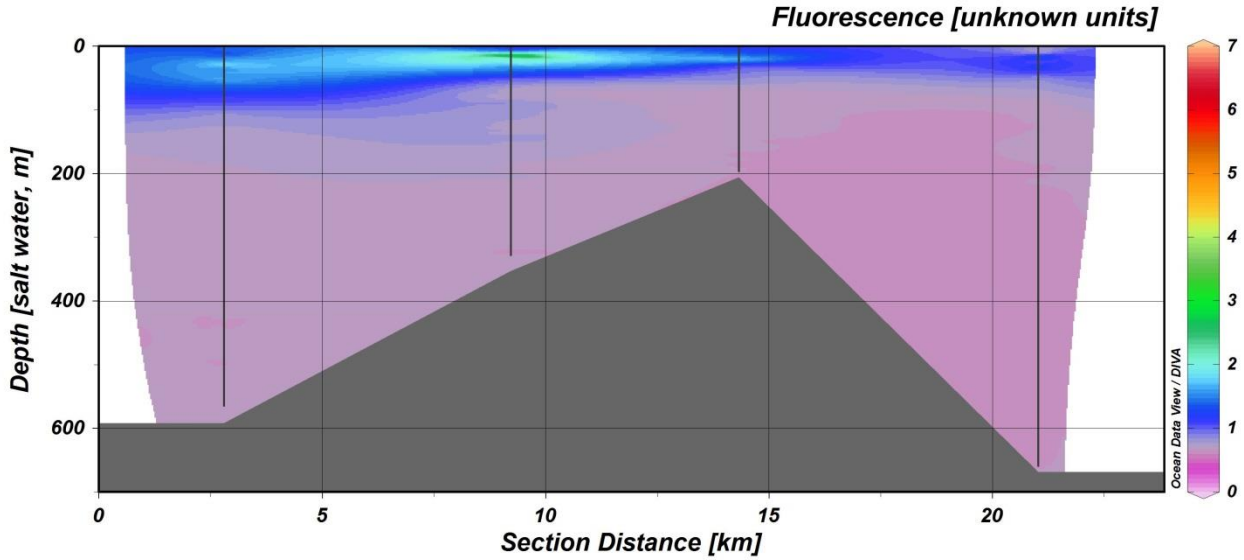
Fluorescence [unknown units]
Depth [salt water, m]
0
200
400
600
0
5
10
15
20
Section Distance [km]
7
6
5
4
3
2
1
0
Ocean Data View / DIVA

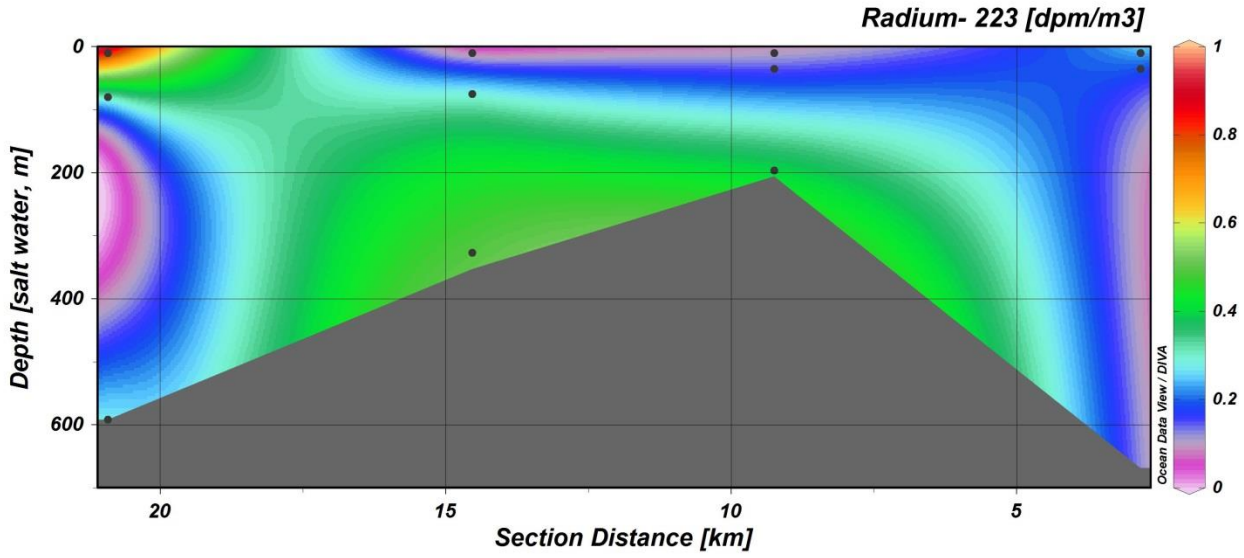
Radium- 223 [dpm/m3]
Depth [salt water, m]
0
200
400
600
20
15
10
5
Section Distance [km]
1
0.8
0.6
0.4
0.2
0
Ocean Data View / DIVA

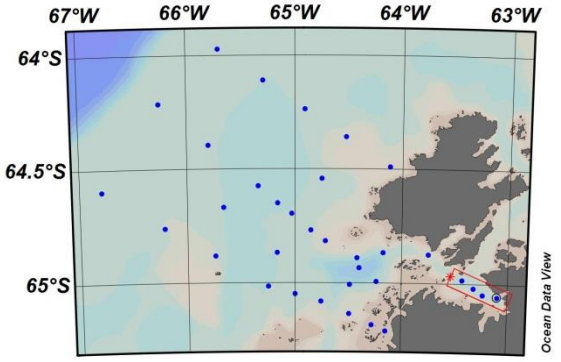
67°W
66°W
65°W
64°W
63°W
64°S
64.5°S
65°S
Ocean Data View

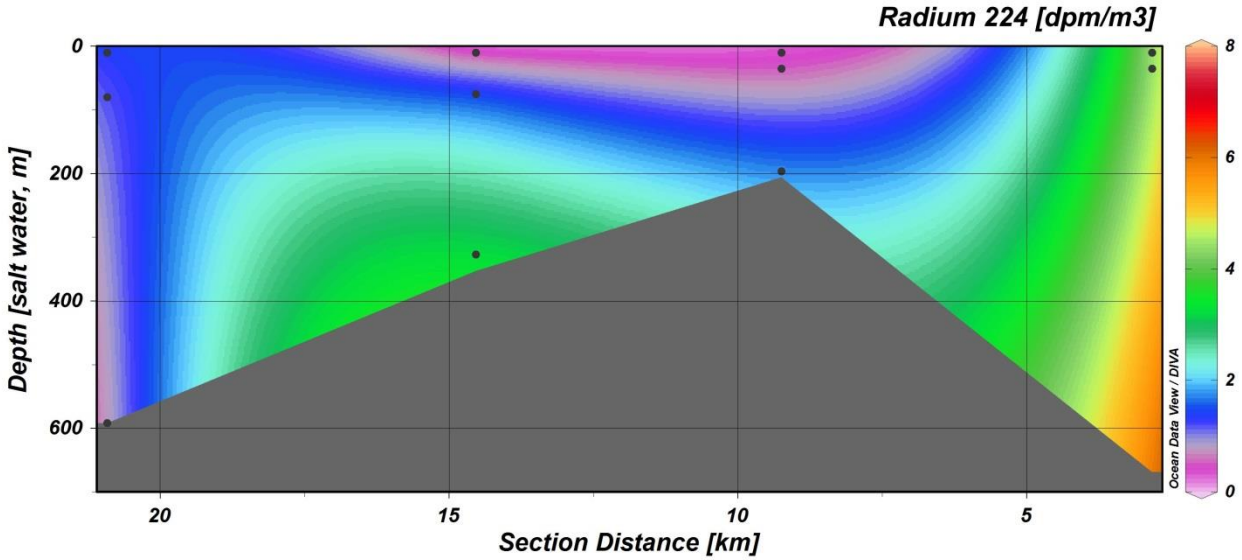
Radium 224 [dpm/m3]
Depth [salt water, m]
0
200
400
600
20
15
10
5
Section Distance [km]
8
6
4
2
0
Ocean Data View / DIVA

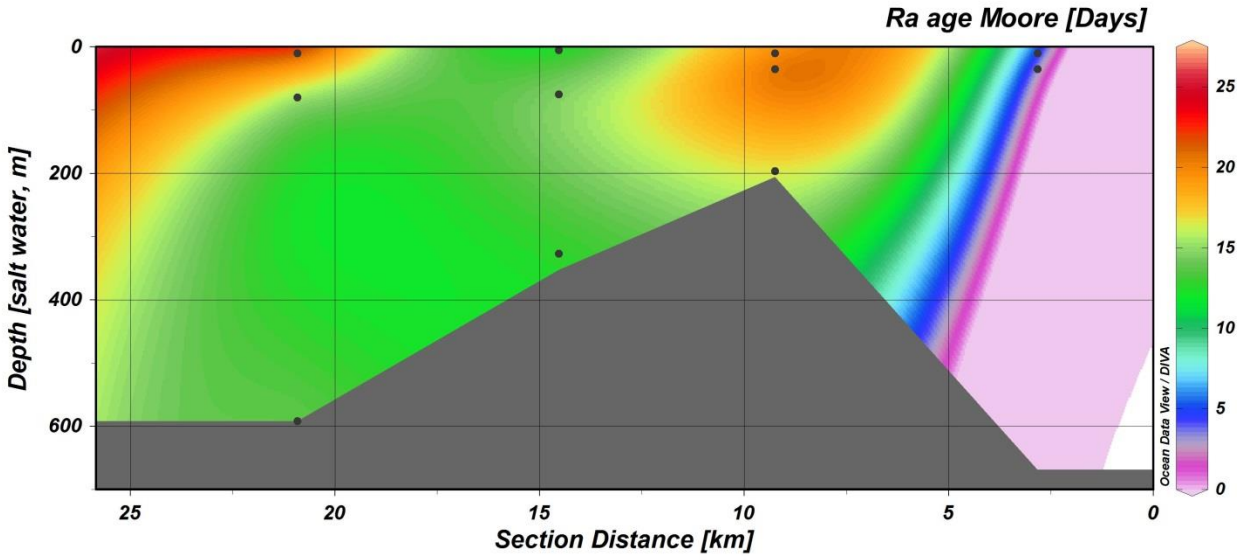
Ra age Moore [Days]
Depth [salt water, m]
0
200
400
600
25
20
15
10
5
0
Section Distance [km]
25
20
15
10
5
0
Ocean Data View / DIVA

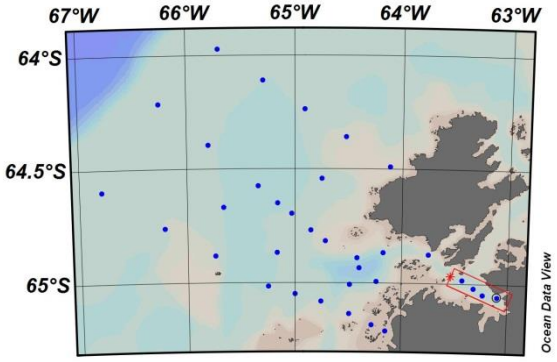
67°W
66°W
65°W
64°W
63°W
64°S
64.5°S
65°S
Ocean Data View

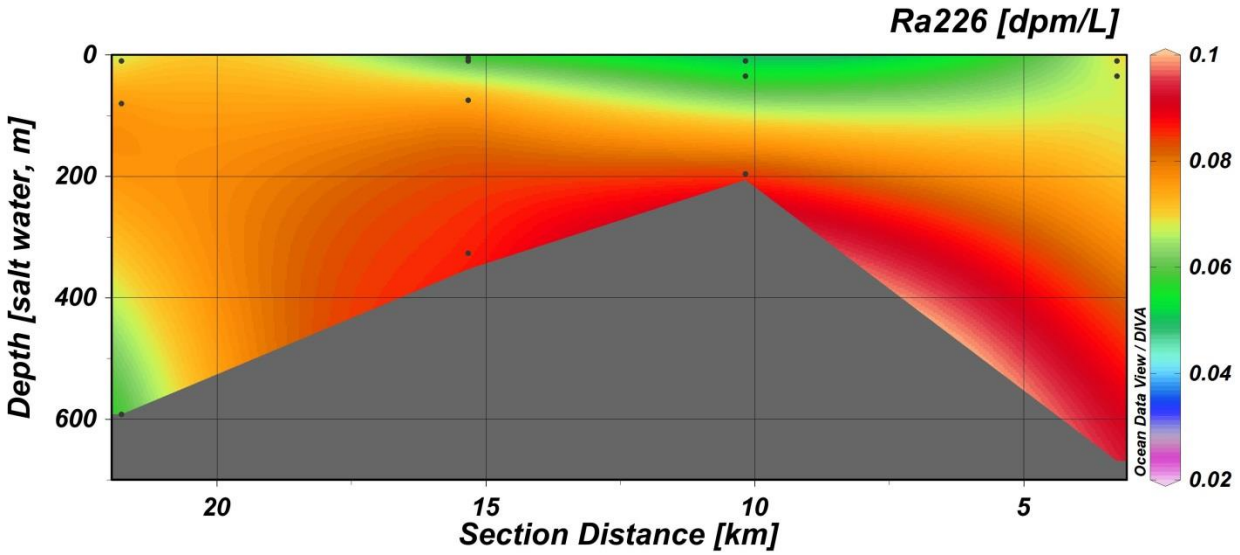
Ra226 [dpm/L]
Depth [salt water, m]
0
200
400
600
20
15
10
5
Section Distance [km]
0.1
0.08
0.06
0.04
0.02
Ocean Data View / DIVA

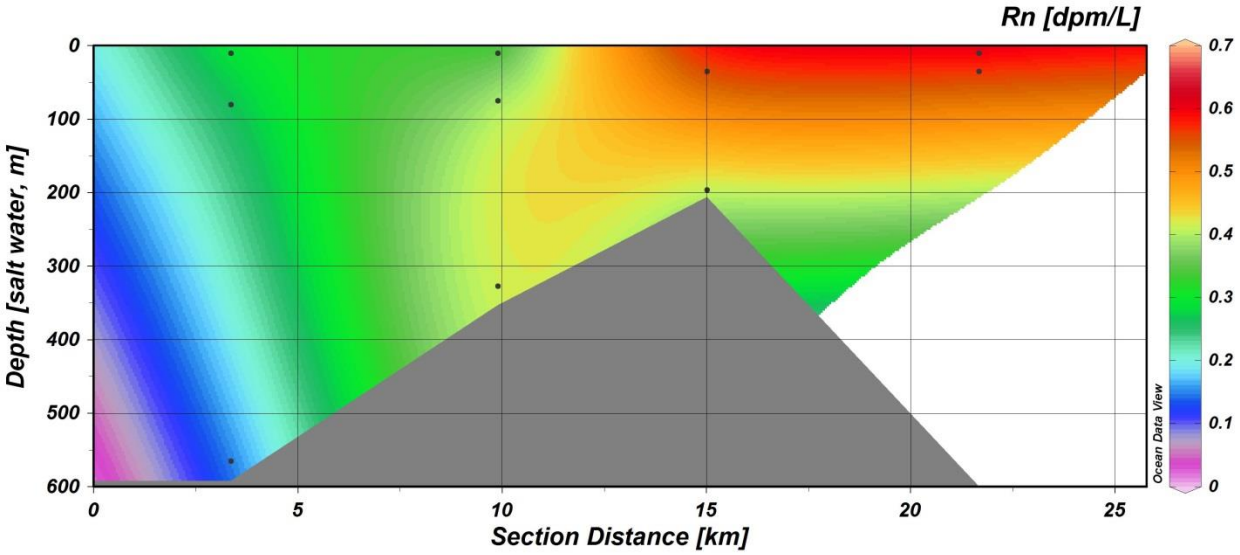
Rn [dpm/L]
Depth [salt water, m]
0
100
200
300
400
500
600
0
5
10
15
20
25
Section Distance [km]
0.7
0.6
0.5
0.4
0.3
0.2
0.1
0
Ocean Data View

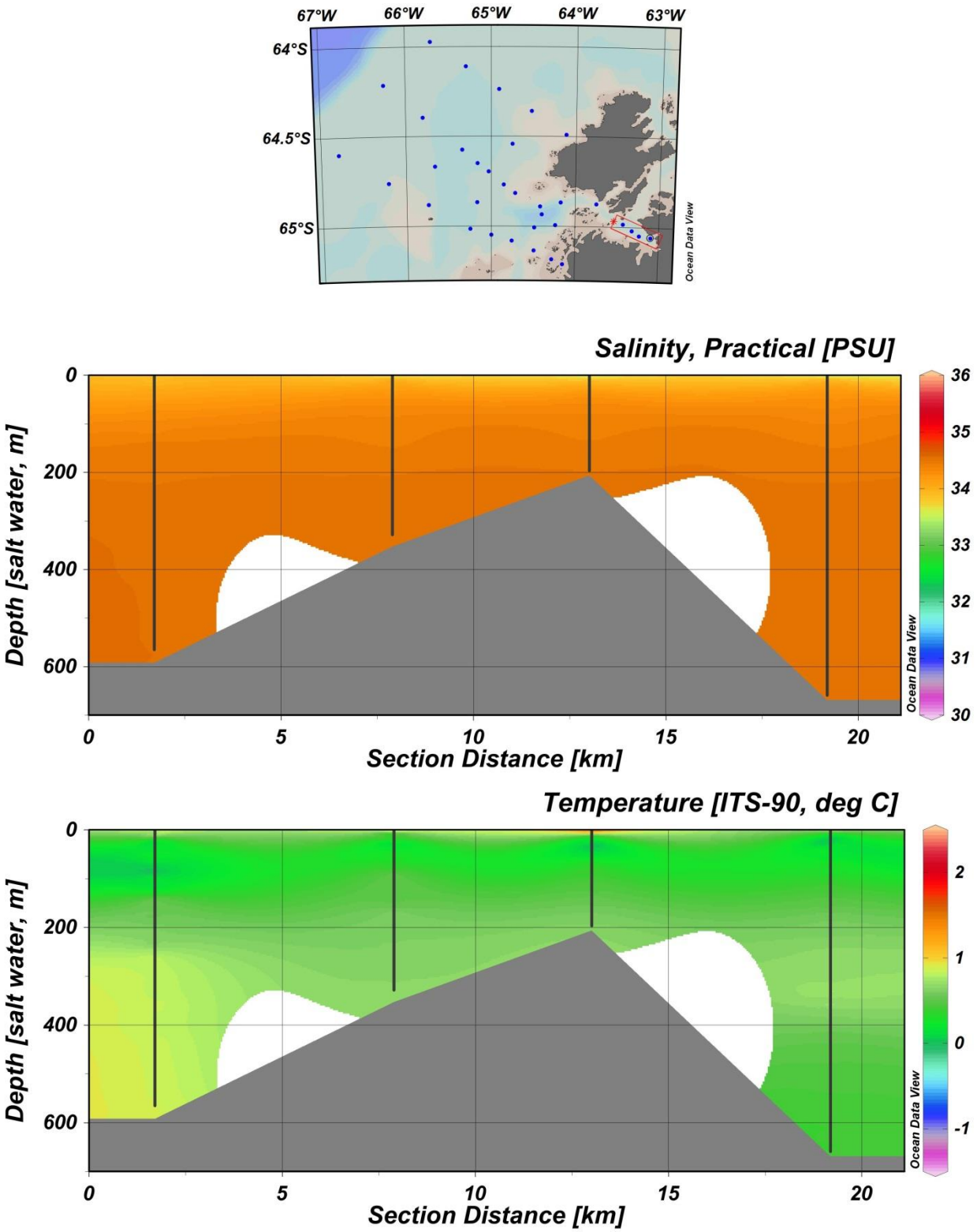
67°W
66°W
65°W
64°W
63°W
64°S
64.5°S
65°S
Ocean Data View
Salinity, Practical [PSU]
Depth [salt water, m]
0
200
400
600
0
5
10
15
20
Section Distance [km]
36
35
34
33
32
31
30
Ocean Data View
Temperature [ITS-90, deg C]
Depth [salt water, m]
0
200
400
600
0
5
10
15
20
Section Distance [km]
2
1
0
-1
Ocean Data View

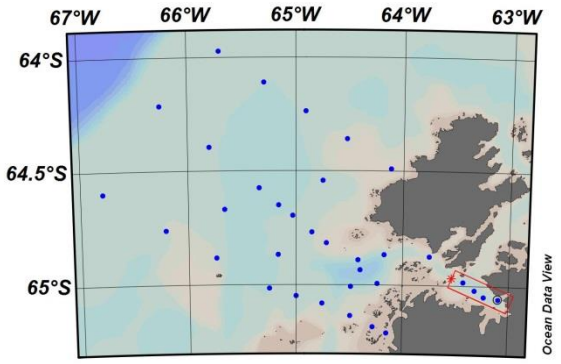
67°W
66°W
65°W
64°W
63°W
64°S
64.5°S
65°S
Ocean Data View

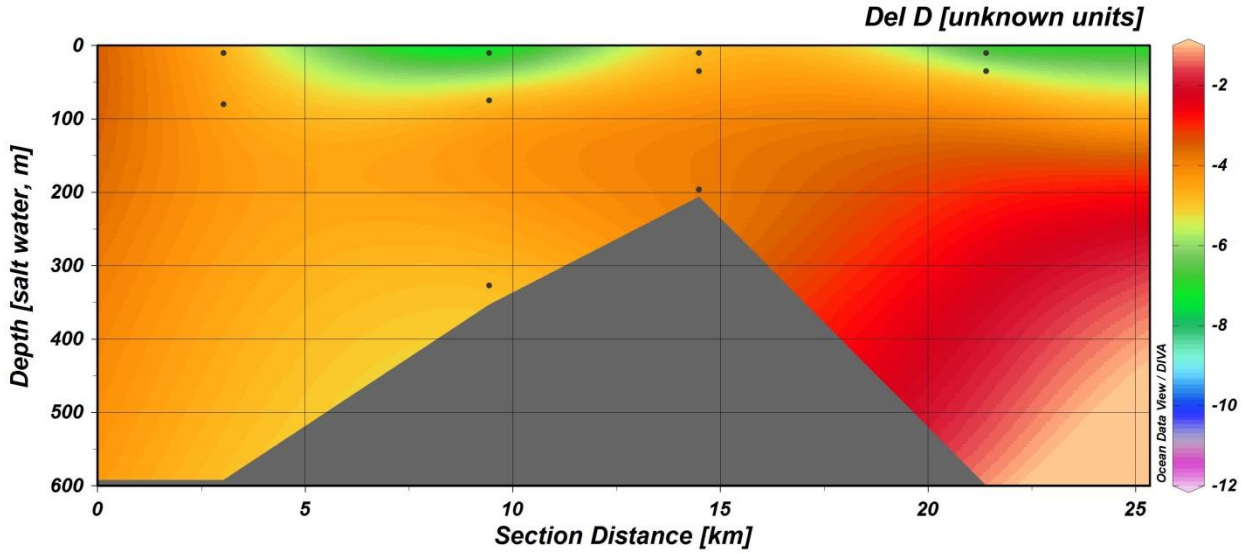
Del D [unknown units]
Depth [salt water, m]
0
100
200
300
400
500
600
0
5
10
15
20
25
Section Distance [km]
-2
-4
-6
-8
-10
-12
Ocean Data View / DIVA

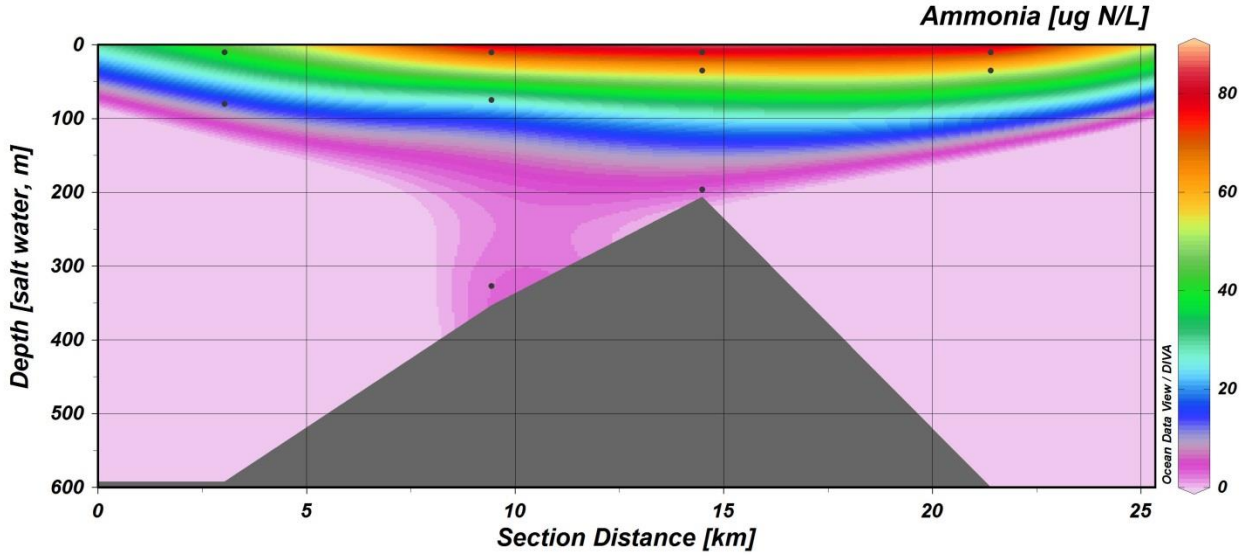
Ammonia [ug N/L]
Depth [salt water, m]
0
100
200
300
400
500
600
0
5
10
15
20
25
Section Distance [km]
80
60
40
20
0
Ocean Data View / DIVA

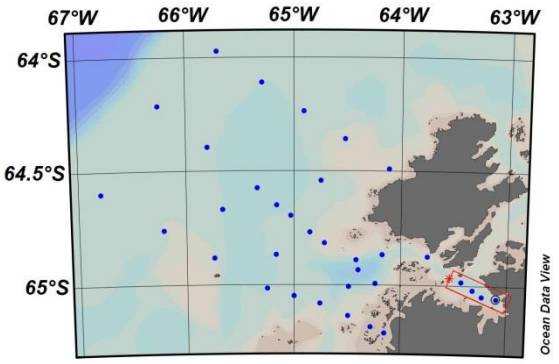
67°W
66°W
65°W
64°W
63°W
64°S
64.5°S
65°S
Ocean Data View

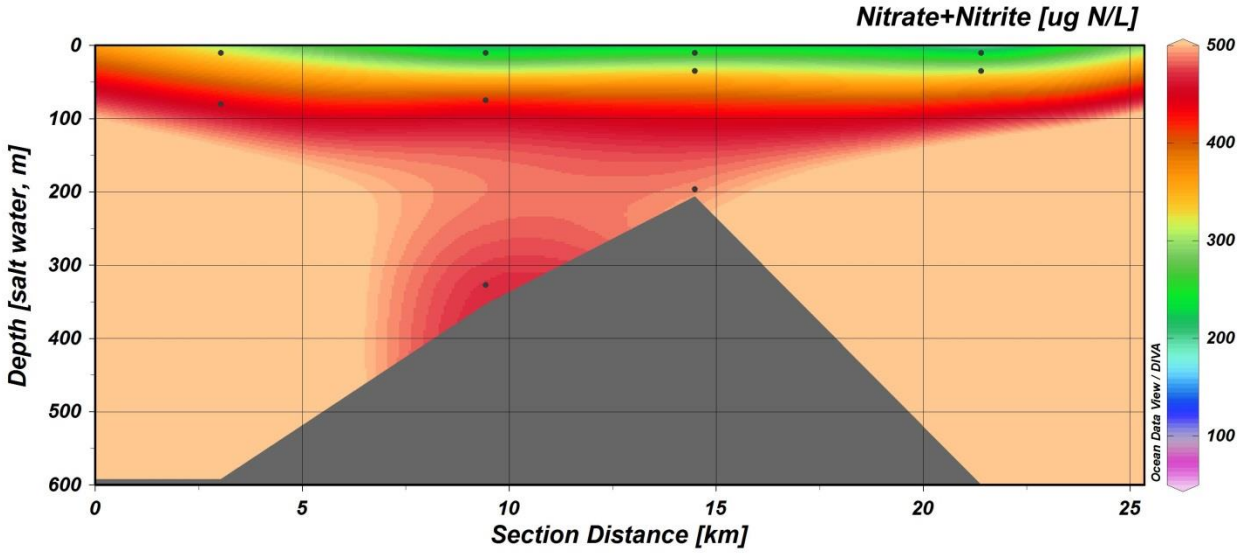
Nitrate+Nitrite [ug N/L]
Depth [salt water, m]
0
100
200
300
400
500
600
0
5
10
15
20
25
Section Distance [km]
500
400
300
200
100
Ocean Data View / DIVA

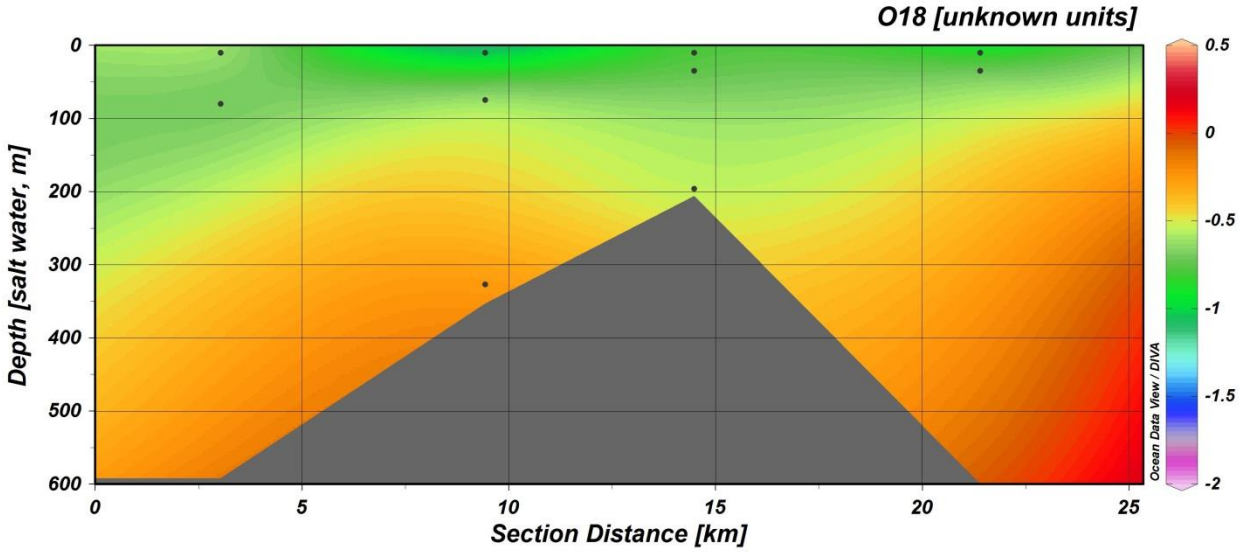
O18 [unknown units]
Depth [salt water, m]
0
100
200
300
400
500
600
0
5
10
15
20
25
Section Distance [km]
0.5
0
-0.5
-1
-1.5
-2
Ocean Data View / DIVA

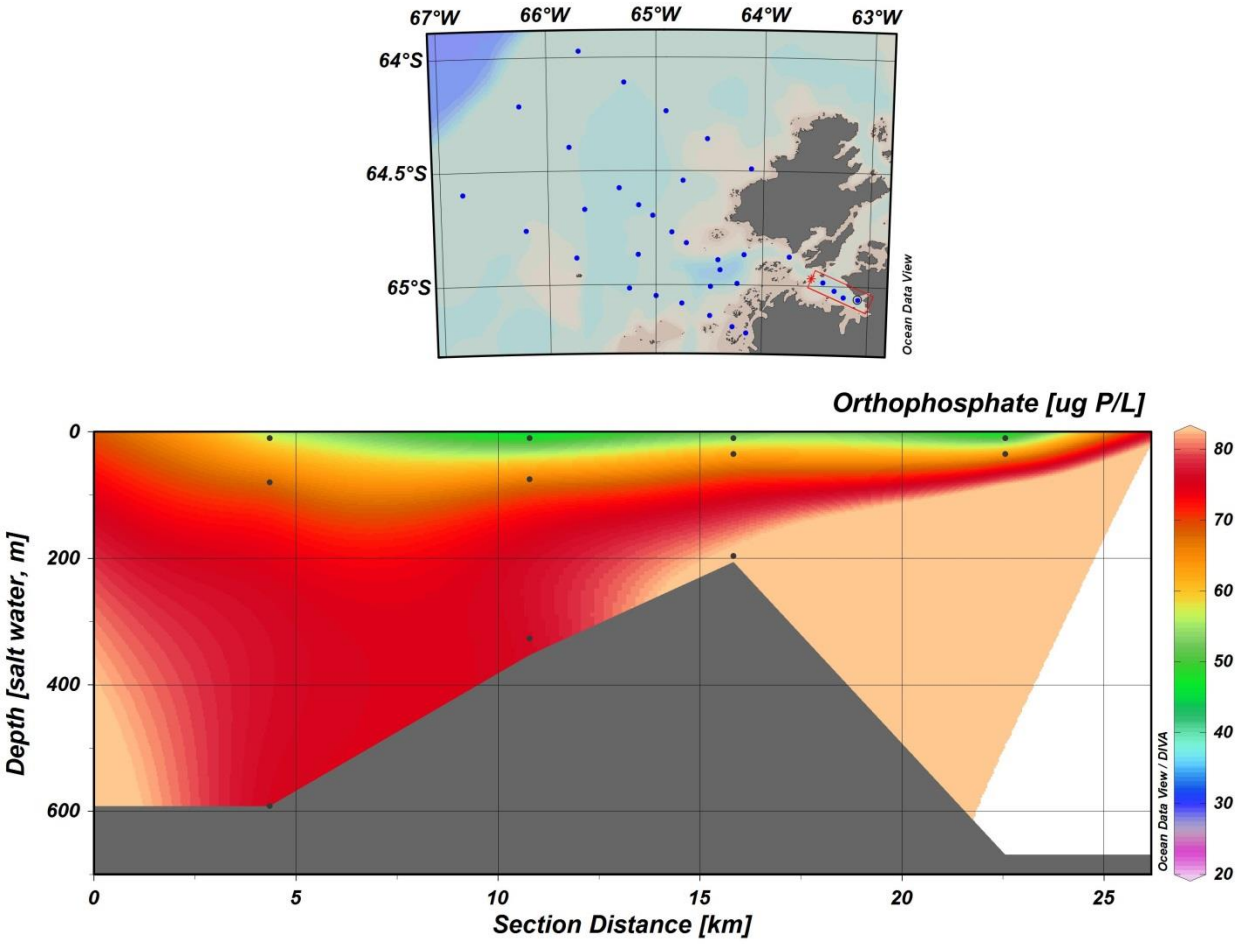
67°W
66°W
65°W
64°W
63°W
64°S
64.5°S
65°S
Ocean Data View
Orthophosphate [ug P/L]
Depth [salt water, m]
0
200
400
600
0
5
10
15
20
25
Section Distance [km]
80
70
60
50
40
30
20
Ocean Data View / DIVA

Appendix II Contour Plots of Geochemical and Physical Parameters during the 2014 Cruise

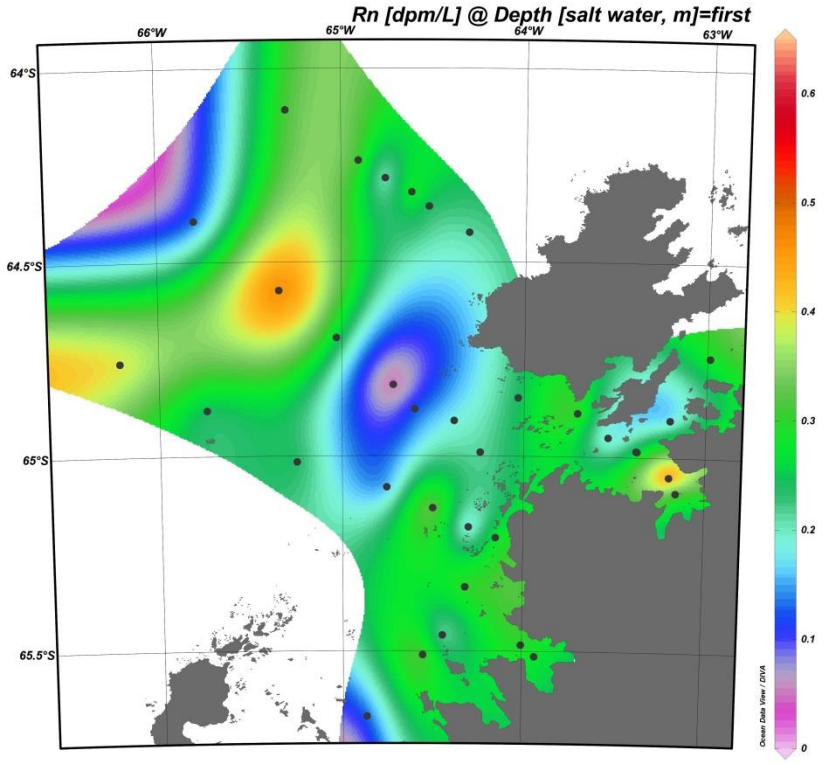
Rn [dpm/L] @ Depth [salt water, m]=first
66°W
65°W
64°W
63°W
64°S
64.5°S
65°S
65.5°S
0.6
0.5
0.4
0.3
0.2
0.1
0
Ocean Data View / DIVA

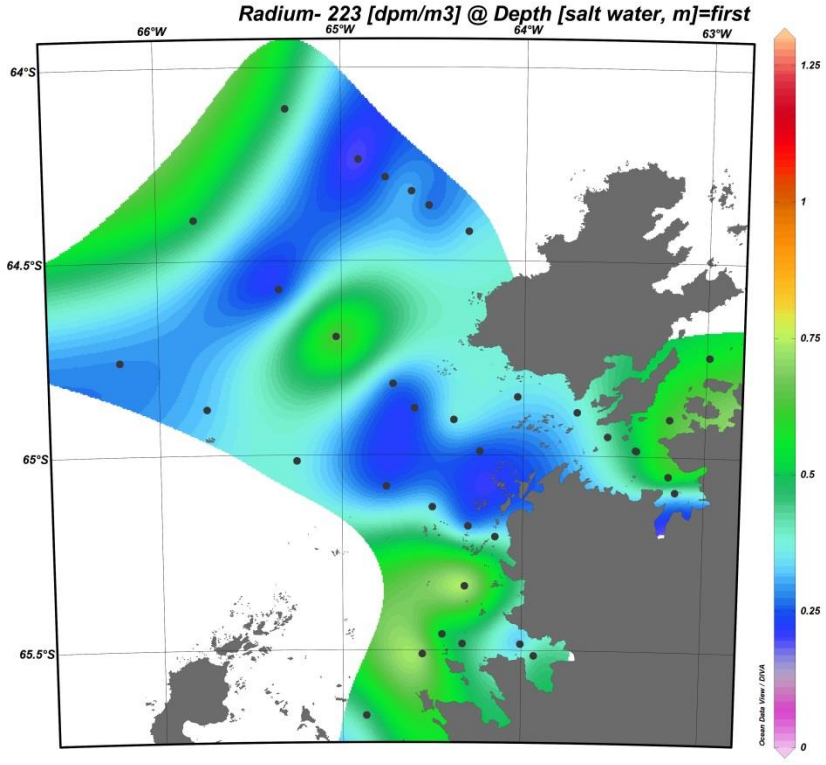
Radium- 223 [dpm/m3] @ Depth [salt water, m]=first
66°W
65°W
64°W
63°W
64°S
64.5°S
65°S
65.5°S
1.25
1
0.75
0.5
0.25
0
Ocean Data View / DIVA

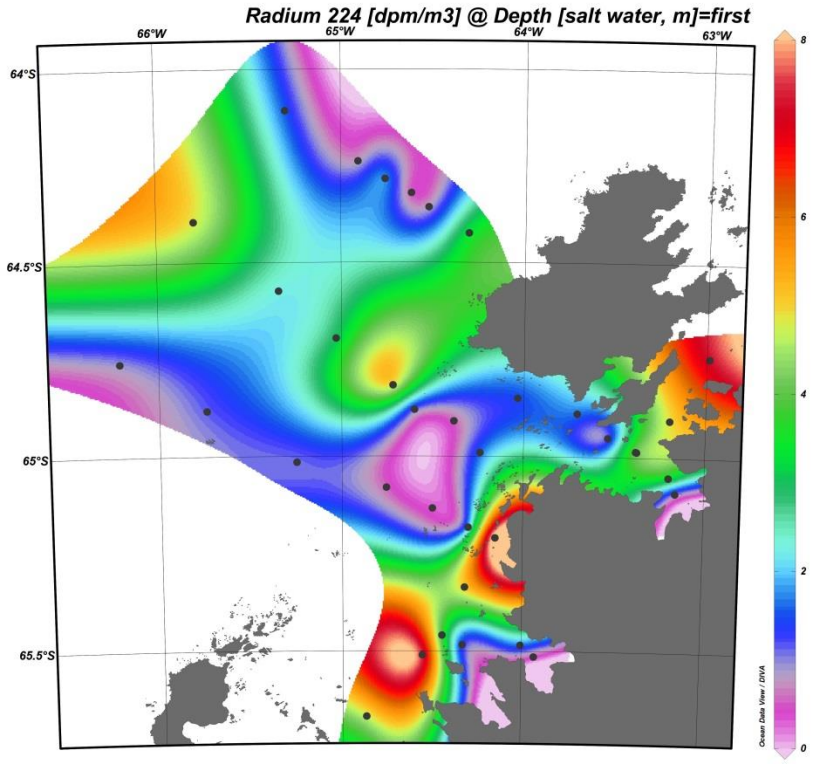
Radium 224 [dpm/m3] @ Depth [salt water, m]=first
66°W
65°W
64°W
63°W
64°S
64.5°S
65°S
65.5°S
8
6
4
2
0
Ocean Data View / DIVA

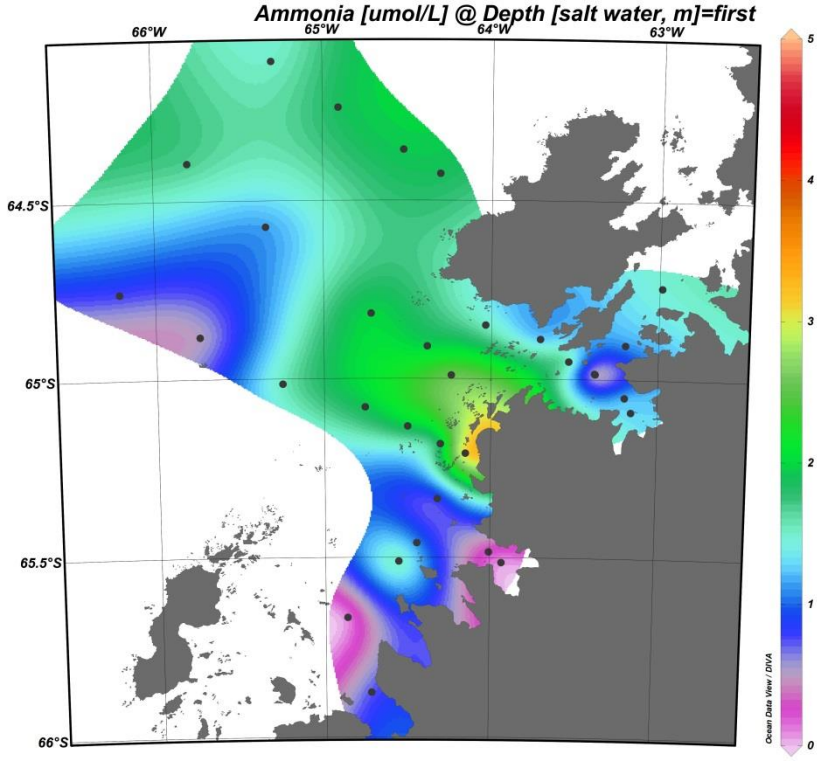
Ammonia [umol/L] @ Depth [salt water, m]=first
66°W
65°W
64°W
63°W
64.5°S
65°S
65.5°S
66°S
5
4
3
2
1
0
Ocean Data View / DIVA

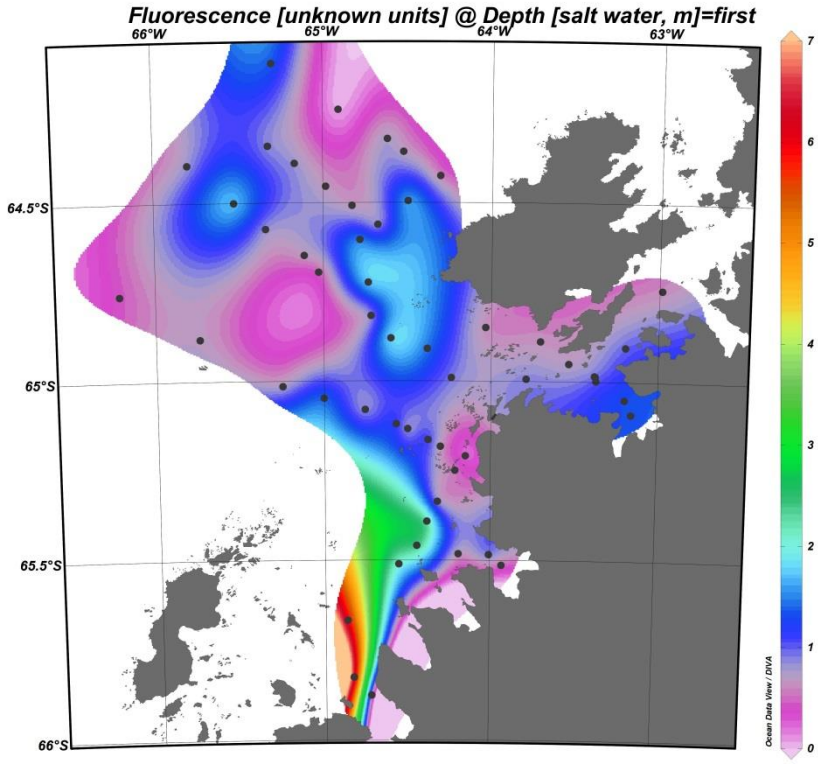
Fluorescence [unknown units] @ Depth [salt water, m]=first
66°W
65°W
64°W
63°W
64.5°S
65°S
65.5°S
66°S
7
6
5
4
3
2
1
0
Ocean Data View / DIVA

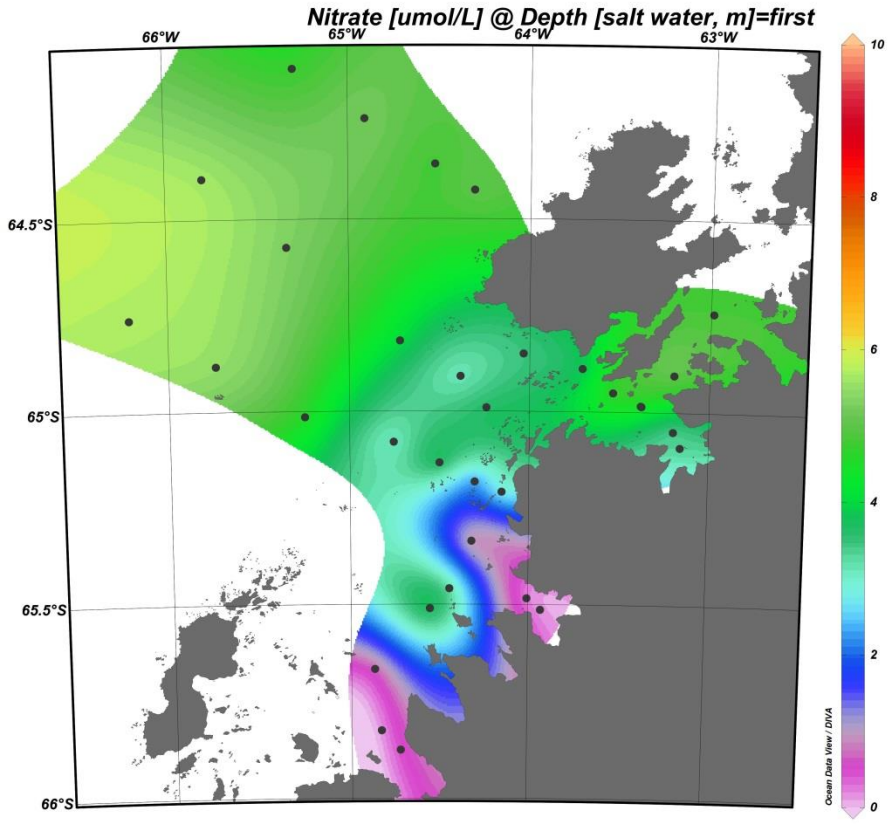
Nitrate [umol/L] @ Depth [salt water, m]=first
66°W
65°W
64°W
63°W
64.5°S
65°S
65.5°S
66°S
10
8
6
4
2
0
Ocean Data View / DIVA

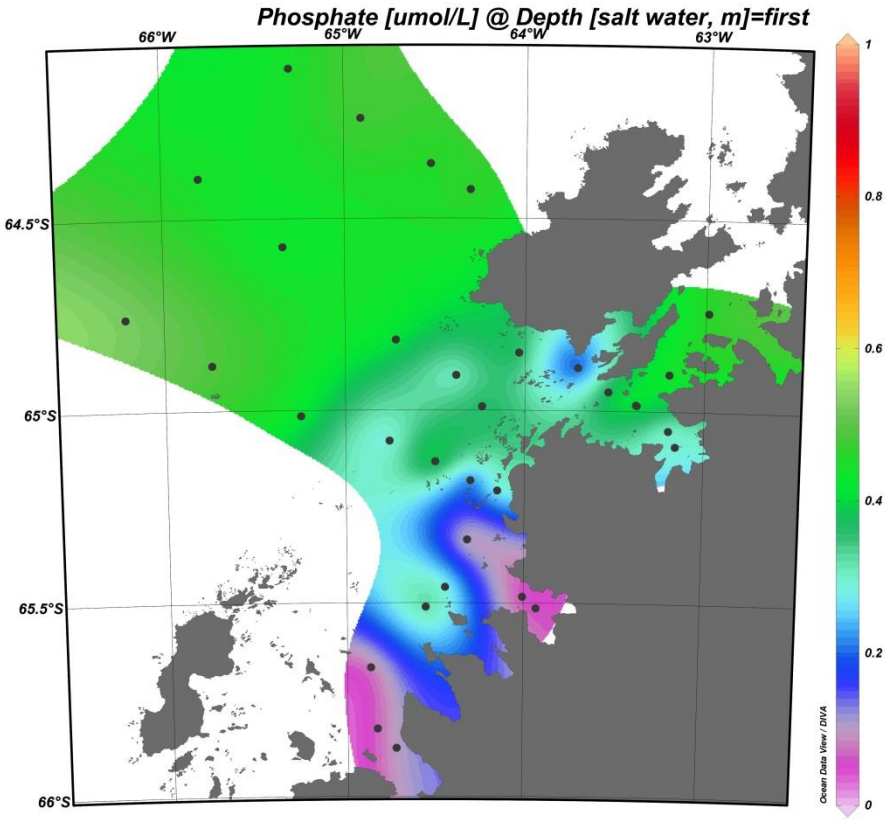
Phosphate [umol/L] @ Depth [salt water, m]=first
66°W
65°W
64°W
63°W
64.5°S
65°S
65.5°S
66°S
1
0.8
0.6
0.4
0.2
0
Ocean Data View / DIVA

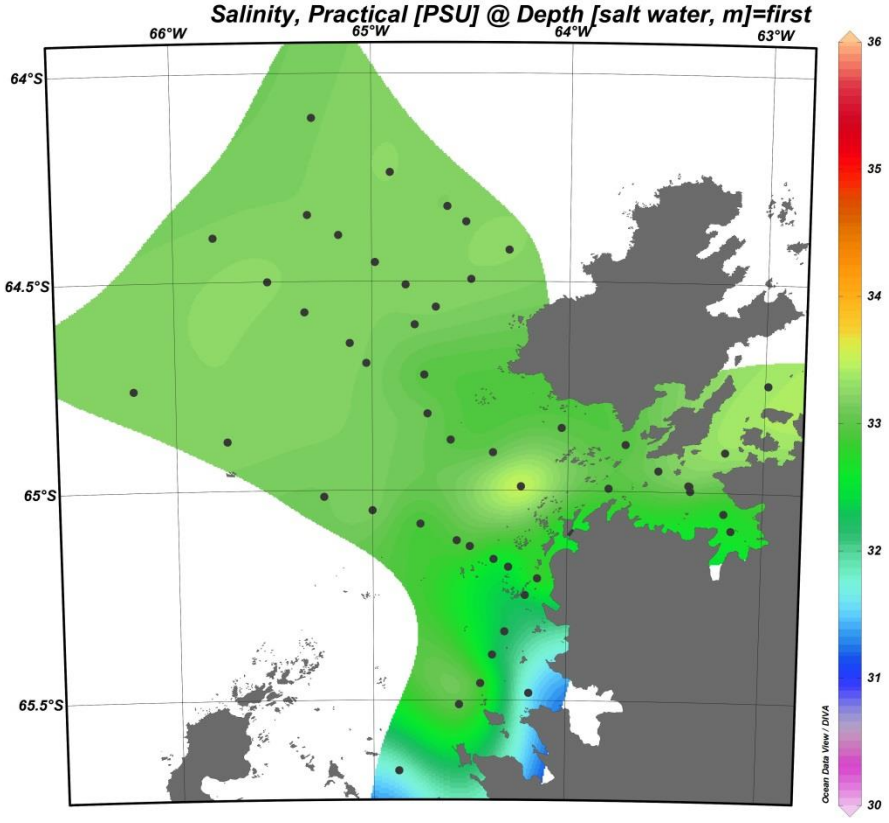
Salinity, Practical [PSU] @ Depth [salt water, m]=first
66°W
65°W
64°W
63°W
64°S
64.5°S
65°S
65.5°S
36
35
34
33
32
31
30
Ocean Data View / DIVA

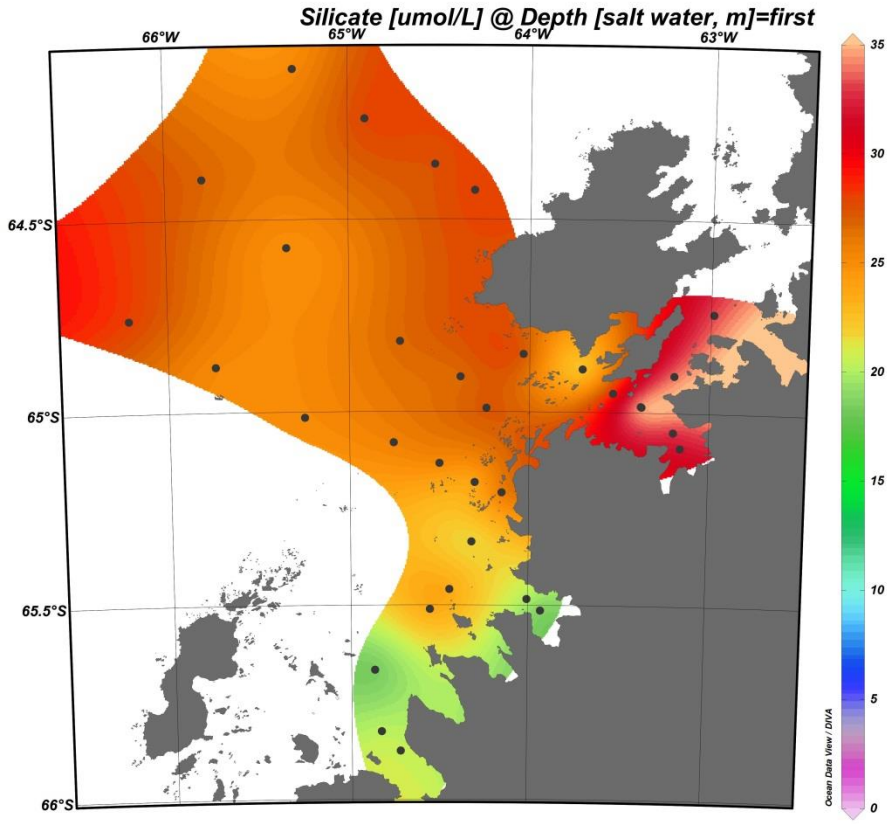
Silicate [umol/L] @ Depth [salt water, m]=first
66°W
65°W
64°W
63°W
64.5°S
65°S
65.5°S
66°S
35
30
25
20
15
10
5
0
Ocean Data View / DIVA

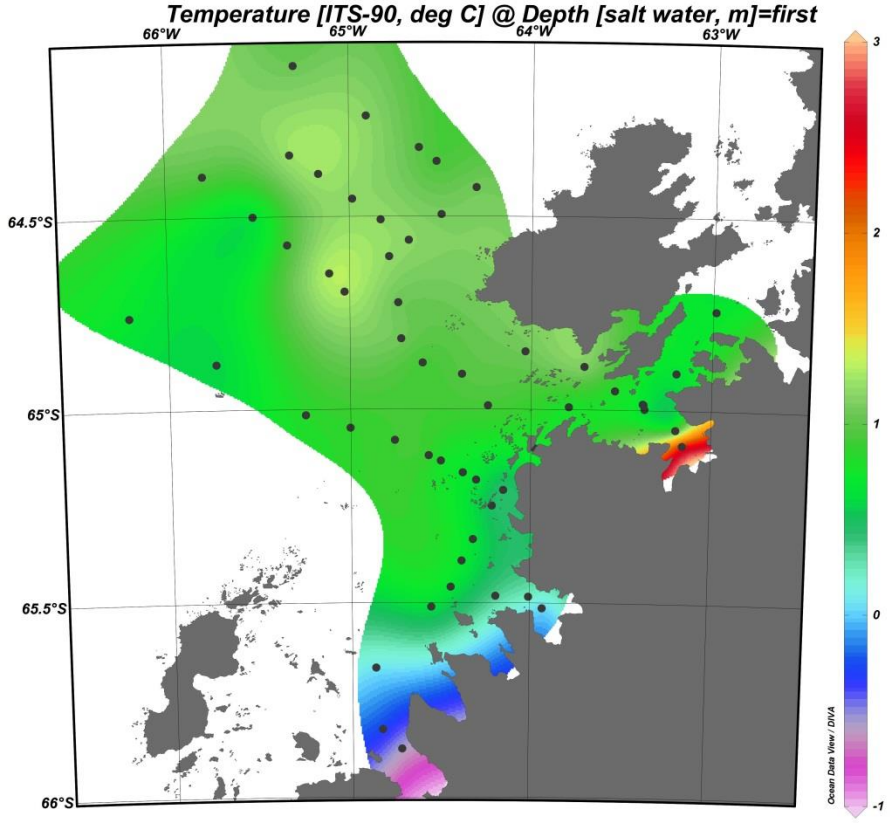
Temperature [ITS-90, deg C] @ Depth [salt water, m]=first
66°W
65°W
64°W
63°W
64.5°S
65°S
65.5°S
66°S
3
2
1
0
-1
Ocean Data View / DIVA

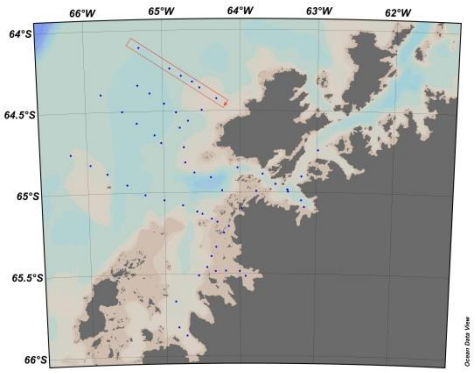
66°W
65°W
64°W
63°W
62°W
64°S
64.5°S
65°S
65.5°S
66°S
Ocean Data View

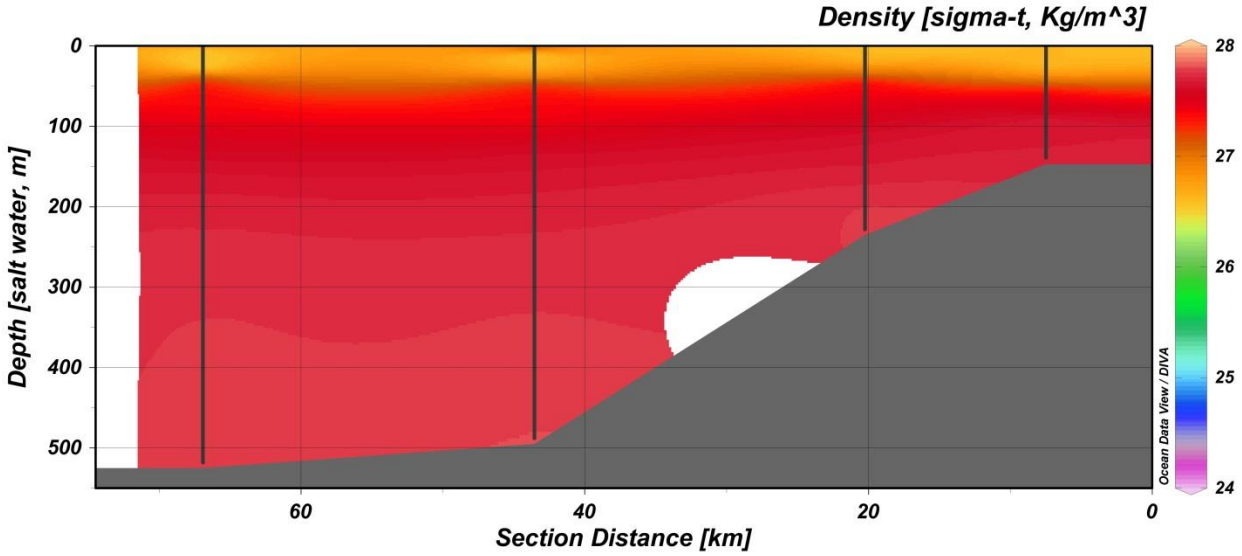
Density [sigma-t, Kg/m^3]
Depth [salt water, m]
0
100
200
300
400
500
60
40
20
0
Section Distance [km]
28
27
26
25
24
Ocean Data View / DIVA

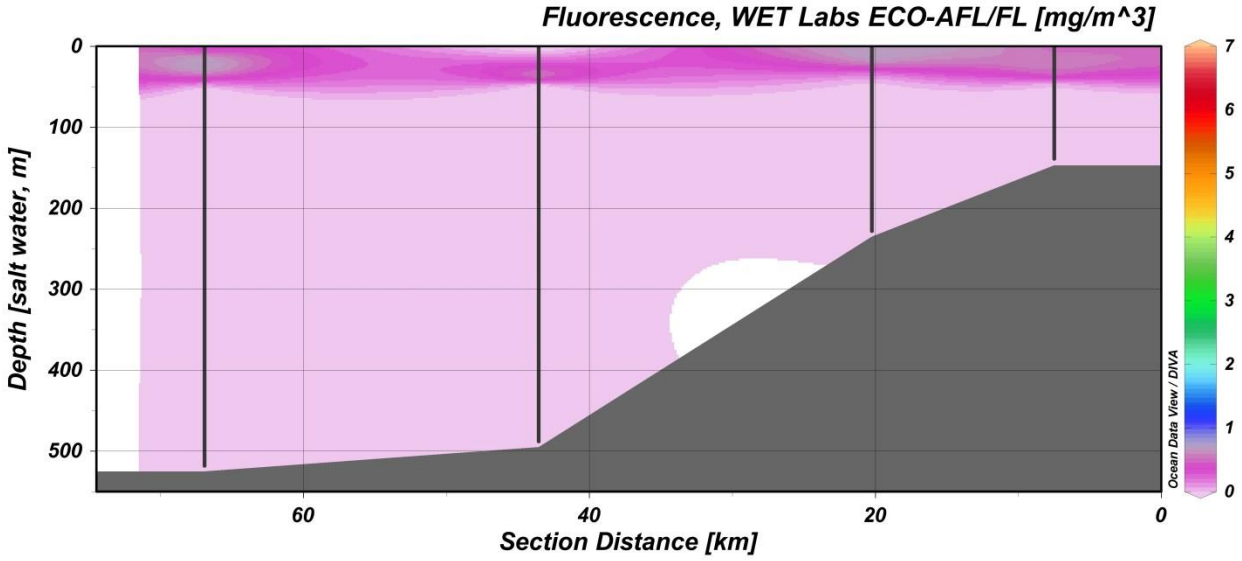
Fluorescence, WET Labs ECO-AFL/FL [mg/m^3]
Depth [salt water, m]
0
100
200
300
400
500
60
40
20
0
Section Distance [km]
7
6
5
4
3
2
1
0
Ocean Data View / DIVA

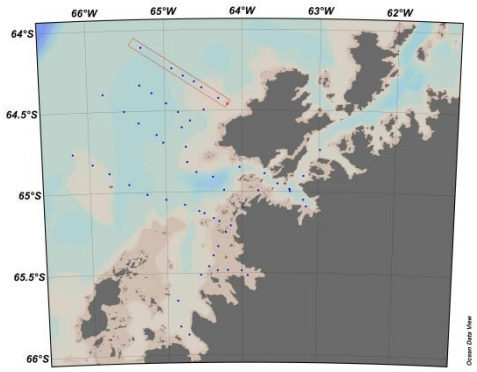
66°W
65°W
64°W
63°W
62°W
64°S
64.5°S
65°S
65.5°S
66°S
Ocean Data View

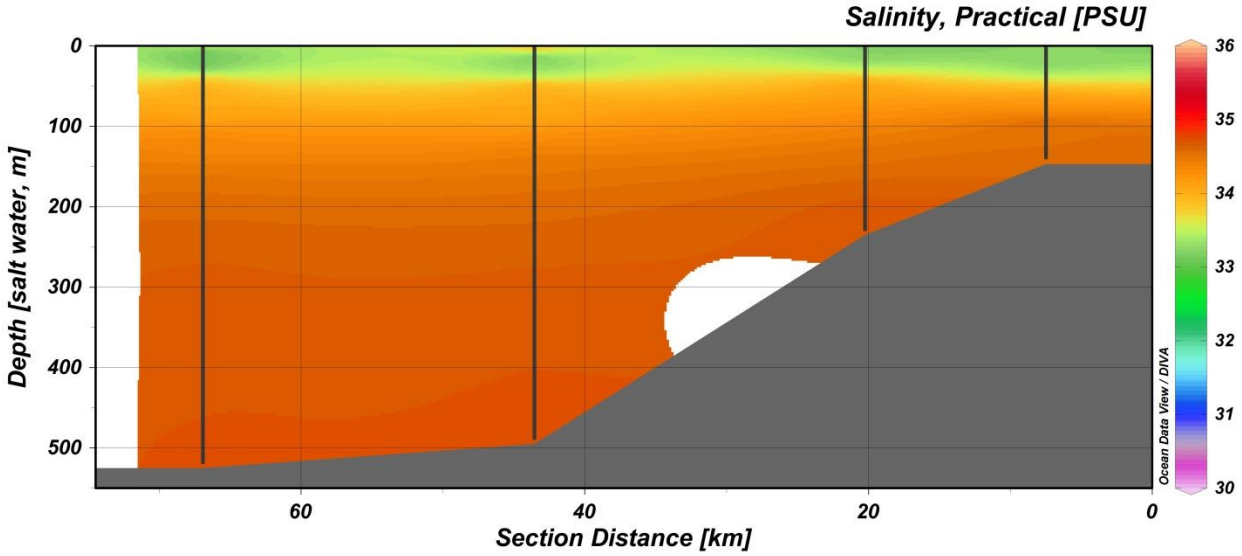
Salinity, Practical [PSU]
Depth [salt water, m]
0
100
200
300
400
500
60
40
20
0
Section Distance [km]
36
35
34
33
32
31
30
Ocean Data View / DIVA

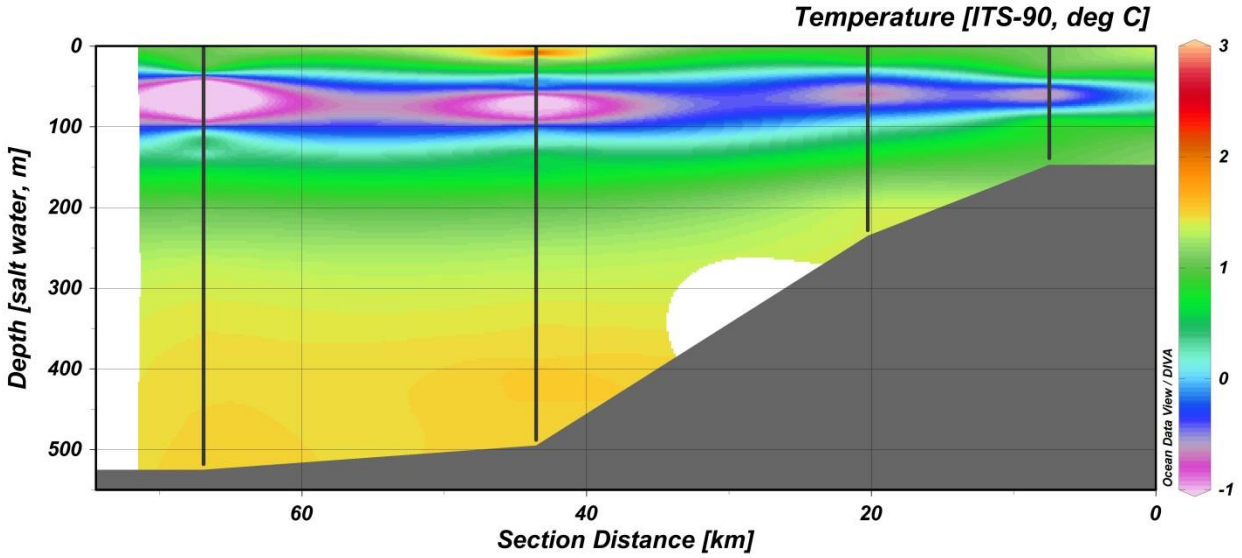
Temperature [ITS-90, deg C]
Depth [salt water, m]
0
100
200
300
400
500
60
40
20
0
Section Distance [km]
3
2
1
0
-1
Ocean Data View / DIVA

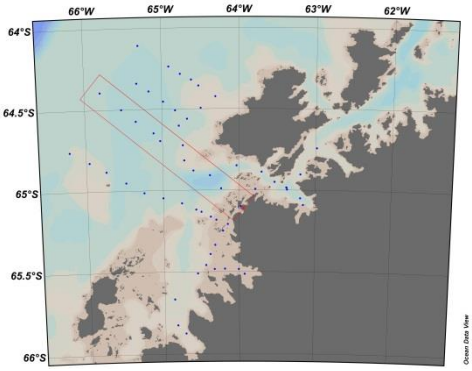
66°W
65°W
64°W
63°W
62°W
64°S
64.5°S
65°S
65.5°S
66°S
Ocean Data View

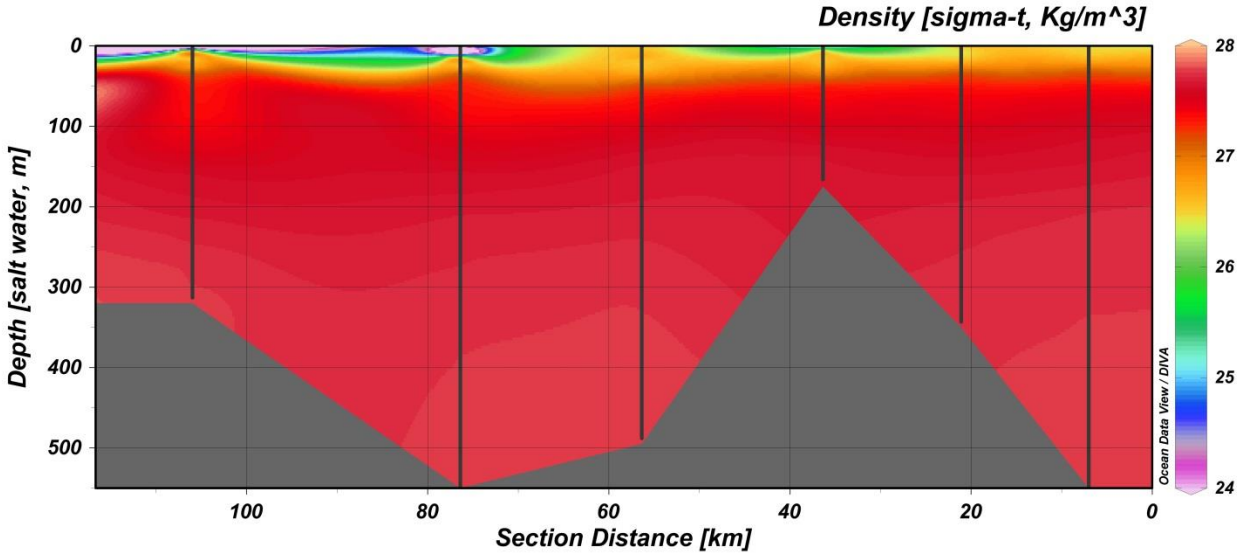
Density [sigma-t, Kg/m^3]
Depth [salt water, m]
0
100
200
300
400
500
100
80
60
40
20
0
Section Distance [km]
28
27
26
25
24
Ocean Data View / DIVA

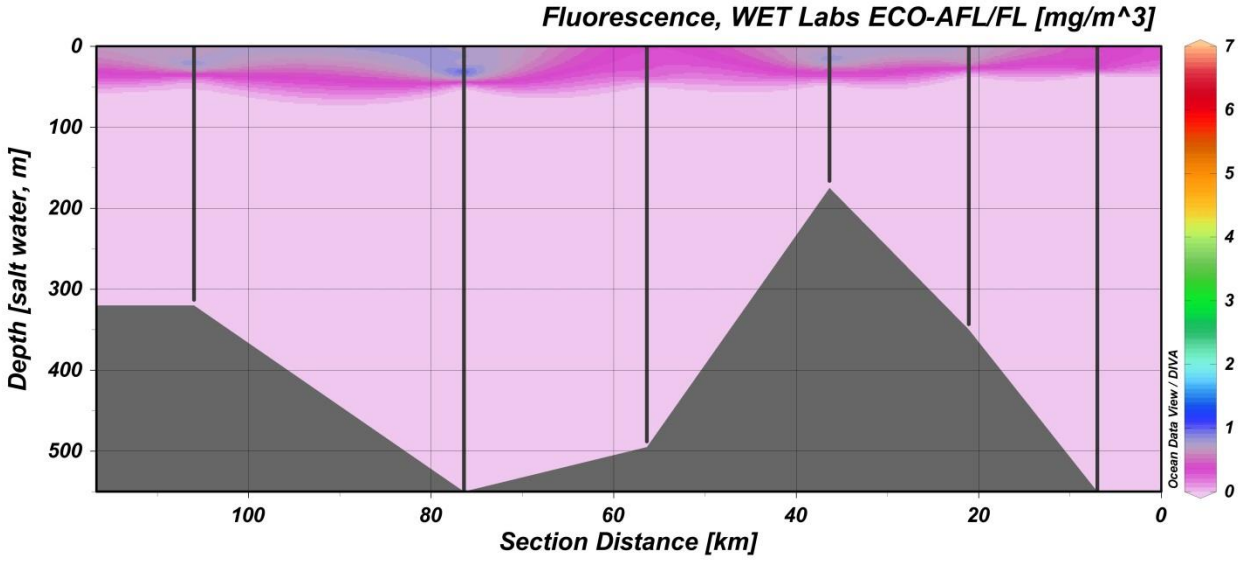
Fluorescence, WET Labs ECO-AFL/FL [mg/m^3]
Depth [salt water, m]
0
100
200
300
400
500
100
80
60
40
20
0
Section Distance [km]
7
6
5
4
3
2
1
0
Ocean Data View / DIVA

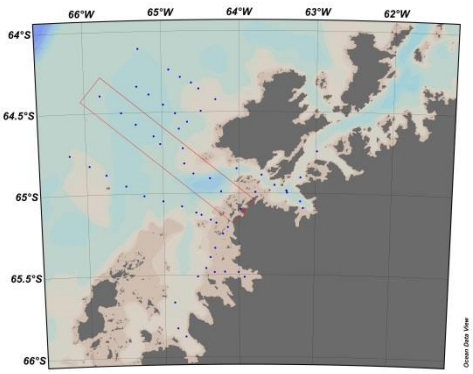
66°W
65°W
64°W
63°W
62°W
64°S
64.5°S
65°S
65.5°S
66°S
Ocean Data View

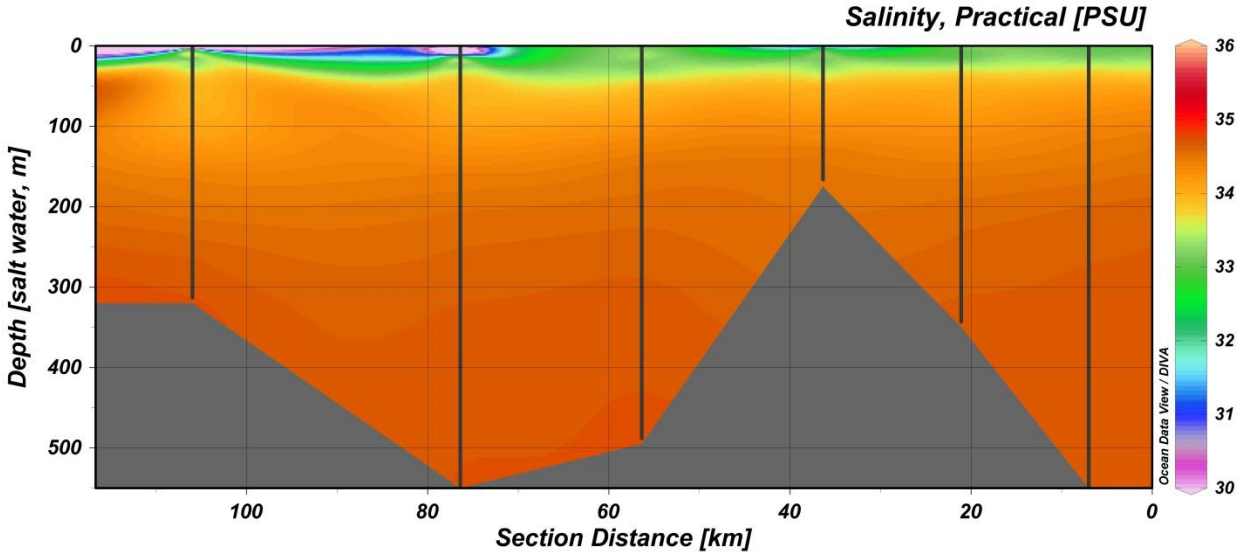
Salinity, Practical [PSU]
Depth [salt water, m]
0
100
200
300
400
500
100
80
60
40
20
0
Section Distance [km]
36
35
34
33
32
31
30
Ocean Data View / DIVA

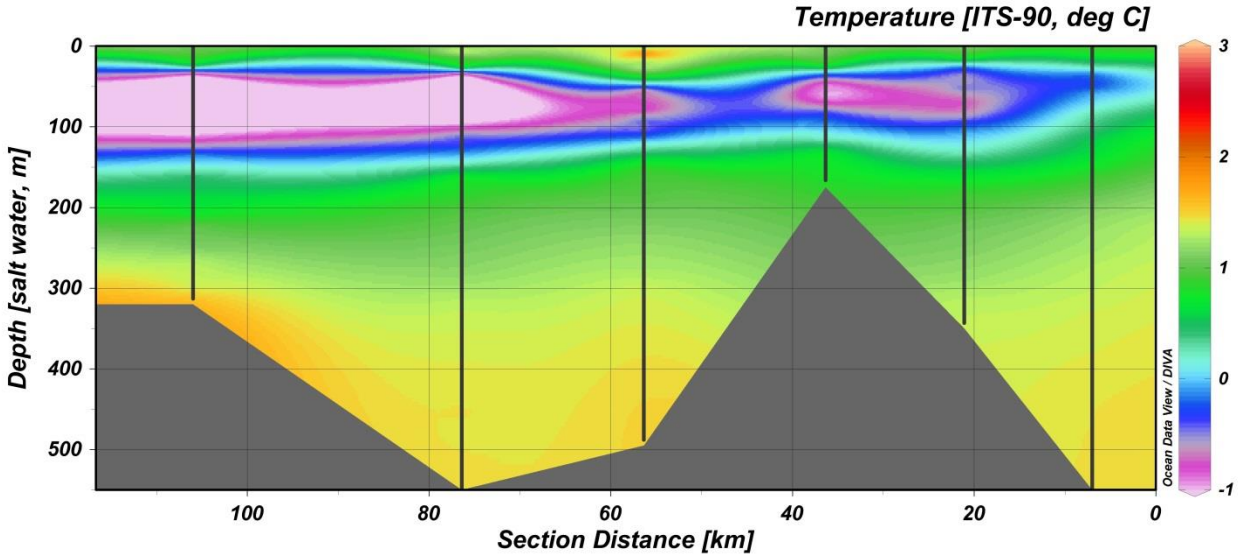
Temperature [ITS-90, deg C]
Depth [salt water, m]
0
100
200
300
400
500
100
80
60
40
20
0
Section Distance [km]
3
2
1
0
-1
Ocean Data View / DIVA

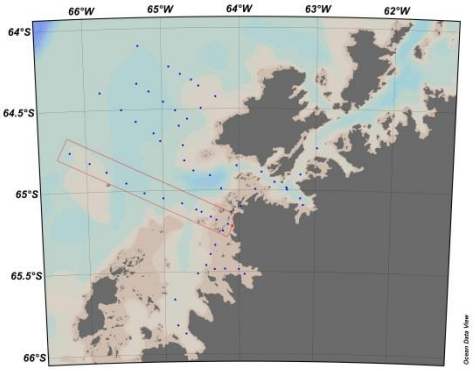
66°W
65°W
64°W
63°W
62°W
64°S
64.5°S
65°S
65.5°S
66°S
Ocean Data View

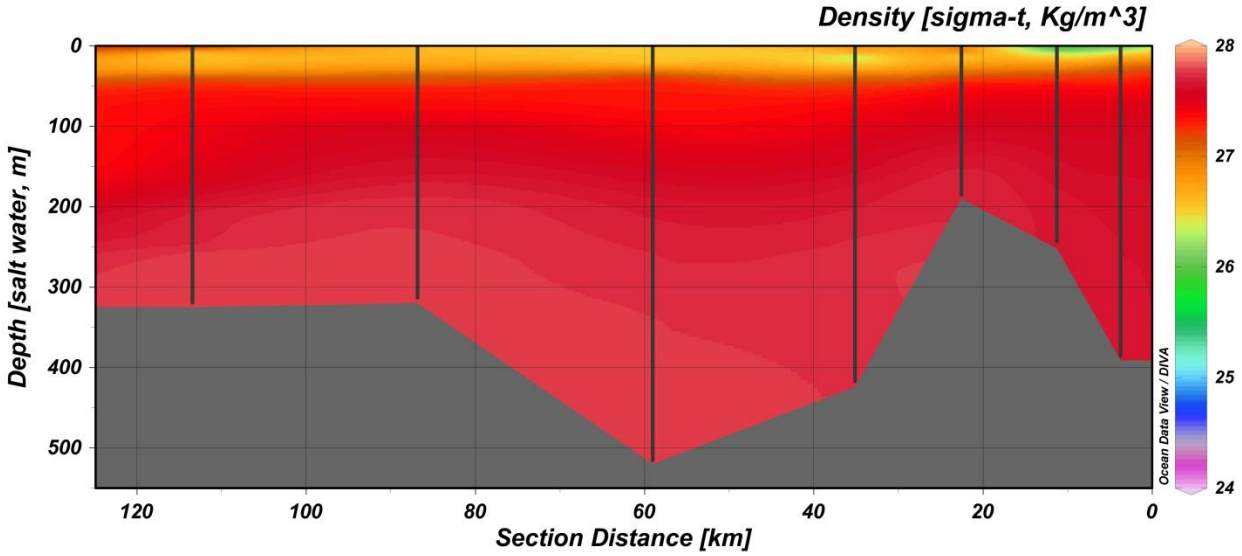
Density [sigma-t, Kg/m^3]
Depth [salt water, m]
0
100
200
300
400
500
120
100
80
60
40
20
0
Section Distance [km]
28
27
26
25
24
Ocean Data View / DIVA

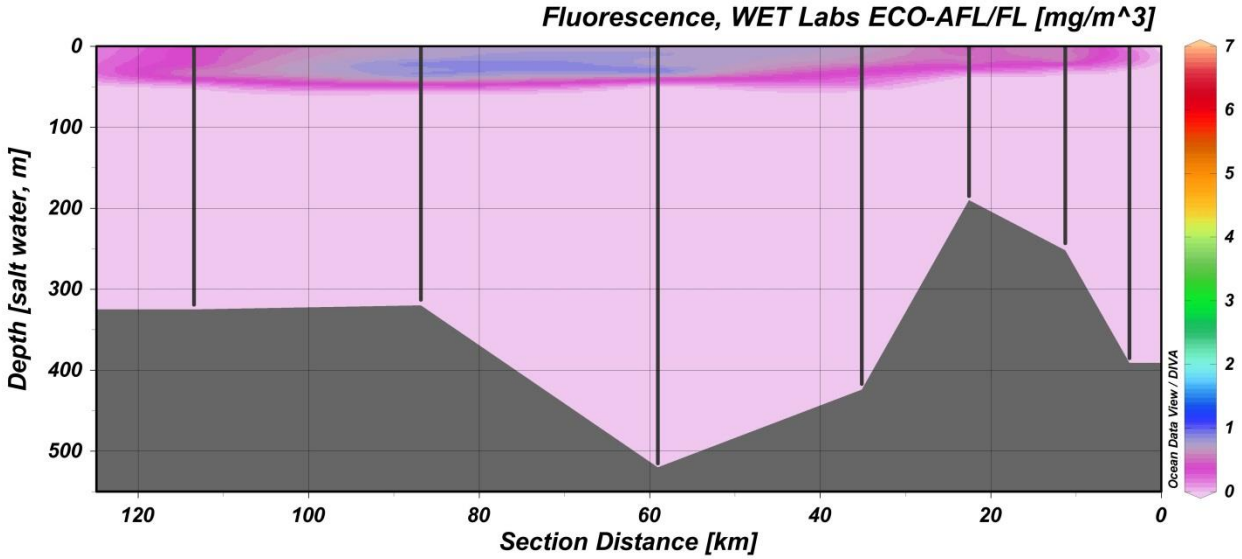
Fluorescence, WET Labs ECO-AFL/FL [mg/m^3]
Depth [salt water, m]
0
100
200
300
400
500
120
100
80
60
40
20
0
Section Distance [km]
7
6
5
4
3
2
1
0
Ocean Data View / DIVA

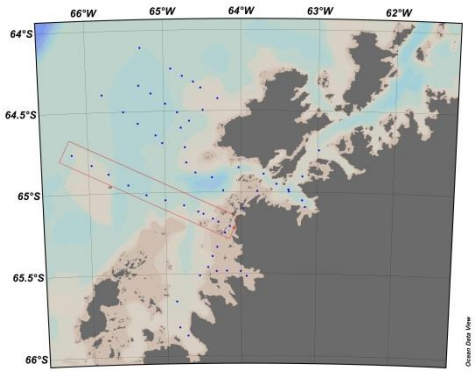
66°W
65°W
64°W
63°W
62°W
64°S
64.5°S
65°S
65.5°S
66°S
Ocean Data View

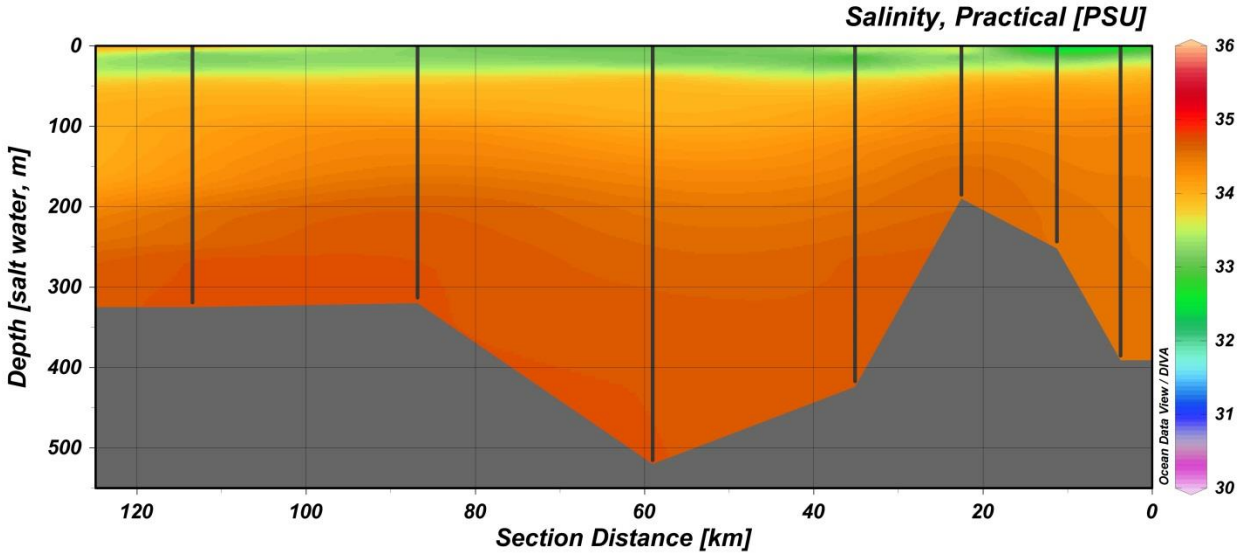
Salinity, Practical [PSU]
Depth [salt water, m]
0
100
200
300
400
500
120
100
80
60
40
20
0
Section Distance [km]
36
35
34
33
32
31
30
Ocean Data View / DIVA

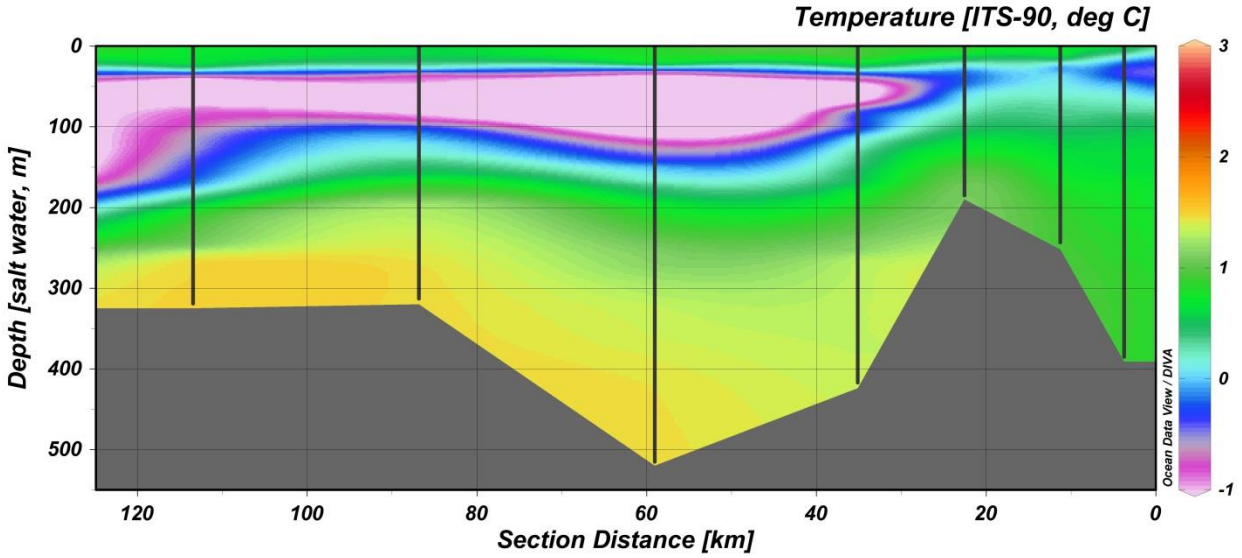
Temperature [ITS-90, deg C]
Depth [salt water, m]
0
100
200
300
400
500
120
100
80
60
40
20
0
Section Distance [km]
3
2
1
0
-1
Ocean Data View / DIVA

Apendix III Data Summary from the 2012 Cruise

Site	Depth	Lat	Long	Salinity	Temp	DO	Fluoresence	Turbidity	Density
T1-1	10			34.06	0	11.14	3.37	0.08	27.35
	55	64.49S	64.12W	34.22	-0.04	9.62	1.97	-0.12	27.48
	125			34.34	0.22	8.42	1.18	-0.15	27.56
T1-2	5			33.96	0.57	11.8	4.89	0.46	27.24
	40.5	64.358S	64.527W	34.1	-0.73	10.739	2.7	-0.11	27.42
	230			34.61	1.19	6.16	0.67	-0.2	27.72
T1-3	10			33.96	-0.26	11.62	4.64	0.26	27.28
	72	64.236S	64.908W	34.03	-1.39	10.94	2.16	-0.18	27.38
	485			34.7	1.55	5.7	0.67	-0.21	27.77
T1-4	10			33.96	-0.029	11.6	4.39	0.26	27.28
	95	64.109S	65.295W	34.06	-1.37	10.6825	1.7509	-0.19	27.4
	510			34.68	1.5	5.62807	0.7033	-0.2	27.75
T1-5	10			33.83	-0.3	11.41	1.34	0.17	27.17
	75	63.972S	65.708W	34.01	-1.43	11.21	2.07	-0.17	27.37
	447			34.69	1.53	5.65	0.64	-0.2	27.76
T2-200	5	64.992S	64.239W	33.58	0.31	10.72	0.99	0.1	26.94
T2-1	10			33.8	0.53	11.338	1.1477	0.15	27.11
	28			34.05	-0.7	11.42	204	0.04	27.37
	80	64.815S	64.716W	34.24	-0.2	9.36415	1.5287	-0.16	27.5
	130			34.37	0.25	8.18	1.08	-0.17	27.58
	182			34.43	0.45	7.59988	0.7985	-0.18	27.6
T2-2	10			33.66	0.71	11.2839	0.989	0.07	26.99
	50	64.695S	65.03W	33.98	-0.89	11.57	3.53	0.01	27.32
	500			34.7	1.53	5.7	0.58	-0.2	27.76
T2-3	10			33.72	-1.49	11.301	3.3065	-0.01	27.22
	30			33.9	-1.51	10.95	3.4	-0.11	27.28
	50	64.757S	65.342W	33.95	-1.54	10.36	1.97	-0.17	27.32
	150			34.33	-0.12	8.43	0.74	-0.2	27.57
	300			34.62	1.46	5.84	0.64	-0.22	27.71
	600			34.71	1.51	5.69	0.61	-0.2	27.78
T2-4	10			33.82	-0.2	11.37	4	0.22	27.17
	100	64.395S	65.801W	34	-1.5	10.93	1.814	-0.17	27.36
	305			34.66	1.49	5.67	0.64	-0.22	27.74
T2-5	10			33.71	-0.41	11.32	3.59	0.25	27.08
	75	64.212S	66.256W	33.94	-1.73	10.5	1.53	-0.2	27.32

	409			34.71	1.55	5.7	0.54	-0.22	27.77
T3-200	4.5	65.209S	64.15W	32.78	0.02	13.45	1.08	0.29	26.31
	40			34.01	-0.29	8.01	0.8938	-0.06	27.33
T3-0	5	65.183S	64.283W	32.81	0.09	12.93	1.62	0.36	26.33
T3-0.5	10	65.135S	64.495W	33.22	0.13	11.66	3.78	0.4	26.68
T3-1	10			33.44	-0.23	11.51	1.75	0.13	26.86
	70	65.08S	64.757W	33.99	-1.17	9.28	1.24	-0.2	27.34
	397			34.6	1.2	6.05	0.64	-0.2	27.71
T3-2	10			33.77	-0.9	11.61	4.51	0.26	27.16
	60	65.014S	65.252W	33.96	-1.47	10.2	2.23	-0.17	27.33
	512			34.69	1.51	5.69	0.64	-0.2	27.76
T3-3	10			34.01	-0.41	10.76	2.29	0.01	27.32
	100	64.882S	65.743W	34.18	-0.51	9.3	1.31	-0.17	27.47
	310			34.65	1.38	5.79	0.77	-0.22	27.74
T3-4	10			33.92	-0.2	11.38	2.32	0.14	27.25
	80	64.759S	66.214W	34.03	-1.26	10.53	1.78	-0.18	27.38
	322			34.65	1.38	5.8	0.74	-0.21	27.74
T3-5	10			33.71	-0.55			0.19	
	80	64.598S	66.796W	34.09	-1.16			-0.21	
	320			34.7	1.58			-0.22	
FB-4	10	65.056S	63.098W	33.91	0.26	10.88	0.77	0	27.21
	35			34.18	0.14	8.54	1.21	-0.12	27.44
FB-3	10			33.86	0.61	11.55	1.31	0.03	27.15
	35	65.047S	63.234W	34.17	0.03	8.4	0.96	-0.13	27.44
	196			34.47	0.61	6.89	0.67	-0.17	27.64
FB-2	10			33.97	0.34	10.38	1.88	0.05	27.26
	75	65.019S	63.321W	34.34	0.33	7.46	0.7	-0.15	27.55
	327			34.51	0.66	6.8	0.61	-0.16	27.67
FB-1	10			33.92	0.67	9.98	1.31	-0.05	27.2
	80	64.984S	63.431W	34.27	0.03	8.35	1.12	-0.18	27.51
	592			34.52	0.87	6.62	0.64	-0.19	27.67
CT-0.5	5	65.006S	64.489W	33.26	0.34			0.31	
CT-2	10			33.52	0.51	11.24	1.78	0.03	26.88
	65	64.866S	65.168W	34.02	-1.07	10.69	1.81	-0.17	37.36

	645			34.7	1.51	5.7	0.67	-0.2	27.77
CT-3	10			33.89	-0.6	11.58	2.61	0.1	27.23
	70	64.667S	65.665W	33.98	-1.38	11.15	2.96	-0.14	27.34
	517			34.69	1.5	5.69	0.61	-0.2	27.76
CT-1	10			33.99	-0.1	11.6	3.69	0.36	27.3
	80	64.542S	64.752W	34.02	-1.19	11.24	2.07	-0.16	27.37
	556.79			34.7	1.54	5.69	0.64	-0.2	27.76
TNS	10			33.7	0.55	11.39	2.07	0.12	27.03
	65			34.06	-1.07	10.17	1.81	-0.17	27.39
	150	64.866S	64.175W	34.36	0.07	8	0.7	-0.21	27.59
	300			34.58	1.12	6.24	0.67	-0.21	27.7
	495			34.66	1.43	5.74	0.64	-0.21	27.74
BS-1	10	64.875S	63.752W	33.82	0.29			0.08	

Site	Depth	224	224 err	223	223 err	226	226 err	222	222 err
T1-1	10	0.44	0.44	0.19	0.05	0.0281	0.0404	0.333	0.111
	55	1.11	0.08	0.35	0.07	0.0486	0.0529	0.304	0.115
	125	2.4	0.12	0.43	0.07	0.0346	0.0392	0.384	0.157
T1-2	5	7.8	0.042	0.55	0.09	0.0563	0.0523	0.125	0.087
	40.5	1.59	0.1	0.43	0.08	0.0518	0.0612	0.1615	0.101
	230	7.82	0.28	0.77	0.09	0.0684	0.0608	0.3625	0.105
T1-3	10	0.58	0.04	0.38	0.06	0.0492	0.0588	0.2305	0.1225
	72	3.01	0.23	0.23	0.05	0.0501	0.0559	0.244	0.109
	485	2.28	0.11	0.77	0.09	0.0334	0.0393	0.507	0.147
T1-4	10	3.6	0.42	0.16	0.06	0.0386	0.052	0.213	0.083
	95	3.65	0.37	0.29	0.07	0.0473	0.0511	0.062	0.049
	510	2.9	0.18	1.52	0.17	0.267	0.0263	0.452	0.173
T1-5	10	0.26	0.03	0.21	0.06	0.03	0.0395	0.2185	0.117
	75	0.05	0	0.27	0.06	0.0559	0.0621	0.335	0.148
	447	5.91	0.31	1.6	0.16	0.0568	0.0568	0.313	0.123
T2-200	5	1.64	0.12	0.34	0.08	0.0336	0.056	0.509	0.147
T2-1	10	0.18	0.02	0.15	0.04	0.0316	0.0623	0.197	0.088
	28	0.15	0.01	0.2	0.05	0.055	0.0675	0.322	0.122
	80	1.11	0.11	0.17	0.06	0.0384	0.0572	0.184	0.092
	130	1.16	0.12	0.47	0.11	0.0324	0.0312	0.499	0.188
	182	0.49	0.05	0.39	0.07	0.0218	0.0431	0.143	0.101
T2-2	10	0.09	0.01	0.15	0.04	0.0351	0.049	0.058	0.058
	50	0.13	0.01	0.16	0.04	0.0257	0.0361	0.609	0.169
	500	1.38	0.13	0.78	0.13	0.0297	0.06	0.575	0.217
T2-3	10	0.55	0.05	0.31	0.07	0.0375	0.072	0.314	0.141
	30	0.63	0.06	0.27	0.06	0.0405	0.0692	0.224	0.08
	50	2.02	0.12	0.54	0.09	0.0573	0.0521	0.102	0.059
	150	0.24	0.02	0.24	0.05	0.47	0.0375	0.186	0.107
	300	1.34	0.1	0.34	0.07	0.0502	0.0448	0.358	0.146
	600	2.41	0.15	1.68	0.18	0.0693	0.09	0.431	0.124
T2-4	10	6.29	0.33	0.65	0.12	0.0406	0.046	0.065	0.065
	100	2.01	0.16	0.2	0.06	0.0413	0.0503	0.166	0.083
	305	3.68	0.25	1	0.17	0.0526	0.0545	0.237	0.131
T2-5	10	0.75	0.05	0.16	0.04	0.0449	0.0533	0.24	0.1005
	75	0.04	0	0.21	0.04	0.0355	0.0445	0.257	0.1045

	409	1.8	0.12	0.62	0.09	0.0394	0.0507	0.608	0.2065
T3-200	4.5	0.49	0.04	0.14	0.04	0.0324	0.045	0.257	0.129
	40	1.51	0.1	0.32	0.07	0.0324	0.0452	0.655	0.207
T3-0	5	0.2	0.02	0.12	0.03	0.0329	0.0434	0.377	0.126
T3-0.5	10	0.99	0.06	0.25	0.05	0.0304	0.0434	0.271	0.111
T3-1	10	0.75	0.05	0.37	0.07	0.0263	0.034	0.137	0.097
	70	0.68	0.05	0.38	0.07	0.0362	0.0333	0.409	0.167
	397	1.34	0.1	0.5	0.09	0.0482	0.0471	0.398	0.12
T3-2	10	0	0.02	0.35	0.07	0.0362	0.0433	0.534	0.202
	60	0.77	0.06	0.37	0.07	0.0532	0.0519	0.306	0.1135
	512	1.47	0.1	0.92	0.12	0.0541	0.046	0.28	0.188
T3-3	10	0.39	0.02	0.35	0.05	0.046	0.0488	0.501	0.177
	100	0.72	0.04	0.36	0.06	0.0668	0.0696	0.358	0.119
	310	1.69	0.09	0.72	0.1	0.0414	0.0429	0.247	0.101
T3-4	10	0.76	0.06	0.18	0.04	0.0321	0.0518	0.196	0.103
	80	0.19	0.01	0.28	0.05	0.0384	0.0512	0.04	0.054
	322	2.02	0.12	0.69	0.1	0.0416	0.0429	0.288	0.144
T3-5	10	0.13	0.01	0.13	0.03	0.0331	0.0536	0.196	0.113
	80	3.25	0.22	0.22	0.04	0.0366	0.0426	0.382	0.171
	320	4.45	0.25	0.87	0.11	0.0368	0.0439	0.352	0.124
FB-4	10	4.48	0.44	0.29	0.08	0.0723	0.007	0.6	0.2
	35	4.31	0.39	0.13	0.04	0.0635	0.006	0.56	0.119
FB-3	10	0.57	0.1	0.13	0.07	0.0545	0.012		
	35	0.23	0.02	0.1	0.05	0.0493	0.012	0.56	0.162
	196	1.72	0.15	0.41	0.1	0.0863	0.018	0.403	0.152
FB-2	10	0.18	0.04	0	0	0.0568		0.319	0.113
	75	1.69	0.13	0.37	0.08	0.0799		0.418	0.171
	327	3.23	0.22	0.48	0.1	0.0842		0.414	0.14
FB-1	10	1.4	0.14	0.96	0.18	0.0666	0.015	0.291	0.146
	80	1.12	0.1	0.17	0.06	0.0778	0.015	0.258	0.108
	592	0.74	0.07	0.29	0.07	0.0578	0.014	0.147	0.104
CT-0.5	5	0.23	0.02	0.2	0.05	0.0469	0.013	0.333	0.111
CT-2	10	0.23	0.02	0.35	0.06	0.0977	0.017	0.337	0.107
	65	0.38	0.03	0.22	0.05	0.0737	0.015	0.554	0.209

	645	1.83	0.13	0.86	0.12	0.0875	0.017	0.371	0.117
CT-3	10					0.0667	0.016	0.364	0.121
	70	0.53	0.04	0.23	0.05	0.0758	0.016	0.706	0.235
	517	2.49	0.14	0.96	0.12	0.1004	0.018	0.238	0.097
CT-1	10	0.1	0.01	0.2	0.05	0.0446	0.0949	0.258	0.129
	80	0	0	0.09	0.03	0.053	0.013	0.142	0.073
	556.79	0.81	0.09	0.57	0.09	0.0341	0.0648	0.355	0.125
TNS	10	0.15	0.01	0.37	0.07	0.0394	0.0514	0.465	0.155
	65	0.27	0.03	0.17	0.05	0.0672	0.014	0.193	0.112
	150	0.48	0.04	0.25	0.05	0.0618	0.016	0.325	0.103
	300	2.7	0.21	0.41	0.06	0.076	0.016	0.169	0.08
	495	1.06	0.11	0.52	0.11	0.0758	0.017	0.124	0.088
BS-1	10	0.98	0.09	0.27	0.07		0.0679	0.549	

Site	Depth	18O	D	N+N mols/uL	NH4 mols/uL	HPO4 mols/uL
T1-1	10	-0.6	-5.54	6.1608	0.512	0.6054
	55	-0.01	-6.62	7.0801	0.7868	0.7013
	125	-0.24	-5.46	6.693	0.3963	0.7128
T1-2	5			4.5964	1.0099	0.5265
	40.5			6.7737	0.3259	0.7318
	230			7.9187	0.6323	0.7865
T1-3	10	-0.59	-5.5	6.1124	0.3347	0.5981
	72	-0.64	-6.62	7.0962	0.4697	0.7013
	485	-0.34	-5.06	7.9187	0.4075	0.7897
T1-4	10	-0.65	-4.49	6.0802	0.3852	0.5981
	95	-0.65	-4.88	7.0962	0.6886	0.5026
	510	-0.27	-2.73	8.0478	0.2995	0.7981
T1-5	10	-0.52	-8.33	6.0156	0.394	0.5717
	75	-0.48	-6.67	6.1124	0.5261	0.6781
	447	-0.25	-4.6	7.6607	0.2049	0.8518
T2-200	5	-0.61	-6.38	4.2739	2.378	0.5233
T2-1	10	-1.95	-11.88	4.4674	1.8378	0.517
	28	-0.66	-5.49	6.2898	0.5384	0.6907
	80	-1.05	-3.29	7.0962	0.7633	0.7097
	130	-0.74	-6.79	7.5639	0.4744	0.7329
	182	-0.81	-11.24	7.1446	0.4427	0.7487
T2-2	10	-0.94	-7.18	4.5319	2.1021	0.0575
	50	-0.68	-2.94	6.6608	0.7457	0.6655
	500	-0.63	-3.72	7.9187	0.3822	0.7992
T2-3	10	-0.81	-7.61	5.0641	1.0041	0.537
	30	-0.71	-5.73	5.5157	0.6694	0.5981
	50	-0.7	-6.53	6.6285	0.411	0.6486
	150	-0.28	-4.16	7.7091	0.3887	0.756
	300	-0.31	-2.76	7.3543	0.4128	0.775
	600	-0.86	-1.01	7.9187	0.364	0.7992
T2-4	10	-0.56	-7.2	5.5963	0.4868	0.5886
	100	-0.46	-6.21	3.79	0.8514	0.5886
	305	-0.78	-9.02	7.5155	0.4234	0.735
T2-5	10	-0.62	-6.05	6.0479	0.4715	0.5896
	75	-0.69	-6.89	6.8865	0.5449	0.6697

	409	-0.21	-4.97	7.9671	0.4057	0.7929
T3-200	4.5	-1.22	-7.51	0.8628	0.218	0.218
	40	-0.56	-4.85	6.7898	1.1274	0.7623
T3-0	5	-0.73	-9.35	3.9513	1.5677	0.3885
T3-0.5	10	-0.8	-8.83	3.1288	2.654	0.4075
T3-1	10	-0.38	-7.46	2.1289	3.3762	0.2874
	70	-0.39	-7.49	4.6287	2.5307	0.5412
	397	-0.51	-1.83	7.7209	0.3705	0.7623
T3-2	10	-1.06	-6.71	4.9351	1.4855	0.5739
	60	-0.84	-6.38	6.6446	0.4645	0.7023
	512	-0.02	-3.17	7.3543	0.3229	0.7876
T3-3	10	-1.25	-6.92	7.322	0.3746	0.7823
	100	-0.97	-2.55	6.564	0.4768	0.7044
	310	-0.08	-2.82	5.4512	0.5361	0.5707
T3-4	10	-0.62	-6.57	4.548	0.5989	0.5781
	80	-0.79	-7.9	6.1769	0.5672	0.6497
	322	-0.61	-9.4	7.2898	1.32	0.7865
T3-5	10	-1.45	-9.81	6.8704	0.448	0.7139
	80	-0.28	-5.07	6.4672	0.5707	0.6834
	320	-0.04	-1.13	7.322	0.377	0.7708
FB-4	10	-1.05	-7.75	2.5643	4.985	0.4233
	35	-0.53	-4.42	6.1769	2.5424	0.7708
FB-3	10	-0.58	-3.71	3.4997	5.0555	0.4823
	35	-0.9	-5.07	6.0963	2.9945	0.7708
	196	-0.64	-4.03	5.13	0.3012	0.8592
FB-2	10	-1.27	-8.41	3.1449	4.756	0.4412
	75	-0.39	-3.98	7.58	0.8044	0.7718
	327	-0.24	-5.05	7.322	0.3928	0.7781
FB-1	10	-0.54	-4.47	5.1448	2.4191	0.5812
	80	-0.8	-4.59	7.2414	0.7105	0.7392
	592	-0.23	-2.17	7.9671	0.3605	0.7897
CT-0.5	5	-0.91	-6.25	2.9836	3.3703	0.0433
CT-2	10	-0.57	-7.32	1.308	1.5795	0.3759
	65	-0.78	-8.69	6.3382	0.9042	0.6802

	645	-0.47	-8.75	7.0478	0.4322	0.7455
CT-3	10	-0.87	-6.01	5.4996	0.4938	0.5833
	70	-0.73	-7.78	6.1769	0.5784	0.6265
	517	-1.36	-5.04	7.3381	0.3887	0.7823
CT-1	10	-1.07	-3.67	5.9511	0.4486	0.5918
	80	-0.9	-9.47	6.9833	0.6224	0.6802
	556.79	0.02	-1.86	7.2091	0.3899	0.7444
TNS	10	-0.63	-6.13	4.6448	2.1373	0.5223
	65	-0.49	-6.18	6.8543	0.9747	0.7107
	150	-0.38	-5.86	6.9349	0.3963	0.7118
	300	-0.49	-8.83	8.0639	0.31	0.8044
	495	-0.39	-3.82	7.4994	0.502	0.7865
BS-1	10	-0.53	-5.48	5.4351	1.4327	0.6139

Apendix IV Data Summary from the 2014 Cruise

Station	Type	Longitude [degrees_east]	Latitude [degrees_north]	Bot. Depth [m]	Depth [salt water, m]	Salinity, Practical [PSU]	Temperature [ITS-90, deg C]
Barb2	CTD	295.27802	-65.875	487	1.1	31.22	-0.59
					24	32.94	0.11
					462	34.6	1.17
BarB3	CTD	295.16901	-65.825	430	0.9	31.89	-0.27
					6	32.64	0.13
					413	34.59	1.15
BEAB34	CTD	295.66876	-65.48338	795	1		
					6		
BEAB-6	CTD	296.06964	-65.51337	575	1		
					6		
BEAB-7	CTD	295.99255	-65.48385	546	1		
					6		
BEAB-8	Intake	295.80688	-65.4818		6	31.561	0.33
CT4-1	Intake	295.21576	-64.60326		6	33.148	1.172
CT4-2	Intake	295.50171	-64.49465		6	33.207	1.087
Flab-18	CTD	296.83978	-65.09068	695	0.3	32.718	2.79
					25.3	33.67	0.45
					671	34.517	0.272
Flab-19	CTD	296.80118	-65.05042	415	0.5	32.62	0.37
					32	33.69	0.52
					412	34.57	0.96
Flab-20	CTD	296.62268	-64.9853	400	1	33.07	0.84
					25	33.57	0.17
					397	34.59	1.12
FlaB-21	CTD	296.46277	-64.95058	498	0.9	33.11	0.77
					27	33.59	0.47
					482	34.61	1.24
FlaB-22	CTD	296.29285	-64.88828		1	32.937	1.17
					25	33.52	0.35
					598	34.64	1.349
Flab-23	CTD	295.96521	-64.8497	380	1	32.98	1.037
					21.5	33.5	0.38
					368	34.668	1.41
FlaB-55	CTD	296.61801	-64.98402	428	1	33.21	0.69
FlaB-58	CTD	296.62784	-64.99718	400	1	32.98	0.55
					6	33.252	0.654
Ger-56	CTD	296.8017	-64.90369	250	1	33.32	0.67
Ger-57	CTD	297.01361	-64.74226	314	1	33.36	0.68
Grand33	CTD	295.55499	-65.459	246	1.4	33	0.65
					34.5	33.39	0.06

GRAND-35	Intake	295.6153	-65.3914		6	32.241	0.704
GRAND-36	Intake	295.78391	-65.24924		6	32.233	0.47
GRAND-37	Intake	296.0191	-65.10005		6	32.482	0.786
GRAND-38	Intake	296.20941	-64.9933		6	32.963	0.735
Grand4	CTD	295.13199	-65.667	403	1.3	31.71	0.05
					25	33.17	-0.25
Grand5	CTD	295.44501	-65.51	200	1.5	33.02	0.63
					17	33.63	-0.24
Grand9	CTD	295.67899	-65.336	265	1.5	32.3	0.65
					37	33.56	-0.5
T4-29	CTD	295.69254	-64.42405	152	6	33.23	1.07
T4-30	CTD	295.47488	-64.35665	245	6	33.21	0.91
T4-31	CTD	295.09235	-64.23788	508	6	33.23	1.16
T4-32	CTD	294.70279	-64.10693	540	6	33.15	1.03
T4-41	Intake	295.23846	-64.2834		6		
T4-42	Intake	295.38	-64.32		6	33.147	0.994
T5-17	CTD	295.75995	-64.99005	600	6	33.614	0.923
					30	33.65	0.519
T5-24	CTD	295.61533	-64.909	369	6	33.005	0.976
T5-25	CTD	295.28024	-64.81654		6	33.08	1.08
T5-26	CTD	294.97015	-64.6953		6	33.16	1.28
T5-27	CTD	294.65866	-64.57378	633	6	33.16	0.91
T5-28	CTD	294.20245	-64.39375	327	6	33.178	0.977
T5-39	Intake	295.39847	-64.8794		6	32.979	0.886
T5-40	Intake	295.2645	-64.72353		6	32.954	1.023
T5-48	Intake	294.88672	-64.6473		6	33.187	1.313
T5-49	Intake	294.47321	-64.50055		6	33.244	0.584
T6-10	CTD	295.84677	-65.2089	390	6	32.97	0.38
T6-11	CTD	295.69623	-65.18233	238	6	32.39	0.716
T6-12	CTD	295.49908	-65.13316	191	6	32.97	0.71
T6-13	CTD	295.2439	-65.07965	427	6	32.851	0.886
T6-14	CTD	294.75076	-65.01456	539	6	33.09	0.82
T6-15	CTD	294.2597	-64.88184	335	6	33.2	0.57
T6-16	CTD	293.78613	-64.75819	341	6	33.201	0.69
T6-50	Intake	294.04172	-64.82477		6		
T6-51	Intake	294.51498	-64.95177		6		
T6-52	Intake	294.99786	-65.0476		6	33.16	0.844
T6-53	Intake	295.43088	-65.11922		6	32.914	0.918
T6-54	Intake	295.6214	-65.16358		6	32.583	0.678
T7-43	Intake	294.67688	-64.34013		6	33.168	1.235
T7-44	Intake	294.83279	-64.38879		6	33.17	1.227
T7-45	Intake	295.01654	-64.45367		6	33.176	1.147
T7-46	Intake	295.17041	-64.50774		6	33.161	1.179

T7-47	Intake	295.32321	-64.5612	6	33.19	1.17

Station	Type	Radium- 223 [dpm/m3]	Radium 224 [dpm/m3]	Rn [dpm/L]
Barb2	CTD	0.461548781	6.155110022	0.26
		0.368303767	7.374330726	0.204
		1.232725595	12.4216005	0.352
BarB3	CTD	0.933455682	3.86709841	0.753
		0.809617036	12.8388971	
		1.555657342	11.87660378	0.472
BEAB34	CTD	0.468896849	0.645924095	
		0.426246329	0.369243728	
BEAB-6	CTD	0.462893632	0.262880174	
		0.274021881	1.021438107	0.272
BEAB-7	CTD	0.275860832	1.892617453	
		0.649296266	2.843288788	0.302
BEAB-8	Intake	0.348387423	2.250875689	0.248
CT4-1	Intake	0.274943522	8.854072078	0.321
CT4-2	Intake	0.391680783	4.715423994	0.444
Flab-18	CTD	0.305831166	0.346973301	
		0.261457691	1.204640297	0.258
		1.515780387	16.1121734	1.116
Flab-19	CTD	0.645102199	3.853037639	0.512
		0.533113175	1.865279913	0
		0.693328562	4.136218159	0.303
Flab-20	CTD	0.285587958	1.112919317	0.198
		0.320234694	5.71154088	0.412
		0.459788713	3.915414308	0.408
FlaB-21	CTD	0.410929281	0.248369111	0.158
		0.32693602	2.218480916	0.35
		0.827713838	3.349848847	0.588
FlaB-22	CTD	0.35256155	1.839612773	0.318
		0.572063473	2.262130983	0.292
		0.9004486	2.591404578	0.333
Flab-23	CTD	0.342609743	1.374193224	0.236
		0.36323453	1.253672525	0.54
		0.636798415	1.494683436	0.395
FlaB-55	CTD	0.677373251	7.570137054	0.307
FlaB-58	CTD	0.487559682	1.711697672	
		0.605795549	1.42878429	
Ger-56	CTD	0.623597724	4.824768211	0.155
Ger-57	CTD	0.554557791	7.254124712	0.285
Grand33	CTD	0.457282976	3.611511551	0.183
		0.298772427	3.596510776	0.483
GRAND-35	Intake	0.346424021	0.825224513	0.221

GRAND-36	Intake	0.339703148	0.966458399	0.305
GRAND-37	Intake	0.416467258	2.077632452	0.208
GRAND-38	Intake	0.280526274	3.143519836	0.414
Grand4	CTD	0.438998248	4.508948475	0.122
		0.389354454	165.8870111	0.321
Grand5	CTD	0.76306309	8.442630504	0.337
		0.293329887	12.88844375	0.206
Grand9	CTD	0.791974899	5.151743058	0.309
		0.491585432	2.306580397	0.245
T4-29	CTD	0.342887968	3.471611396	0.209
T4-30	CTD	0.243519278	0.694305821	0.225
T4-31	CTD	0.177506196	0.491966305	0.323
T4-32	CTD	0.45775884	1.54055129	0.312
T4-41	Intake	0.263736451	2.338981187	0.167
T4-42	Intake	0.326885478	0.111183697	0.313
T5-17	CTD	0.236062957	1.689800103	0.21
		0.50535355	1.178971575	0.157
T5-24	CTD	0.375393279	0.502653568	0.182
T5-25	CTD	0.260911111	5.452045548	0.034
T5-26	CTD	0.655798927	2.850343731	0.261
T5-27	CTD	0.206206527	2.202415726	0.472
T5-28	CTD	0.500374051	4.889130202	0.125
T5-39	Intake	0.22231392	0.650733837	0.127
T5-40	Intake	0.365127413	3.027007276	0.16
T5-48	Intake	0.352797282	0.940378698	0.172
T5-49	Intake	0.478800557	1.38838784	0.363
T6-10	CTD	0.384063626	9.676535571	0.287
T6-11	CTD	0.244583982	0.556048674	0.15
T6-12	CTD	0.357655988	0.469912842	0.354
T6-13	CTD	0.235066422	0.557677669	0.142
T6-14	CTD	0.367563894	1.020066211	0.241
T6-15	CTD	0.319941947	1.140828835	0.235
T6-16	CTD	0.281781866	0.882271934	0.396
T6-50	Intake	0.177402127	1.504419483	0.413
T6-51	Intake	0.475217785	4.788931205	0.212
T6-52	Intake	0.372765217	0.756145182	0.216
T6-53	Intake	0.179979879	4.043630799	0.426
T6-54	Intake	0.194207452	0.15194079	0.281
T7-43	Intake	0.442015433	1.324997755	0.225
T7-44	Intake	0.582873631	1.782239209	0.164

T7-45	Intake	0.302863898	1.096932336	0.323
T7-46	Intake	0.276010441	1.224557342	0.396
T7-47	Intake	0.38179572	0.49106689	0.24

Station	Type	Orthophosphate [ug P/L]	Nitrate+Nitrite [ug/l]	Ammonia [ug/l]	Silicate [ug/l]	Fluorescence
Barb2	CTD	9.49	29	12.7	1230	0.3
		10	123	13.2	1450	4.6
		73.7	486	0	2440	
BarB3	CTD	6.27	6.85	0	1220	6.8
		77.2	495	0	2710	
BEAB34	CTD					
BEAB-6	CTD	5.82	10.7	0.451	1100	0.42
		5.32	36.1	4.99	1180	
BEAB-7	CTD	4.41	5.5	3.74	1210	1.05
		4.37	5.77	0	1200	
BEAB-8	Intake					0.56
CT4-1	Intake					1.65
CT4-2	Intake					1.72
Flab-18	CTD	28.9	213	20.9	1920	1.26
		36.2	256	31	2040	
		79.6	508	6.68	3000	
Flab-19	CTD	25.9	194	23.1	1930	1.31
		59.8	375	51.8	2480	
		79.5	500	0	3030	
Flab-20	CTD	34.6	263	0.845	2090	0.76
		49.4	319	42.8	1990	
FlaB-21	CTD	37	294	31.2	1710	0.69
		53.8	360	34.5	2190	
		73.6	495	0	2820	
FlaB-22	CTD	15.4	229	19.5	1300	0.63
		45.1	311	43.4	1980	
		74	520	0	2900	
Flab-23	CTD	35.8	215	25.9	1660	0.6
		45.9	267	49.3	1840	
		75.4	492	0	3030	
FlaB-55	CTD	43.1	285	11.2	2100	0.92
FlaB-58	CTD					1.14
Ger-56	CTD	41.9	315	19.6	2030	0.97
Ger-57	CTD	43.4	298	24.6	1990	0.59
Grand33	CTD	28.5	212	17.9	1420	2.5
						1.9
GRAND-	Intake					2.61

35						
GRAND-36	Intake					0.69
GRAND-37	Intake					0.74
GRAND-38	Intake					0.88
Grand4	CTD	5.98	30.5	0	1080	6.01
Grand5	CTD	30.7	238	27.9	1420	1.91
		43.5	267	51.7	1630	
Grand9	CTD	7.36	41	11.4	1280	0.507
		60.2	307	92.6	1900	
T4-29	CTD	44.2	311	31.7	1680	0.52
T4-30	CTD	42.7	294	32.6	1640	0.63
T4-31	CTD	45.4	323	31.6	1670	0
T4-32	CTD	42	290	25.4	1510	1.36
T4-41	Intake					
T4-42	Intake					0.83
T5-17	CTD	35.1	228	43.9	1640	0.91
		56.1	359	66.7	2210	
T5-24	CTD	27.9	188	32.8	1590	1.42
T5-25	CTD	39.1	251	34.1	1600	0.62
T5-26	CTD					0.33
T5-27	CTD	40.6	328	19	1490	0.76
T5-28	CTD	42.1	348	28.7	1610	0.761
T5-39	Intake					1.93
T5-40	Intake					1.84
T5-48	Intake					0.71
T5-49	Intake					1.78
T6-10	CTD	29	186	58.8	1570	0.09
T6-11	CTD	16.4	120	26.1	1400	0.538
T6-12	CTD	40.4	244	34.1	1520	0.507
T6-13	CTD	25.5	181	32.2	1530	0.729
T6-14	CTD	40.05	284	26.25	1505	0.71
T6-15	CTD	46.2	340	8.08	1510	0.69
T6-16	CTD	49.7	351	13.1	1680	0.41
T6-50	Intake					
T6-51	Intake					
T6-52	Intake					1.46
T6-53	Intake					1.39
T6-54	Intake					1.36
T7-43	Intake					0.82

T7-44	Intake	0.84
T7-45	Intake	0.68
T7-46	Intake	0.61
T7-47	Intake	0.61